Western Australian School of Mines: Minerals, Energy and Chemical Engineering

Kinetic Analysis and Modelling of Cellulose Pyrolysis

Samreen Hameed

This thesis is presented for the Degree of
Doctor of Philosophy
of
Curtin University

March 2019

DECLARATION

To the best of my knowledge this thesis contains no material previously published by any other person except where due acknowledgment has been made.

This thesis contains no material which has been accepted for the award of any other degree or diploma in any university.

Signature:

Date:

ABSTRACT

The process of pyrolysis essentially entails heating of biomass in the absence of oxygen. It has been used to produce charcoal in the past, however, recently it has received significant attention for its ability to produce liquid fuels (bio-oil). Being the most abundant component of any biomass, cellulose has been often used as the model compound to study the process of pyrolysis. The process of biomass pyrolysis is challenging to model because of complicated chemical structure of biomass and underlying chemical reactions. Although several kinetic, network and mechanistic models for this process have been developed, a generalized model taking into account the kinetics, heat and mass transfer effects, the effect of inorganic species and possible interactions among particles is required to fully understand the process.

In this study, a reactor scale model for pyrolysis of cellulose has been developed. Firstly, kinetic analysis of cellulose has been performed using experimental and literature data. A distributed activation energy model was developed to determine the intrinsic kinetics of pure and NaCl-loaded cellulose pyrolysis in a thermogravimetric analyser (TGA). A set of experiments was performed for a range of heating rates (5 to 250 K/min) and for different concentrations of NaCl in cellulose (0.25 to 2 wt. %) which showed a pronounced effect of salt on the primary pyrolysis reactions of cellulose. The data obtained have then been used in a two component distributed activation energy model (DAEM) to calculate the kinetic parameters. The optimized kinetic parameters for the pure and NaCl-loaded cellulose were used in the Chemical Percolation Devolatilization (CPD) model, which was then used to predict the product yield. The model predictions showed that the fraction of gases and char in the pyrolysis products increased in the presence of salt, which is consistent with the literature.

Secondly, the hydrodynamics of fluidized bed was studied using computational fluid dynamics (CFD) modelling. A multiphase model based on the kinetic theory of granular flow was developed to study the mixing behaviour of cellulose and sand particles in a bubbling fluidized bed. After model validation using available experimental data from literature, the effect of various operating parameters such as superficial gas velocity, mixture composition and particle size were analysed. The impact of these parameters on the particle segregation number, which is used to quantify the segregation behaviour of the fluidized bed, has been emphasized. The

results showed that the degree of mixing increased with gas velocities thus giving lower values of particle segregation numbers. Increase in the ratio of biomass in the mixture led to greater segregation while the increase in biomass particle diameter promoted the mixing.

Finally, the reaction kinetics and hydrodynamic model were integrated to form a multi-phase reactive model to simulate cellulose pyrolysis using CFD model and cellulose pyrolysis kinetic scheme. The model developed for cellulose pyrolysis using Broido-Shafizadeh kinetic scheme was first validated and then kinetic parameters predicted from DAEM were used to compare the product yield obtained from a single value and distribution of activation energy. It was found that tar and char yield increased while gas yield decreased with the inclusion of DAEM. This shows that the distribution of activation energies has a profound effect on the rate of reaction and product yield, it is thus recommended to use distribution of activation energies instead of single activation energy for the accurate prediction of pyrolysis product yield.

PUBLICATIONS RELATED TO THE CURRENT RESEARCH

JOURNAL PUBLICATIONS

1. S. Hameed, A. Sharma, V. Pareek, H. Wu, Y. Yu, *A Review on Biomass Pyrolysis Models: Kinetic, Network and Mechanistic Models,* Biomass & Bioenergy. 123 (2019) 104-122.
2. Samreen Hameed, Abhishek Sharma, Vishnu Pareek, "*Modelling of particle segregation in fluidized beds*". Powder Technology. 353 (2019) 202-218.
3. Samreen Hameed, Adhirath S. Wagh, Abhishek Sharma, Vishnu Pareek, Yun Yu, "*Kinetic modelling of pyrolysis of cellulose: Effect of salt*". Industrial & Engineering Chemistry Research. Submitted in July 2019.

CONFERENCE PAPERS

1. Samreen Hameed, Abhishek Sharma, Vishnu Pareek, Hongwei Wu, Yun Yu, "*Mixing/Segregation behavior of Cellulose and Sand Particles in a Bubbling Fluidized Bed".* Chemeca 17, 23-26 July, 2017 Melbourne, Australia

ACKNOWLEDGEMENTS

First and foremost, I would like to express my sincere gratitude to my supervisor Prof. Vishnu Pareek for the support of my Ph.D study, for his patience encouragement and immense knowledge. I am genuinely thankful to him for providing me an opportunity to work under his supervision and with his team.

I would also like to thank Prof. J. B. Joshi for his guidance. Despite his busy schedule, Prof Joshi has been very kind to make himself available for discussions over web meetings especially in the first 18 months of my study.

I would also like to thank my co-supervisor, Prof. Hongwei Wu. His guidance helped me throughout the research and writing of this thesis. His useful comments during my research write-up have helped improving my writing skills.

My sincere thanks also go to my associate supervisors Dr. Yun Yu, Dr. Abhishek Sharma who have always been there to offer help in experimental modelling and simulation techniques. I would like to express my appreciation to my colleagues and group members who were there for discussions and help. I particularly thank Adhirath Sajay Wagh who has been a source of insightful discussions that helped me in the project. I also would like to acknowledge all the technical and administrative staff of Chemical Engineering Department for their assistance.

I am truly thankful to my family for their immense moral support throughout my PhD journey, especially my father who has always been my strength and support.

Financial support from Higher Education Commission, Faculty Development Program through University of Engineering and Technology, Lahore Pakistan and partial funding from Curtin University, Australia are also highly acknowledged.

DEDICATION

Dedicated to my beloved parents

TABLE OF CONTENTS

LIST OF FIGURES

LIST OF TABLES

NOMENCLATURE

SYMBOLS

A	Pre-exponential factor (s^{-1})
C_p	Specific heat (J/kg-K)
D	Diffusivity (m^2/s)
E	Activation Energy (J/kgmol)
M	Molecular weight (kg/kgmol)
P	Particle pressure (atm)
T	Temperature (K)
U	Gas inlet velocity (m/s)
U_{mf}	Minimum fluidization velocity (m/s)
υ	Vapour velocity (m/s)
V	Particle volume (m^3)

GREEK LETTERS

α	Volume fraction
k	Thermal conductivity (W/m-C)
ρ	Density (kg/m^3)
μ	Viscosity (kg/m-s)
θ	Granular temperature $(m/s)^2$
ϕ	Specularity coefficient
σ	Standard deviation
σ+1	Co-ordination number
δ	Side chains

SUBSCRIPT

A.Cell	Active cellulose
b	Bridge breaking
Cell	Cellulose

C	Char
cross	Cross linking
G	Gases
T	Tar
g	Gas phase
gas	Gas formation
l	l^{th} fluid phase
v	Vapour phase
s	Solid phase

ABBREVIATIONS

BFB	Bubbling Fluidized Bed
CFD	Computational fluid Dynamics
CNMR	Carbon-13 Nuclear Magnetic Resonance
CPD	Chemical Percolation Devolatilization
CPMD	Car-Parinello Molecular Dynamics
DAEM	Distributed Activation Energy Model
DEM	Discrete Element Model
DFT	Density Functional Theory
DPM	Discrete Particle Model
EE	Eulerian-Eulerian
EL	Eulerian-Lagrangian
FBR	Fluidized Bed Reactor
FTIR	Fourier-Transform Infrared Spectroscopy
GB	Glass Beads
GWS	Ground Walnut Shells
LMWPs	Low Molecular Weight Products
MD	Molecular Dynamics

MFIX	Multiphase Flow with Interphase eXchanges
ODE	Ordinary Differential Equation
PSN	Particle Segregation Number
QUICK	Quadratic Upstream Interpolation for Convective Kinematics
TFM	Two Fluid Model
TGA	Thermo-Gravimetric Analysis

CHAPTER 1 INTRODUCTION

It is expected that contribution of renewable sources into global energy demand will grow by one-fifth in the next five years. Among the renewable sources, which includes hydropower, wind, solar PV, solar thermal, geothermal and marine, bioenergy is currently the major contributor, and is likely to remain the biggest source in the period of 2018-2023 [1].

1.1. Research Background

Several technologies have been developed for converting biomass into bio-fuels, including physical, thermal, chemical, thermochemical and bio-chemical processes. Figure 1.1 shows the respective operating conditions and the type of products of these processes. Via physical processes, the biomass is converted into solid fuels using crushing, grinding, drying and pressing under different temperature and pressure conditions. Transesterification is a chemical route for converting oil crops to bio-diesel in the presence of an acidic or basic catalyst. Alternatively, the biomass can also be directly combusted to produce heat which is then used to produce electricity. Bio-chemical processes produce bio-oil, gas and ethanol from biomass via fermentation, anaerobic digestion and enzymatic hydrolysis processes. Pyrolysis, gasification, hydrolysis, liquefaction, torrefaction and carbonisation are examples of the thermochemical conversion methods which are used to produce fuel and energy from biomass under different operating conditions. Pyrolysis thermally decomposes biomass in inert atmosphere to produce several useful products including bio-oil, gases, tar and char that can further be used for energy production. It is one of the oldest thermochemical conversion techniques used for different solid material such as coal, biomass, oil shale, polymers, etc.

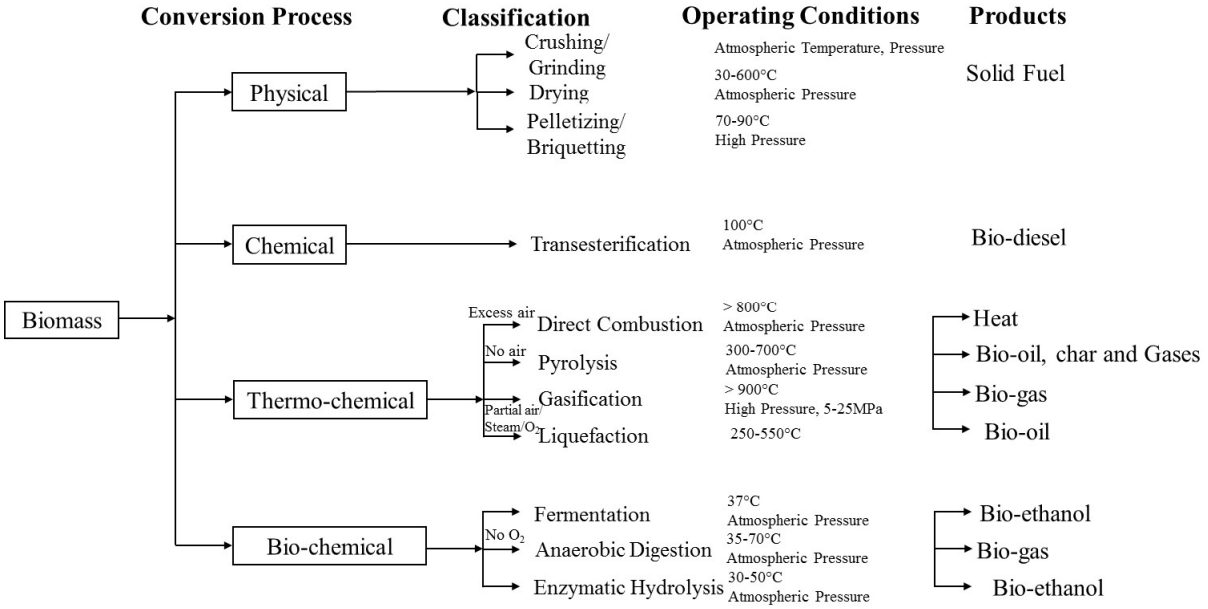

Figure 1.1. Conversion processes for biomass to produce different bio-fuels.

As a renewable energy resource, biomass comprises of cellulose, hemicellulose, lignin and other compounds such as ash and extractives. Figure 1.2 [2] presents the typical contents of these constituents in lignocellulosic biomass. Cellulose may be in the form of clusters of straight chains made of various number of glucose units, bounded by inter-chain hydrogen bonds,whereas hemicellulose has an amorphous polymeric structure. Sugars are the building blocks for hemicellulose. Lignin is a complex non-crystalline phenolic macromolecule. The base unit for lignin is an aromatic compound such as sinapyl, coniferyl, and coumaryl alcohols. Ash is considered to be a mineral matter and its composition depends on the type of biomass. It consists of sodium, potassium, calcium, silicon, phosphorous and magnesium which are found as oxides or salts as sulphates, phosphates and carbonates [3,4]. Biomass structure, its chemical composition and amount of components varies for different biomass materials depending on the source [5]. Although the amount of inorganic species is often small, it can significantly affect the biomass pyrolysis process, leading to a decrease in the bio-oil yield and increase in the yield of char and gas [6,7]. It also changes the decomposition temperature and the rate of pyrolysis [8]. In certain reactions, it acts as a catalyst such as biomass dehydration and volatiles cracking [9]. The catalytic effect of inorganic species on the biomass pyrolysis is one of the major challenges for the pyrolysis process as well as its modelling.

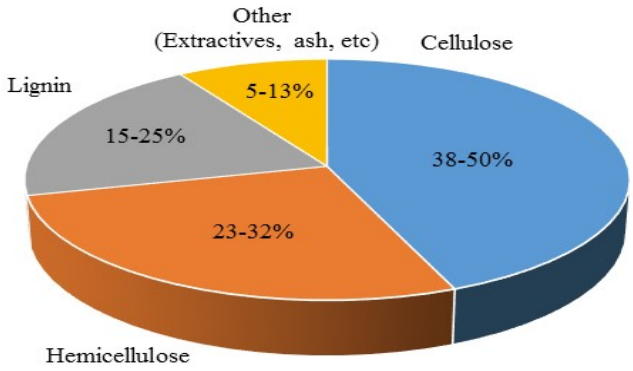

Figure 1.2. Lignocellulosic biomass composition [2].

Mathematical modelling and simulation tools have always aided the understanding of mechanism of biomass pyrolysis. Researchers have worked tremendously in the field of biomass pyrolysis and modelling to reveal the basic reaction mechanism, reaction kinetics, predicting the product yield. Biomass contains three main components, i.e. cellulose, hemicellulose and lignin. These components are often modelled independently, and then superpositioned to predict the behaviour of bionass. Koufopanos et al. [10] used the Shafizadeh model [11] originally developed for cellulose, for the three components of biomass and concluded that the overall pyrolysis rate of one type of biomass can be obtained by adding the rates of its basic constituents. Later, heat transfer effects were included into these kinetic models for accurate calculation of pyrolysis rate [12,13]. Chemical kinetics and intra-particle heat transfer have also been coupled with the external heat transfer effects for cellulose particles in a fluidized bed reactor [14]. Modelling of biomass pyrolysis based on the model compounds led to some errors on pyrolysis products because of the effect of inorganic species on reactions and other possible interactions between different components in biomass [9]. Despite the major developments in the field, there is still need of further improvements in cellulose pyrolysis modelling. Few of the research gaps which need to be addressed are: understanding of the cellulose pyrolysis behaviour, effect of inorganic species on cellulose pyrolysis, integration of kinetics and hydrodynamics of pyrolysis systems, etc. These research gaps are discussed in detail in chapter 2 of this study.

1.2. Objectives

This thesis focuses on the modelling and simulation of cellulose pyrolysis in a fluidized bed reactor. The main aims of this research are to analyse the kinetics of cellulose particles at slow and fast pyrolysis conditions in the absence and presence of inorganic species, to observe the mixing and segregation behaviour of cellulose particles, to develop a reactor scale model for cellulose pyrolysis in a fluidized bed reactor. The specific objectives in the present work are to:

1. Determine the kinetics of cellulose pyrolysis, in the absence and presence of inorganic species under slow pyrolysis conditions. This is to accomplish through experiments and modelling using thermogravimetric analysis (TGA) and distributed activation energy model (DAEM).
2. Study the effect of inorganic species on the product yield of cellulose pyrolysis using chemical percolation devolatilizaion (CPD) model.
3. Develop a computational fluid dynamics (CFD) model to examine the hydrodynamics of cellulose particles in a bubbling fluidized bed.
4. Quantify the mixing and segregation behaviour of cellulose particles in the fluidized bed using particle segregation number and examining the effect of parameters such as mixture composition, superficial gas velocity and particle size on the segregation phenomena.
5. Develop a CFD model to combine the reaction kinetics with the hydrodynamics to study the cellulose pyrolysis in the fluidized bed reactor and then incorporate the distributed activation energy model to compare the product yield with and without distribution of activation energy.

1.3. Thesis Structure

To accomplish these objectives, the tasks performed have been organized in this thesis as follows:

Chapter 1 introduces the biomass pyrolysis and modelling with some research background and focuses the research objectives of this study.

Chapter 2 reviews the literature including different models developed for the biomass pyrolysis. Specifically, it discusses about the kinetic, network and mechanistic models for biomass pyrolysis. It also highlights the challenges of biomass pyrolysis modelling including:

importance of inorganic species, interactions among the constituents of biomass and multi-scale modelling of biomass pyrolysis. This chapter also analyses the ways to use kinetic and network models for biomass pyrolysis in computational fluid dynamics. Advantages and disadvantages of pyrolysis models and their quantitative comparison have also been discussed. The importance of cellulose to be used as a resource and its modelling has also been briefly described in this chapter.

This chapter also includes the research gaps, methodology and approach used in this work.

Chapter 3 highlights the effect of inorganic species on the cellulose pyrolysis using CPD model scheme. For this purpose, the kinetic parameters for pure cellulose have been determined using TGA data and distributed activation energy model, and later the kinetic parameters of the salt-loaded cellulose have been determined using the same approach. Optimized parameters have been then used to predict the product yield, and comparisons made between the product yield obtained from the pure cellulose and salt-loaded cellulose.

Chapter 4 reports the mixing and segregation behaviour of cellulose particles in an inert bed of sand of a fluidized bed using multi-phase CFD model. It analyses the segregation behaviour qualitatively as well as quantitatively. The impact of different parameters such as mixture composition, particle size and superficial gas velocity has also been analysed.

Chapter 5 discusses the details for the formulation of a multi-phase CFD model, aiming at developing a model for cellulose pyrolysis to include the distribution of activation energies rather than single activation energy. Yields of pyrolysis products have also been compared with or without including the DAEM in the CFD scheme.

Chapter 6 offers concluding remarks on the experimental and modelling work of cellulose pyrolysis based on the results obtained from this study. It also provides some recommendations for the future work.

Map of the thesis is presented in Figure 1.3.

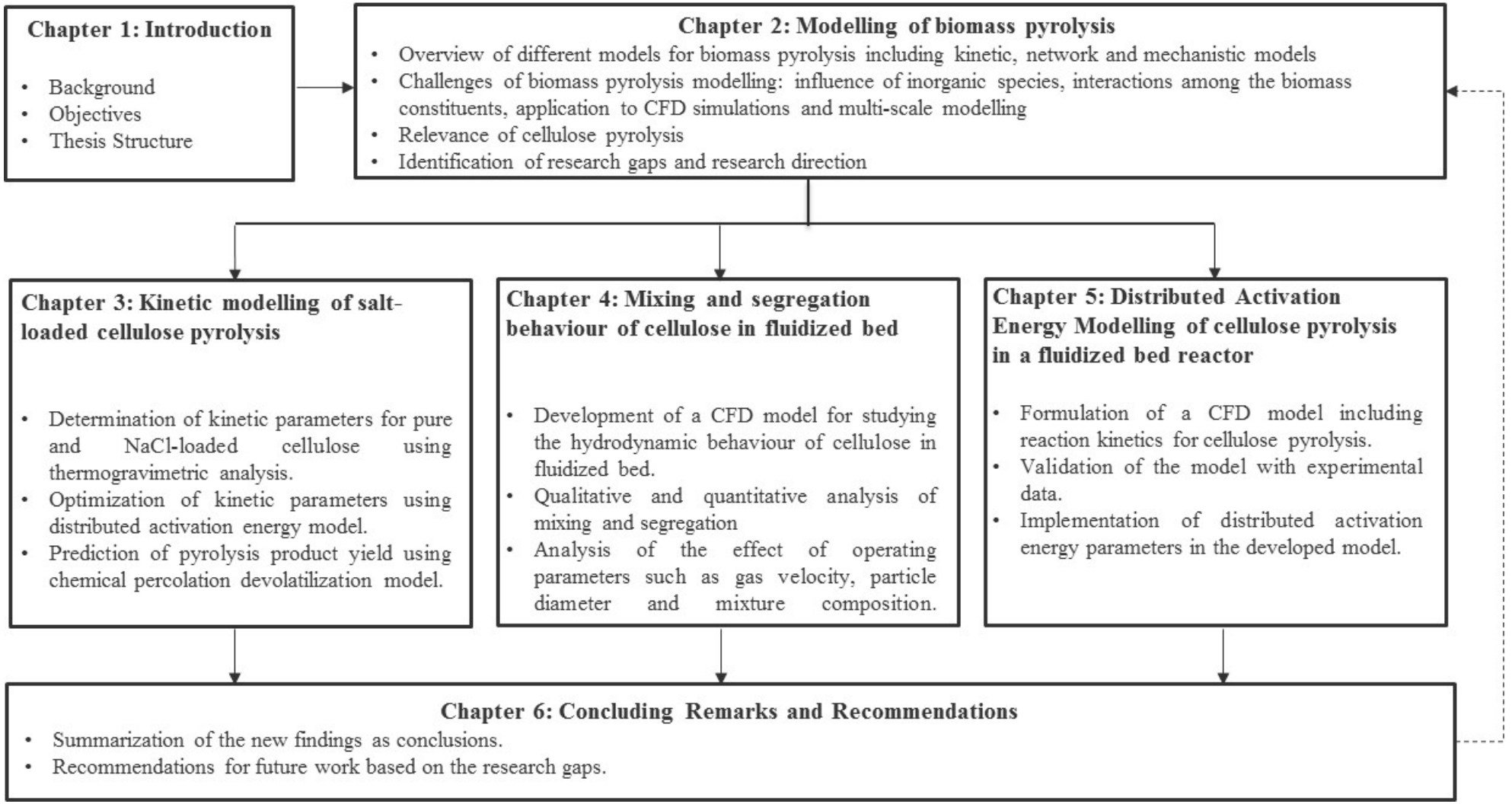

Figure 1.3. Map of the thesis

CHAPTER 2 MODELLING OF BIOMASS PYROLYSIS

2.1. Introduction

Pyrolysis is one of the most promising technologies for converting biomass into bio-oil, biochar and gases [15]. Research on biomass pyrolysis in the literature has been extensive [16–20], and near-commercial pyrolysis processes have also been developed for bio-fuel production [21–24]. From process optimisation point of view, developing models for simulating biomass pyrolysis becomes increasingly important. Previous studies [10,12,25–29] reported the understanding on fundamental reaction mechanisms and reaction kinetics of biomass pyrolysis, ranging from simple single-step kinetic model to complex reaction model that includes hundreds of reactions.

In the open literature, there are several classic reviews available on biomass pyrolysis reaction mechanisms and modelling. Di Blasi [4] presented a detailed overview of the biomass pyrolysis modelling including kinetics, transport and reactor scale models. Detailed modelling is required to better understand the pyrolysis of either single particle or particles at reactor scale. Understanding the detailed mechanisms of primary and secondary reactions, structural changes, gas and particle behaviour in a bed and requirement of an accurate model were few of the research gaps highlighted in the review. Since then extensive studies were carried out in this direction, largely addressing these research gaps. Later, Sharma et al. [30] discussed kinetic, particle and reactor models for biomass pyrolysis along with the process parameters and catalytic pyrolysis. In the review presented by Sharma et al. [30] different model discussed are kinetic (lumped and distributed), particle and reactor (phenomenological and CFD) models, however no comparison is made among the different types of models which has been focused in the current review. Anca-Couce [31] has recently given a detailed analysis of pyrolysis mechanisms including basic constituents, kinetic schemes, product compositions and pyrolysis models at molecular, particle and reactor level. The present work compliments the previous reviews and summarizes key topics that have not been thoroughly discussed previously, particularly those on key network models. It further summarises the contribution of network models to simulate biomass pyrolysis and also compares these network models with other significant (e.g. kinetic and mechanistic) pyrolysis models.

2.2. Pyrolysis Models

2.2.1. Kinetic Models

Chemical kinetics play a key role in explaining the characteristics of pyrolysis reactions and developing mathematical models. There have been extensive studies on biomass pyrolysis kinetics in the past decades for developing various kinetic models [32–34]. Most of kinetic models are considered as lumped models, because the kinetics are based on the yields of lumped products (i.e. char, tar and gas). The recent advances in kinetic models have been well reviewed in the literature [35–40]. Table 2.1 summarizes the key findings of some recent review articles on the kinetic models.

Kinetic models typically include one-step global kinetic model, parallel and competitive reactions model, models with secondary tar cracking, detailed lumped kinetic model, distributed activation energy model (DAEM) and nucleation growth model. Some typical models with respective reaction mechanisms are presented in Table 2.2, together with kinetic data (first order) for different reaction schemes determined experimentally and validated through modelling.

Table 2.1. Existing review articles on kinetic modelling of biomass pyrolysis in the open literature [35–40].

Reference	Year of publication	Key aspects covered	Key findings
Sinha et al. [36]	2000	• Modelling of physical and chemical parameters affecting pyrolysis and chemical kinetic schemes. • Uncertainties in kinetic parameters estimation for different types of biomasses.	• Modelling should consider key parameters (e.g. temperature, heating rate, residence time, structural factors etc.) • To model biomass pyrolysis, experimental data inputs are required.
Moghtaderi [37]	2006	• Kinetic modelling of biomass pyrolysis at high temperature and high heating rate. • Simplification in modelling thermal and transport effects via respective assumptions.	• Modelling requires the development of more accurate and robust chemical kinetic mechanism. • Hybrid models may be developed with both thermal and comprehensive scheme as sub-models.
Babu [38]	2008	• Considering single- and multi-step mechanisms for isothermal pyrolysis. • Estimating kinetic parameters via modelling. • Modelling reaction mechanisms and scheme for thermal plasma pyrolysis.	• There is a need of designing a suitable pyrolysis reactor which can give gaseous products for a variety of feed mixtures under different operating conditions. • Modelling of plasma pyrolysis maybe improved via computational fluid dynamics.
Prakash and Karunanithi [39,40]	2008, 2009	• Use of Koufopanos kinetic mechanism for determining the distribution of primary and secondary products under various operating conditions. • Comparison among various kinetic models for single-particle pyrolysis.	• A generalized model needs to be developed, taking into account particles of different shapes under different operating conditions.
Papari and Hawboldt [35]	2015	• Review on various pyrolysis reactors. • Comparison among published biomass pyrolysis reaction models.	• Spectrum for the feedstock properties and operating conditions should be broadened.

		• Application of chemical percolation devolatilization model for maximizing bio-oil or biochar yield.	
Wang et al.[41]	2017	• Review on new experimental techniques used for biomass pyrolysis • Macroscopic kinetic models analysis • Understanding the molecular simulations for biomass model compounds	• Quantitative and qualitative technologies are required to unravel the complexity of biomass pyrolysis and to characterize pyrolysis products.

Table 2.2. An overview of kinetic data for different pyrolysis models [25–27,35,42–47]

Model	Reaction mechanism	Feed	Analysis technique	Activation energy, (kJ/mol)	Frequency factor (s^{-1})
One-step kinetic model [35,43]	$\text{Woody Biomass} \xrightarrow{k} \text{Volatile gases + Char}$	Cellulose	TGA-MS	$E = 221$	$A = 1.47\times10^{7}$
Three parallel reactions model [44,45]	$\text{Biomass(xCellulose + yHemicellulose + zLignin)} \longrightarrow \text{Volatiles + Char}$	Beechwood, Sawdust, Rice husk	TGA, DTG	$E_1 = 184\text{-}192$ $E_2 = 129\text{-}133$ $E_3 = 64\text{-}87$	$A_1 = 1.14\times10^{6}$ $A_2 = 2.69\times10^{4}$ $A_3 = 2.22\times10^{1}$
Six independent first order reactions [46]	$S_{v1} \xrightarrow{k_1} G\uparrow$ $S_{v2} \xrightarrow{k_2} G\uparrow$ $S_{v3} \xrightarrow{k_3} G\uparrow$ $S_{v4} \xrightarrow{k_4} G\uparrow$ $S_{v5} \xrightarrow{k_5} G\uparrow$ $S_{v6} \xrightarrow{k_6} G\uparrow$	Pinewood	Steel reactor	$E_1 = 83$ $E_2 = 146$ $E_3 = 77$ $E_4 = 60$ $E_5 = 139$ $E_6 = 130$	$A_1 = 0.70\times10^{5}$ $A_2 = 0.20\times10^{10}$ $A_3 = 0.43\times10^{4}$ $A_4 = 0.29\times10^{2}$ $A_5 = 0.51\times10^{7}$ $A_6 = 0.32\times10^{6}$
Competitive reactions model [42]	$\text{Solid} \xrightarrow{k_1} \text{Gas}$ $\text{Solid} \xrightarrow{k_2} \text{Tar}$ $\text{Solid} \xrightarrow{k_3} \text{Char}$	Cellulose, Wood	Pyrex reactor	$E_1 = 140$ $E_2 = 133$ $E_3 = 121$	$A_1 = 1.3\times10^{8}$ $A_2 = 2.0\times10^{8}$ $A_3 = 1.08\times10^{7}$

Mechanism with secondary interactions between charcoal and volatiles [18,19]	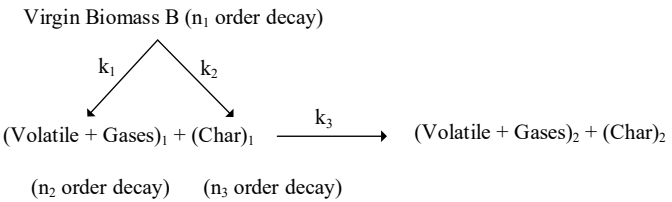	Wood sawdust	Isothermal-mass change determination	*G_1=17254.4 *G_2=10224.4 *L_1=-9061227 *L_2=-6123081 E_3=81	$A_1 = 9.973\times10^{-5}$ $A_2 = 1.068\times10^{-3}$ $A_3 = 5.7\times10^{5}$
	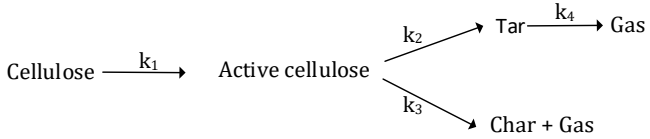	Cellulose	Pyrolysis reactor	E_1=58 E_2=47 E_3=36	$A_1 = 1.7\times10^{21}$ $A_2 = 1.9\times10^{16}$ $A_3 = 7.9\times10^{11}$
Detailed lumped kinetic model [27]	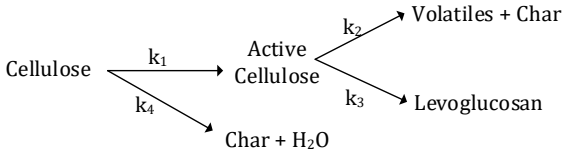	Cellulose	FTIR, TG-MS	E_1=192.5 E_2=125.5 E_3=133.9 E_4=41.8	$A_1 = 8.0\times10^{13}$ $A_2 = 1.0\times10^{9}$ $A_3 = 8.0\times10^{7}$ A_4 = 4**T
Distributed activation energy model [47]	$f(E) = \frac{1}{\sigma\sqrt{2\pi}} exp\left(-\frac{1}{2}\left(\frac{E-E_M}{\sigma}\right)^2\right)$	Wood	TGA	E=102.7±6.06 σ=1.92±0.42	A=5.98×10^6±0.18

* Fitting parameters for modified Arrhenius equation $\boldsymbol{K_1 = A_1 exp\left[\left(G_1/T\right) + \left(G_1/T^2\right)\right]}$, f (E) is the Gaussian distribution of activation energies

**T represents the temperature.

One-step global kinetic models are the simplest models available which represent the conversion of biomass to the volatiles and char as a first order single-step reaction. Since pyrolysis products only consist of char and volatiles [48], most of the researchers have used the global reaction model coupled with appropriate heat transfer and volume reaction models [39,49]. Kinetic parameters of these models can be estimated either experimentally or using different models such as Kissenger Model, Kissenger-Akahira Sunose (KAS) and Flynn-Wall-Ozawa (FWO) [35] models.

However, global kinetic models have certain limitations as they do not include elaborate reaction mechanism and only consider the primary reactions. Hence, other kinetic models were later formulated to include the secondary reactions [50]. The formation of gases from tar decomposition and the conversion of tar to char by polymerization were included in the kinetic model as secondary reactions [51]. Shafizadeh and Bradbury model [11] included both primary and secondary decomposition reactions. In this model, cellulose was first converted to active cellulose, which is further decomposed to other secondary products. This model gave good predictions for the product yield, but the determination of activation energy was difficult for this model as the composition of the active material was unknown. This model has been used extensively by researchers in its original form as well as extended forms [4,12,52].

A detailed lumped kinetic model for biomass pyrolysis was proposed by Cuoci et al. [53]. This mechanism included 15 reactions with 30 lumped species. Ranzi et al. [27] extended this mechanistic model to describe the biomass pyrolysis, devolatilization and gas phase reaction of the released gas species from the three reference components of biomass. Generalized form of this model for cellulose is presented in Table 2 along with the feed and kinetic parameters, while the detailed mechanism proposed for hemicellulose and lignin can be found in the literature [27]. The recent development in this regard is given by Corbetta et al. [29]. The previous multi-step model [27] has been revised with new experimental data and modelling of secondary gas phase reactions has also been included. These reactions have been discussed by Couce et al. [54].

Recently, distributed activation energy model has also been employed to better understand the complexity of biomass pyrolysis, as it takes into consideration the

decomposition of species over a large number of independent parallel reactions with different activation energies, represented by a continuous distribution function usually Gaussian distribution [55]. In some cases, when there exist auto-accelerated reactions during cellulose pyrolysis such as random nucleation or nuclei growth, first order reaction kinetics are not enough to model the process [56]. Hence, nucleation growth model using either Avrami-Erofeev or Prout-Tompkins equation is used. This model was first formulated for the decomposition kinetics of potassium permanganate, and later used for other solid materials like cellulose, paper, algal kerogens, etc [57–59]. Weight loss data obtained from thermogravimetric analysis of cellulose fits best to the Avrami-Erofeev equation in the form of equation 2.1, with α representing degree of degradation against time, t [62,63].

$$\mathbf{kt} = [-\boldsymbol{ln}(\mathbf{1}-\boldsymbol{\alpha})]^{\mathbf{1}/\boldsymbol{n}} \quad , \boldsymbol{where}\ \boldsymbol{n} = \mathbf{2} \tag{2.1}$$

Reynolds and Burnham [62] compared the different types of kinetic models with the experimental data for cellulose and paper. Kinetic parameters were determined using different methods including discrete distribution, the modified Friedman, modified Coats-Redfern, three-parameter nucleation and nth-order methods. The pyrolysis profiles for different cellulose materials and the regression analysis indicated that the three-parameter kinetic model shows good fitting data as compared to other methods [59,62]. These kind of models have not been addressed much for biomass and need more attention. Kinetic models have been implemented to the whole biomass [29] as well as the biomass constituents individually [63–65]. However, cellulose being the most abundant component of the biomass has gained the maximum attention [56,66–68]. Xiong et al. [69] assessed different kinetic model schemes for biomass pyrolysis using computational fluid dynamics (CFD) simulations. Three reaction schemes were compared: Scheme I: single-component single-step, Scheme II: single-component two-step and Scheme III: multi-component multi-step. The modelling results were then compared with the experimental data.

Kinetic models have made enormous contribution to biomass pyrolysis modelling. However, there are certain limitations in their applications. Thermogravimetric analysis has been widely used to determine the reaction kinetics at low heating rates, but the kinetics under slow pyrolysis conditions may not be applicable to pyrolysis at higher heating rates. Biomass pyrolysis performed at high heating rates may give

appropriate reaction kinetics but come with a challenge of limitations in heat transfer. Also except detailed kinetic schemes, all the other models give lumped product compositions (tar, char and gases) which are not sufficient to explain the complex heterogeneous reactions taking place during biomass pyrolysis and formation of hundreds of species. Therefore, other types of models (i.e., network models) have been employed to address the issues related to kinetic models.

2.2.2. Network Models

Pyrolysis is also sometimes referred as devolatilization, which is a term often only reserved for removing volatiles from coal before its conversion to liquids or gas. It involves reactions including molecular level deployerization and repolymerization [17,70], mechanisms [71,72] of which can be divided into 4 stages as shown in Figure 2.1. These 4 steps are the basics for network models.

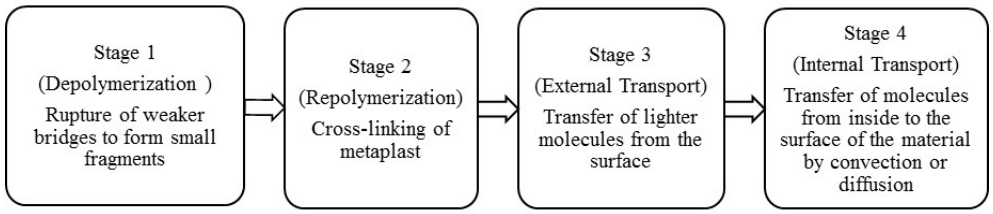

Figure 2.1. Devolatilization mechanism for network models [71,72].

Network models were first proposed for coal devolatilization and later modified for biomass pyrolysis. Reviews on network models of coal devolatilization are available in literature [72–74]. Network models consider the detailed structural changes of material during pyrolysis, thus they are also known as structural models. The typical network models for biomass are Bio-FG-DVC (Functional Group Depolymerization Vaporization Crosslinking) model [75], Bio-FLASHCHAIN model [76] and Bio-CPD (Chemical Percolation Devolatilization) model [77].

FG-DVC is the model consisting of two sub-routines, one is FG (Functional Group or species evolution model) and the other is DVC (Depolymerization, Volatilization, and Cross-linking or tar formation model) [78,79]. It comprises of six important concepts: functional groups, macromolecular network, network coordination number, bridge breaking, cross-linking and mass transport of tar. The whole concept can be defined as the formation of light gases as a result of decomposition of functional groups and at the same time depolymerization of macromolecular network due to breakage of

bridges and formation of some new fragments which are transported to form tar. The composition of volatile species can be analysed using functional group (FG) model, while DVC determines the amount and molecular weight distribution of tar and char formed [80,81]. Solomon and co-workers [78,82–84] have made significant contributions to the development of FG-DVC model for coal.

FLASHCHAIN model includes a four step reaction mechanism which depicts the chain structure and its analogy with flash distillation. Niksa [85–88] proposed the FLASCHAIN model for the rapid coal pyrolysis. The same model was modified for biomass pyrolysis, named Bio-FLASHCHAIN [89]. Three concepts were used to formulate this model from previous research, i.e., DISCHAIN, DISARAY and FLASHTWO theory. DISCHAIN theory includes the straight chain configuration model to determine the qualitative impact of the macromolecular configuration [90,91]. This is explained by two different phenomena: depolymerization and cross-linking. Depolymerization indicates the evolution of tar from the main reactant chains to small fragments. The monomers may reattach to the long fragments forming tar precursors by cross-linking to char. DISARAY theory is same as that of DISCHAIN theory. The only difference is, instead of straight chains it is implemented to the two dimensional structures, i.e., bethe lattice [92]. FLASHTWO theory depicts the pressure effects which have not been included in the previous models.

CPD model considers the biomass as a macromolecular structure of aromatic clusters connected through chemical bridges. When biomass is heated some bridges break to form light gases and tar, while others remain intact and form char. Percolation theory gives the mathematical expressions based on lattice statistics for the modelling of devolatilization processes therefore it is termed as chemical percolation devolatilization model. The model was developed to calculate the tar, char and gas yield on the basis of structural properties. Residence time, temperature, pressure and heating rate are the key parameters for predicting product yield. The coal pyrolysis has been well studied in the past using CPD model. Fletcher and co-workers [93–97] proposed a chemical model for coal pyrolysis using Percolation Lattice statistics instead of Monte Carlo techniques (proposed by Solomon et al. [83]). They extended their research for black liquor and biomass as well [98,99]. Sheng and Azevedo [77] proposed the CPD model for the main components of biomass. Lewis et al. [100,101]

assumed that biomass pyrolysis takes place as a weighted average of its main components, i.e., cellulose, hemicellulose and lignin. CPD model was applied to all the three components individually and then calculated the weighted average yield from all the three components to determine the yield of whole biomass.

2.2.2.1 Defining the Networks for Biomass

Biomass pyrolysis modelling started with the characterization of the macromolecular structure of biomass, which was based on the three basic constituents of biomass, i.e., cellulose, hemicellulose and lignin. The structural configurations of these components are shown in Figure 2.2.

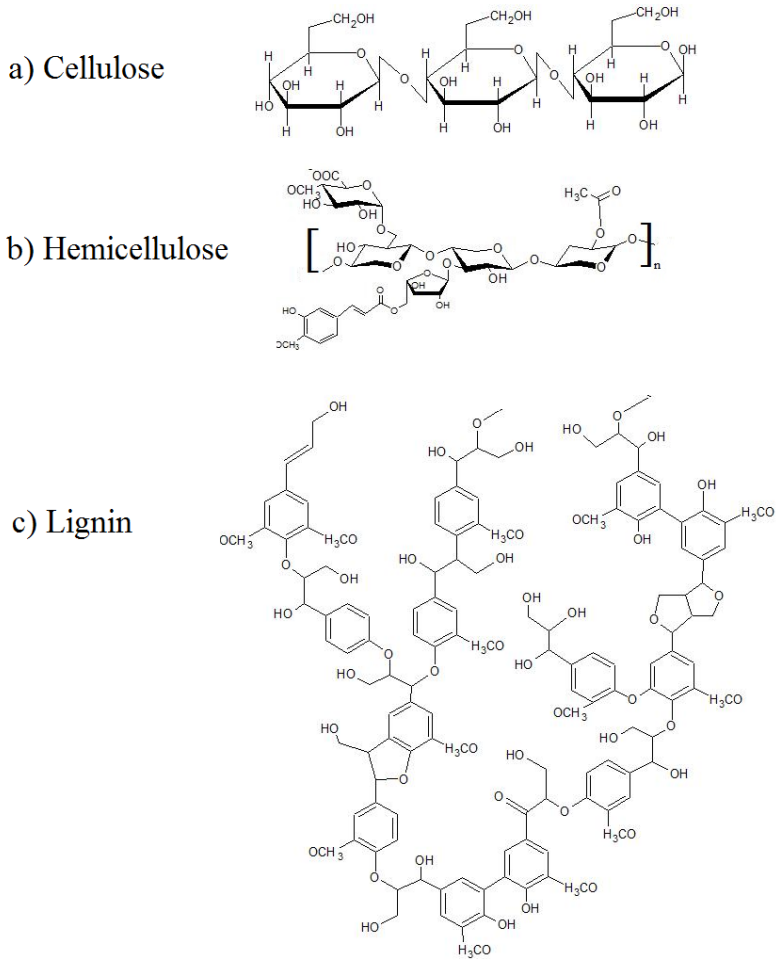

Figure 2.2. Structure of major biomass components: (a) cellulose; (b) hemicellulose; (c) lignin [102].

For network models the structures are defined based on statistical techniques either Monte Carlo or Percolation lattice theory. Serio et al. [103] used Monte Carlo calculations for FG-DVC model, which has been implemented particularly for lignin

pyrolysis, since the structure of lignin is considered to be analogous to coal. A typical macromolecular network for lignin consists of a chain of 'l' monomers having a molecular weight distribution and these clusters of monomers are connected through crosslinks as shown in Figure 2.3 [103]. However, for percolation theory bethe lattice is used which allows the number of free monomers to be expressed as a function of coordination number and the probability of bonds being unbroken. Percolation statistics are preferred over the Monte Carlo for biomass components because of the use of bethe lattice, better understanding of the network behaviour and being less computationally demanding [93]. Statistics of two and three dimensional arrays are quite complex therefore pseudo-lattices (bethe lattice) were developed to provide the analytical solutions. Coordination number defines the number of possible bridges per cluster and plays an important role for the characterization of lattices. In FG-DVC, for a bethe lattice co-ordination number is 2 (σ+1), one of which represents the evolution of volatile species and the other is for the tar formation at the same time [104,105].

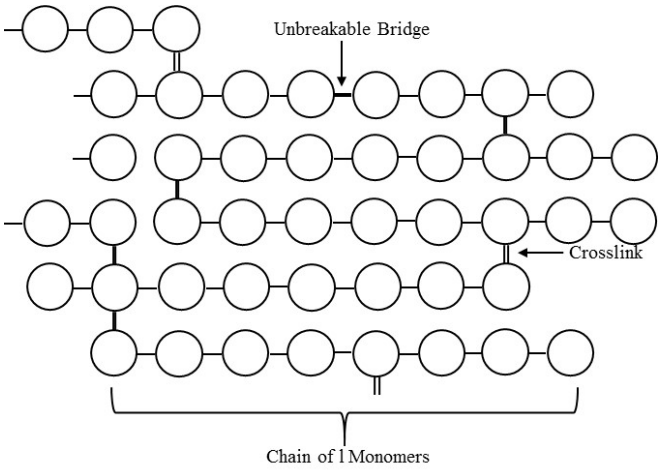

Figure 2.3. Macromolecular network used in Monte Carlo simulation [103].

In Bio-FLASHCHAIN biomass is represented as a chain copolymer of cellulose and lignin like component with the coordination number, σ+1=2.0. The size of these chain fragments may vary from one monomer to an infinite chain [89].

The macromolecular network for CPD model is often the bethe lattice with different coordination number. An example of trigonal bethe lattice with the coordination number, σ+1=3 is shown in Figure 2.4.

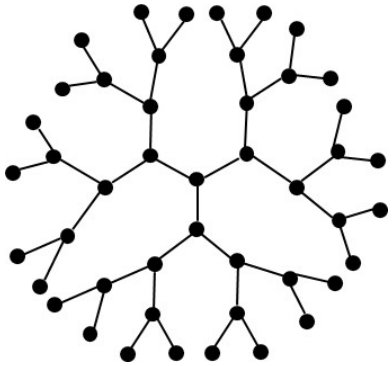

Figure 2.4. Trigonal bethe lattice structure with coordination number 3 [93].

2.2.2.2 Biomass Geometric Characterization

Structural parameters are one of the input parameters for all three network models. These are feed specific parameters and totally depend on the type of biomass. These parameters include coordination number, initial bridge population, molecular weight of monomers, initial fraction of labile bridges, charred bridges, molecular weight of one cluster, side chains molecular weight, etc. The parameters including the aromatic nuclei are specified only for coal and do not play any role for biomass feedstock [106]. The structural parameters are determined using different experimental techniques such as py-FIMS, ^{13}CNMR, SEM/X-ray, etc.

For implementation of FG-DVC to lignin, the important parameters are molecular weight of monomers (M_{avg}), molecular weight between cross-links (M_c), standard deviation (σ), oligomers length (Q) and crosslinks per gram (m_o). The method of their determination has been discussed by Serio et al. [103] in detail. There are three basic structural parameters which are important for Bio-FLASHCHAIN i.e. bridges, dehydrated bridges and char links. For CPD model, these parameters are based on the three components of biomass i.e. cellulose, hemicellulose and lignin. Since the structure of cellulose and hemicellulose is considered to be analogous so the base unit for both of them is the fixed anomeric carbon and attached hydrogen. Lignin bears the structure same as that of low rank coals, so the base unit for lignin is coniferyl, coumaryl and sinapyl alcohol which are shown in Figure 2.5 [100].

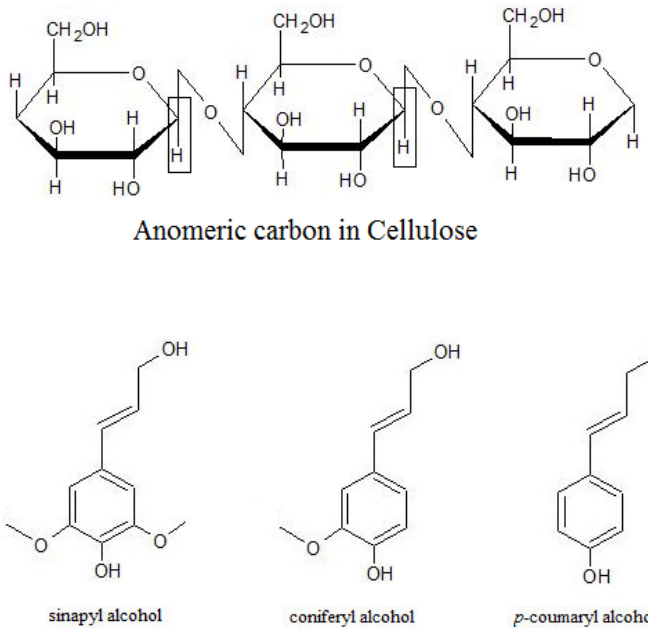

Figure 2.5. Base units for cellulose and lignin used in CPD model.

Structural parameters have different values for different materials, some of which are shown in the Table 2.3. Initially, there were no advanced characterization tools (CNMR data) for biomass, and these parameters were essentially assumed based upon the structure of biomass components [77]. In recent studies, these parameters have been determined using the CNMR techniques [107].

Table 2.3. Structural parameters for different biomass [98,99,108].

Structural Parameters	**Materials**				
	Sawdust			Black Liquor	Green River Oil-Shale
	Cellulose	Hemi-cellulose	Hardwood Lignin		
Molecular weight of cluster, MW_{cl}	81.0	77.5	208	297	776
Molecular weight of side chains, M_{δ}	22.7	21.5	39	37	131
Initial fraction of intact bridges, p_0	1.0	1.0	0.71	0.71	0.5
Coordination number, $\sigma+1$	3.0	3.0	3.5	3.6	5.0
Initial fraction of char bridges, c_0	0.0	0.0	0.0	0.0	0.0

2.2.2.3 Reaction Mechanism

The basic mechanism of bridge breaking and forming for lignin according to FG-DVC is shown in Figure 2.6, where the monomers are shown as circles and the number in them is the molecular weight of the monomer and attached bridges. Pyridine was used to extract the two types of lignin (ALC and SEYP) which are 100% soluble in pyridine [103]. Grey circles represent the fraction of char molecules insoluble in pyridine while pyridine soluble fraction is represented as white circles, and tar formed is represented as rectangles. Single lines represent the breakable bridges while the double lines are for stable or unbreakable bridges. The original biomass represented as a polymer would have both breakable and unbreakable bridges. During the tar formation, some breakable bridges may donate hydrogen so that there are only unbreakable bridges in the final char.

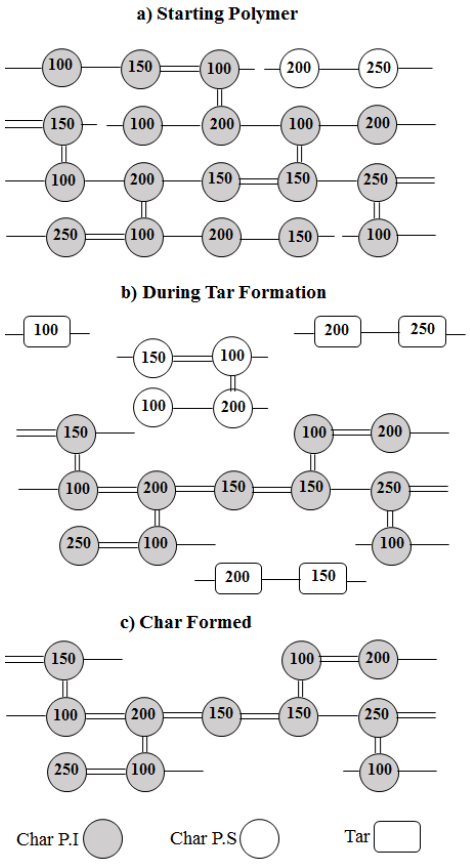

Figure 2.6. Representation of lignin molecule in DVC simulation [103].

In the bio-FLASHCHAIN mechanism, there are four basic steps: bridge scission, spontaneous condensation, bimolecular recombination and peripheral group elimination as shown in Figure 2.7. The fraction of fragments which are reacting to

form intermediates, metaplast, tar and non-condensable gases are determined using statistical probability relationships [89].

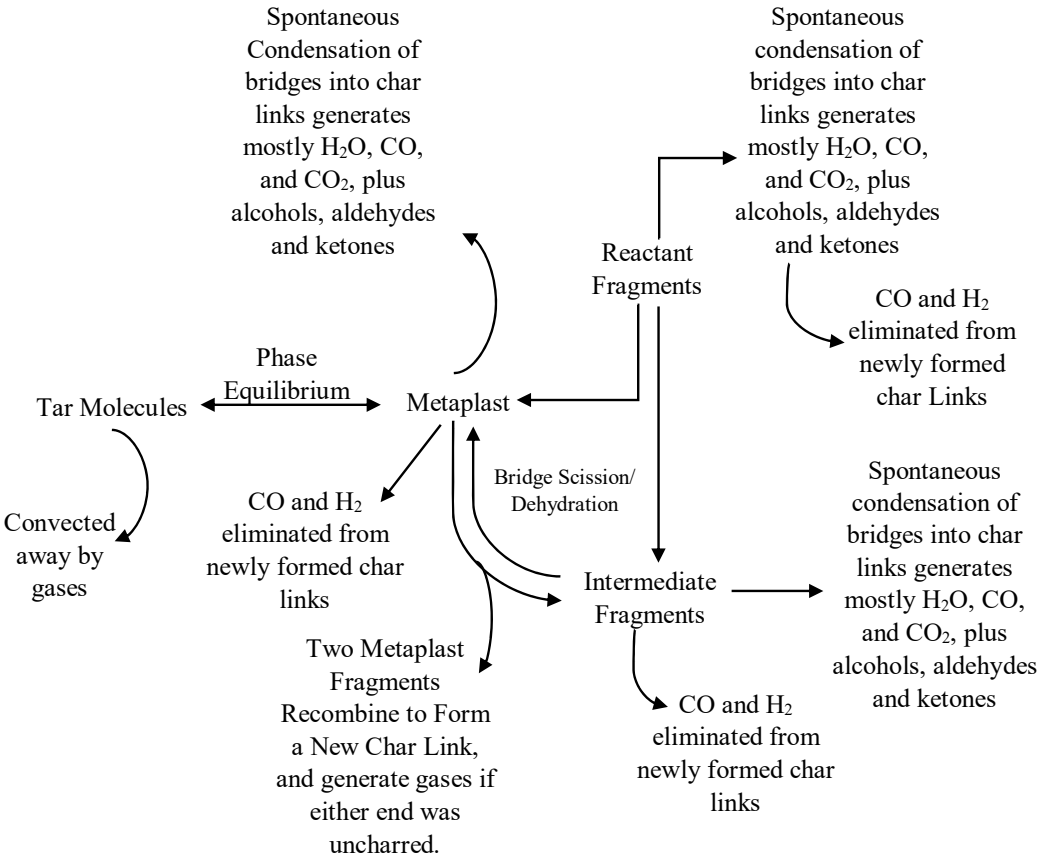

Figure 2.7. Reaction mechanism in Bio-FLASHCHAIN model **[89]**.

In the CPD model, the bridges which break easily are named as labile bridges and the ones which remain stable are the charred bridges. The three basic reactions which take place during the thermal decomposition of biomass are: bridge breaking, gas and char formation and cross-linking. The reaction scheme for this bridge breaking and formation of intermediates and the stable products is shown in Figure 2.8 [94].

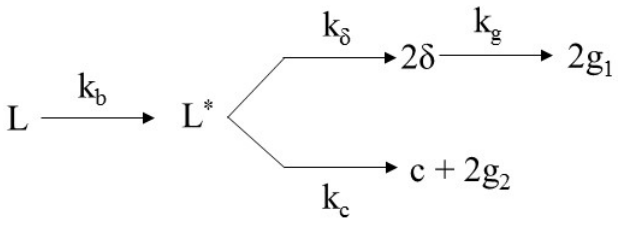

Figure 2.8. CPD reaction scheme [93].

The labile bridges (L) break to form an intermediate (L*) which is quite unstable and is converted to the stable products by the two parallel reactions. The side chains (δ) represent the finite fragments which dictate the mechanism of tar release. The fragments are divided into three categories: (i) the low molecular weight species which condense at room temperature are classified as tar, (ii) species of intermediate molecular weight which do not get vaporized and are termed as metaplast, and (iii) the species which do not condense follow reaction path to form light gases (g_1). In addition, stable char forms with the release of light gas (g_2) in parallel to the tar formation [93].

2.2.2.4 Reaction Kinetics for the Basic Processes

The basic processes which control the network devolatilization are bridge breaking, cross-linking and the distribution of the products. Rate of each process depends on the reaction kinetics. Hence, kinetic parameters are second input parameters for these three models other than the structural parameters. For FG-DVC and CPD the reaction kinetics are determined using TGA-FTIR analysis. The reaction rates for these models are based upon distributed activation energies. These processes with their kinetics and the most commonly used rate equations are elaborated in below sections.

2.2.2.5 Bridge Breaking

In FG-DVC model for lignin, the rate of bridge breaking reaction is: $k_b = 1.0 \times 10^{14}\exp(-24500 \pm 2000/RT)\sec^{-1}$ [104]. In this model, when a labile bridge breaks it requires a hydrogen to form a stable free radical. For coal it was assumed that all labile bridges contain donatable hydrogens and some of them break while the others donate hydrogen for stabilization. However, this concept is not true for biomass. As discussed by Serio et al. [103] for lignin pyrolysis, donating hydrogen does not produce unbreakable bonds. For Bio-FLASHCHAIN the bridge breaking step goes into two pathways: scission and spontaneous condensation, while the assigned values for these have not been reported in literature [89]. For CPD model the rate of bridge breaking reaction needs to be calculated for all the three species individually. The rate specified for pure cellulose on the basis of kinetic parameters is as : $k_b = 1.0 \times 10^{18}\exp(-59000 \pm 1800/RT)\sec^{-1}$ [77]. Similarly, rate of bridge breaking reaction has also been determined for hemicellulose and lignin [77].

2.2.2.6 Cross-linking

For FG-DVC of coal, the cross-linking reaction is due to the gas evolution particularly CO_2 and CH_4, while in case of biomass particularly lignin, it is assumed that the evolution of high temperature water and methanol is responsible for cross-linking reactions [103]. In Bio-FLASHCHAIN, the small fragments produced as a result of scission recombine to form char links which is analogous to cross-linking. Initially, it was assumed that there was no cross-linking process in CPD, later it was considered that cross-linking arise due to the reattachment of the metaplast to the infinite char matrix, and was included with the rate of reaction as: $k_{cross} = 3.0 \times 10^{15} \exp(-65000/RT) sec^{-1}$ [77]. Kinetics of the cross linking reaction of biomass have been kept same as that of coal and same value has been used for different materials.

2.2.2.7 Product Distribution

In the FG-DVC model, the FG part becomes dominant for the gaseous product evolution. TGA-FTIR has been used for different materials to determine the reaction kinetics and evolution of the gaseous species [103,105,109]. In the initial versions of FG models, around 19 functional groups were defined to determine the product yield. However, in the recent studies for biomass, only CO, CO_2, H_2O, CH_4 and tar were specified. Tar evolution for the coal FG-DVC was considered as a part of the DVC but for biomass it is modelled along with gaseous species.

In bio-FLASHCHAIN, the intermediate fragments produced as a result of bridge scission and spontaneous condensation tend to produce the metaplast. Tar is formed from this metaplast by flash distillation [89]. Flash distillation with chemical kinetics and fragmentation statistics determines the fragments going into the vapour phase or in the condensed phase and then overall product yield.

For CPD model the reaction kinetics for the gas evolution are determined on the same basis as that for FG. The overall reaction rate for gas evolution is taken as the weighted average of its functional groups [104]. The rate of gas formation for pure cellulose using functional group is: $k_g = 8.23 \times 10^{12} \exp(-43180 \pm 3000/RT) sec^{-1}$ [77]. As char formation and the gas evolution goes parallel to each other in the CPD mechanism, so a constant kinetic ratio, ρ for these reactions is defined ($\rho = \frac{k_\delta}{k_c}$). The

value of ρ differs for different materials. Tar release is included in the CPD model using Raoult's law and flash distillation. When the CPD model was first implemented to the biomass, only primary pyrolysis reactions were considered [77] but later, the secondary tar cracking model was also included in the CPD to predict the more accurate yield of tar and gas.

2.2.2.8 Overall Pyrolysis Product Yield

Chen et al. [104,105] studied six different biomass materials and analysed them using TG-FTIR. The yield of volatile species and the functional groups amounts were determined at three different heating rates, 3, 30 and 100 K/min using experimental data. FG-DVC model was also used to predict the volatiles at higher heating rate of 1000 K/sec but the results obtained were not satisfactory. Figure 2.9 shows rate of formation of different gaseous species and tar predicted from FG-DVC at 30 K/min.

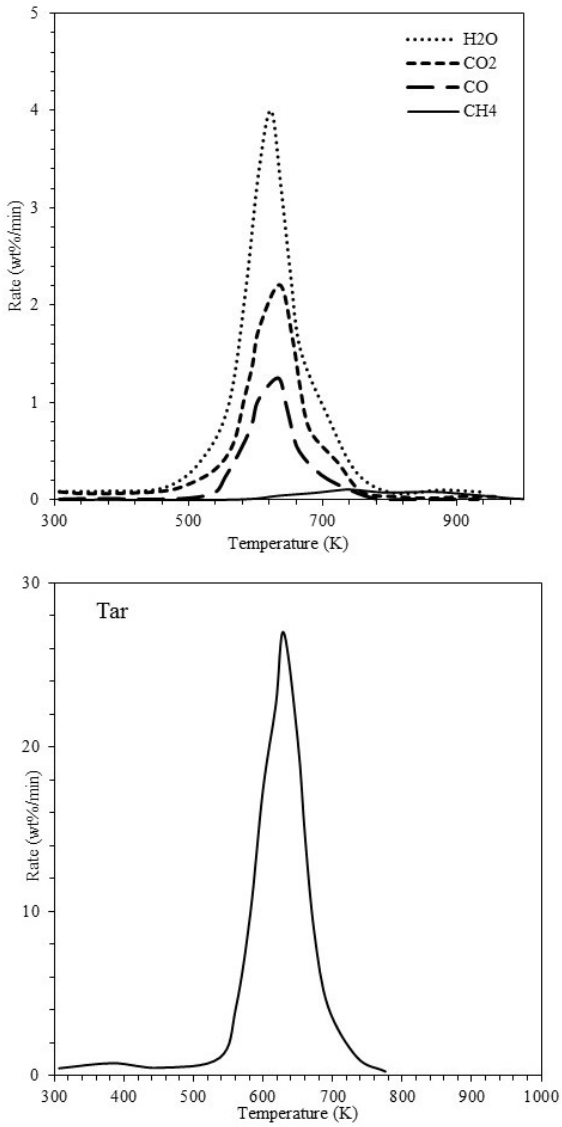

Figure 2.9. Product yield predicted from FG-DVC model for populus deltoids at 30 K/min [105].

Pyrolysis product yield for different biomasses such as bagasse, beech, silver birch and eucalyptus were predicted using bio-FLASHCHAIN model assuming two components pure cellulose and lignin. Experimental data was used to predict the input parameters and then those parameters were used in the model to predict the char, tar and gas yield and the effect of ash catalysis was studied comparing the pyrolysis yield from original, potassium exchanged and acid washed beech [110]. The results obtained from bagasse devolatilization at 1000 K/sec and 0.1MPa pressure for total weight loss and the tar yield are shown in Figure 2.10 [89]. The graph represents that predicted total weight loss and the tar yield from bio-FC model is comparable to experimental data points above 800K.

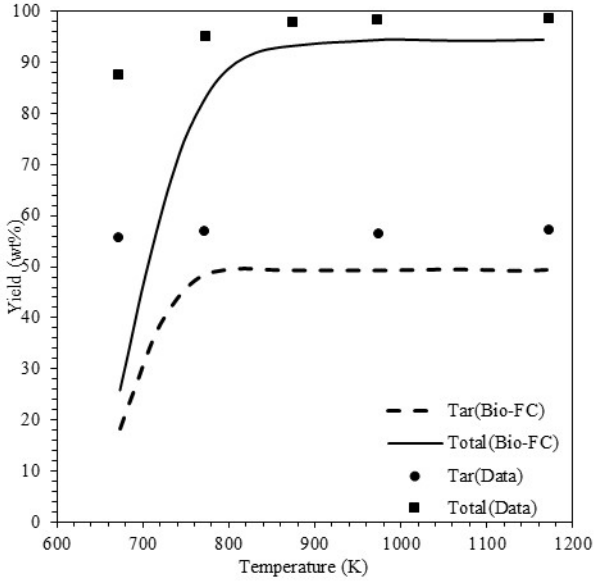

Figure 2.10. Product distributions for bagasse devolatilization[89]**.**

For the CPD model, the overall yield of tar, char and gas for the biomass pyrolysis was determined using the weighted average of the yield of cellulose, hemicellulose and lignin. Lewis and Fletcher [100] predicted the sawdust pyrolysis yield using CPD model and compared the results with the experimental data obtained from flat-flame burner experiments. Bio-CPD model has been implemented to various biomass under different conditions [111–113]. For all the cases, CPD model has been used for the individual components such as cellulose, hemicellulose, lignin, kraft lignin, black liquor, xylan and glucomannan, Predicted pyrolysis yields of tar, char and gas has been compared to different experimental data available in the literature there exists a good agreement between experimental and modelling results. Comparison of the pyrolysis product yield for xylan and glucomannan obtained from experimental data [114] and the CPD model predictions is shown in Figure 2.11 [108]. Other than biomass, the CPD model calculations have been extended to the green river oil shales as well [107,115,116].

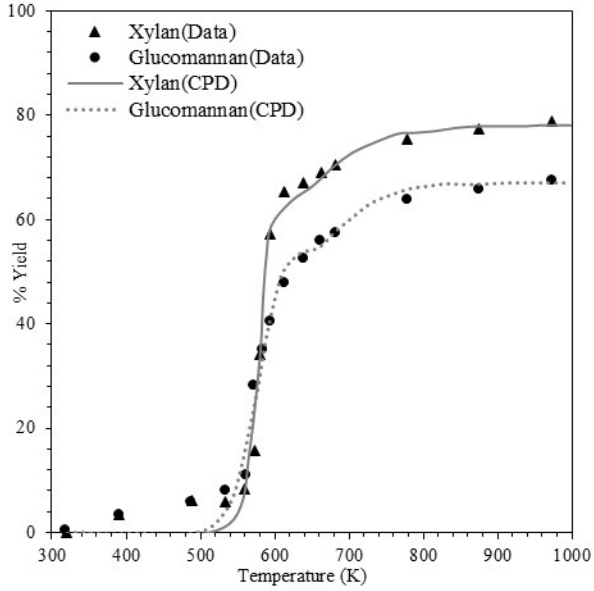

Figure 2.11. Comparison of pyrolysis product yield from CPD model and experimental data [108].

2.2.2.9 Summary of Network Models

Network models discussed in the previous sections, are essentially feed specific, and have been used only for few materials because of the structural limitations. However, they have still produced accurate results for biomass pyrolysis. The objective of this study is to highlight all the features of network models including the areas which need attention for the future applications. A summary of these models is given in Table 2.4.

Table 2.4. Key points summarizing network models.

Model	Heating Rate	Influence of mineral matter	Interaction among particles	Future Work
FG-DVC [104]	Low heating rates	Implemented to the whole biomass and its components individually, however did not consider the effect of minerals.	Has been implemented to the whole biomass and for pure lignin. Interaction among constituents has been neglected.	Secondary reactions, effect of minerals, interaction among species and heating rate effects should be included.
Bio-FLASHCHAIN [89]	High heating rates	Implemented to two components of biomass and also included the impact of ash catalysis.	Only cellulose and lignin are considered as feed, neglecting hemicellulose and other constituents.	Understanding the chemistry of bond breaking and cross-linking reactions.
CPD [100]	For both low and higher heating rates	Cellulose, hemicellulose and lignin have been modelled neglecting mineral matter and ash contents	Product yield is predicted individually for model compounds.	Using the model for the whole biomass including inorganic species and interaction among biomass constituents.

2.2.3 Mechanistic Models

The mechanistic models reveal the mechanism of biomass pyrolysis, including all the reaction paths and the components formed. These are mechanism based models which are not lumped and explain elementary reactions. Efforts have been made by different researchers to reveal the biomass pyrolysis mechanism, however not many literature data are available for such models [117,118].

The mechanistic modelling at a molecular level is normally based on two different methods, the force field method based on molecular mechanics and the first-principles or ab initio method based on electronic structure calculation. To model and simulate the physical and chemical interactions, different methods used are shown in Figure 2.12. Molecular dynamics and Monte-Carlo techniques are used for the simulation of mechanistic models at molecular levels.

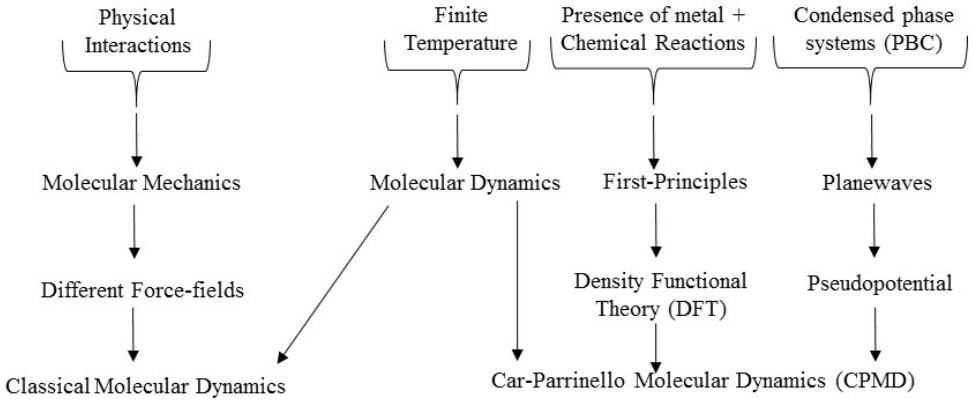

Figure 2.12. Molecular level methods to model physical and chemical interactions [119].

For the complex structures of biomass, first-principle methods or the density functional theory (DFT) are more suitable. Density functional theory was used to study the dehydration of cellulose using cellotriose as model compound [120], which showed that the location of hydroxyl groups plays a significant role in cellulose dehydration. The work was further extended to understand the mechanism of pyran ring breaking [121]. Since a typical biomass contains thousands of species, it is practically not possible to include all of them in the modelling. Hence, the researchers have focused on understanding the pyrolysis mechanism of cellulose and other major constituents of biomass rather than considering the whole biomass. An overview of the work published on mechanistic modelling using different simulation methods such as MD, DFT and CPMD is shown in Table 2.5.

Table 2.5. An overview of the existing literature on mechanistic models [64,118,122–129].

Reference	Year of publication	Simulation method	Material	Outcomes
Agarwal et al. [122]	2012	CPMD	Cellulose	• Revealing the mechanism of conversion of cellulose to pre-levoglucosan and other products.
Mettler et al. [123]	2012	ab-initio CPMD	Cellulose Carbohydrates	• α–cyclodextrin was used for simulations instead of cellulose. • Revealing the condensed-phase pyrolysis chemistry. • Furans and glycoaldehyde formation takes place as a result of glycosidic bond cleavage. • Glycosidic bond cleavage and intra-pyran chemistry are interconnected.
Huang et al. [124]	2012	DFT	Xylopyranose	• Xylopyranose is first converted to an isomer through ring opening reaction which is converted to final products through five reaction pathways, among them two has been considered more feasible.
Seshadri and Westmoreland [125]	2012	Quantum chemistry statistical mechanics	β-D-glucose	• Activation energies for all the reactions: dehydration, ring-opening and formation, ring contraction, retro-aldol condensation and keto-anol tautomerization) were determined.
Huang et al. [126]	2013	DFT	Lignin	• Syngas and acetylene are formed as a result of decomposition of poly p ethylene which is the model compound of lignin in the presence of hydrogen plasma.
Bland and Silva [64]	2013	ab-initio quantum chemical DFT	Chroman	• An intermediate is produced as a result of retro-Diels-Alder mechanism which is further decomposed to benzene and fulvene.
Mayes et al. [118]	2014	Quantum mechanics	Cellulose	• Simulations for glycosidic bond cleavage and levoglucosan formation. • Rate coefficient for glycosidic cleavage is four times more than ionic breakage.

		DFT		
Lu et al. [128]	2014	DFT	β-D-glucopyranose Cellobiose	• The most favourable pathways for the conversion of β-D-glucopyranose and cellobiose to levoglucosenone are 1.2 dehydration, hydrogen transfer and enol-keto tautomerization which is the rate determining step.
Lu et al. [129]	2018	DFT	Cellulose	• Chain ends produced during the decomposition are levoglucosan-terminated end, non-reducing, reducing and a-cyclic glucose end which are significant for final product distribution.

One such mechanistic model was proposed by Vinu and Broadbelt [130]. The formation of levoglucosan from glucose-based carbohydrates involved two steps: mid-chain glycosidic bond cleavage and unzipping of levoglucosan from the chain ends. A series of four reaction schemes was proposed: (i) conversion of cellulose to levoglucosan and glucose, (ii) formation of glycoaldehyde and low molecular weight products (LMWPs), (iii) conversion of glucose to a range of intermediates and (iv) conversion of low molecular weight products (LMWPs) to glyoxal, acetaldehyde, 3-oxobutanal, formaldehyde and char. First reaction scheme for conversion of cellulose to levoglucosan and glucose is shown in Figure 13. The model tracked a large number of cellulosic species and 40 LMWPs in 99 individual reactions along with the time evolution. The results of the models were compared with the experimental results of Patwardhan et al. [131]. The predicted product yields matched well with the experimental data. This mechanistic model proposed for neat glucose was also used to study the effect of inorganics on the glucose pyrolysis [132] which is discussed in detail in Section 3 of this chapter.

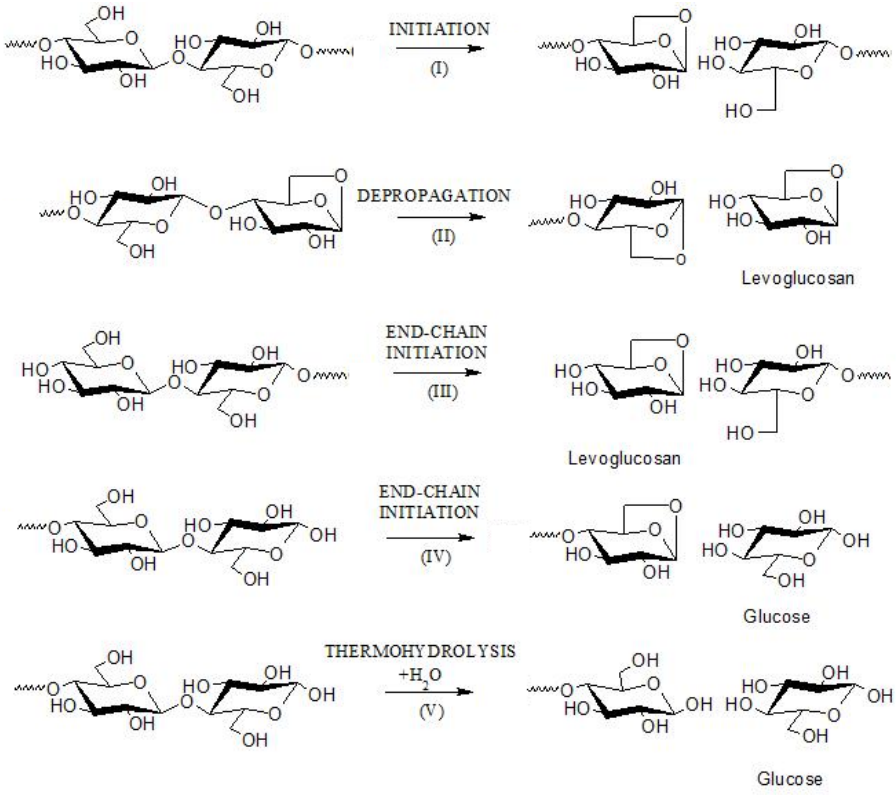

Figure 2.13. Mechanism of formation of levoglucosan and glucose through glycosidic bond cleavage and hydrolysis [130].

Zhou et al. [133] also developed a mechanistic model using the elementary steps and respective kinetic parameters to predict 103 species in 342 reactions involving reactions of cellulosic chains and LMWPs. The fast pyrolysis mechanism of glucose, cellobiose, maltohexaose, cellulose and levoglucosan is revealed using the mechanistic modelling approach based on DFT. The model developed in this study was then validated using experimental data for fast pyrolysis at different temperatures and for different carbohydrates [127]. The model was able to predict the major products (levoglucosan, 5-HMF, glycoaldehyde, char, CO, CO_2, H_2O and methyl glyoxal), minor products (levoglucosenone, furfural, acetone, dihydroxyacetone, propenal) and some other pyrolysis products which were not quantified in experimental results. In addition to the product yield, the reaction time was also predicted using the mechanistic model. For example, it takes 1.75 s for the formation of levoglucosan during cellulose pyrolysis [127]. Broadbelt and colleagues [28,117,118] have carried out extensive work on the mechanistic modelling for fast pyrolysis of glucose-based carbohydrates.

To better understand the use of glucose as a starting point for the molecular modelling of cellulose pyrolysis, Mettler et al. [134] studied the chain length effect and came up with less complex a more-established chemistry of glucose pyrolysis. Levoglucosan which is one of the major products of cellulose pyrolysis, is deoxygenated when present in the molten biomass, this was validated through experiments conducted for levoglucosan only and co-pyrolysis of levoglucosan and fructose [135].

Researchers have worked extensively on understanding the mechanism for the pyrolysis of model compounds of biomass, but this approach still needs development to completely reveal the complex mechanism of whole biomass pyrolysis.

2.3. Challenges of Pyrolysis Models

2.3.1. Influence of Inorganic Species

There are significant experimental data in the literature on the influence of inorganic species on biomass pyrolysis. The effect of inorganics on cellulose pyrolysis at low temperatures has been observed by the change in the primary products yield [136]. The influence of inorganic salts on the primary and secondary pyrolysis reactions has been studied by Patwardhan et al. [137]. The results show that the primary pyrolysis

reactions are catalysed in the presence of inorganic species and produce more low-molecular-weight species like formic acid and glycoaldehayde while the yield of levoglucosan is reduced. Comparison of the experimental data of almond shells pyrolysis in a fluidized bed reactor with the two kinetic models, i.e. single step and three parallel reactions showed good agreement [138]. However, pyrolysis of $CoCl_2$ impregnated almond shells could not be simplified using these simple schemes [138]. The effect of mineral matter and other organic salts has been discussed by several other researchers [6,9,68,139–144]. The effect of metals and metallic salts has also been studied [68,145–147]. Biomass ash sometimes acts as catalyst in the pyrolysis [148]. Alkali and alkaline earth metallic species (K, Na, Mg, Ca, etc.) have profound effect on pyrolysis product yield for different biomass species. These species can be removed by water and acid washing treatment and as a result the yield of water in bio-oil decreases and the yield of sugars and lignin-derived oligomers increases [149]. A brief analysis of the experimental literature discussed above shows that some inorganic species reduce the bio-oil yield and promote the char formation however, certain inorganic species increase the formation of light oxygenates and gases. For example, calcium oxide have a negligible effect on levoglucosan product yield while other inorganics such as ash have a profound effect on it [137].

Biomass pyrolysis models have been developed to incorporate the effect of inherent inorganic species as catalysts. Previously, impact of inorganic species on the product yield was studied through lumped kinetics only but recently emphasis has been given to detailed kinetic and mechanistic modelling to better understand the mechanism of biomass pyrolysis in the presence of inorganics. Trendewicz et al. [150] evaluated the effect of potassium on the cellulose pyrolysis kinetics and proposed a new mechanism. The Ranzi scheme [151] has been modified to include the catalytic effects of potassium on cellulose pyrolysis product yield. The results showed that presence of 1 % potassium in cellulose decreased the oil yield from 87.9 % to 46.2 %, but the char yield increased from 3.7 % to 14.0 % and similarly the gas yield increased from 8.4 % to 39.8 %. The same reaction scheme including the effect of potassium has been used in CFD simulations by Eri et al. [152] to observe the change in pyrolysis product yield using multi-phase reactor model. Hence, the ignorance of this effect and considering only three components for modelling of biomass pyrolysis may lead to poor reactor design for industrial applications.

For all the three network models, the reaction mechanism including the catalysis by inorganic species has been neglected. However, Niksa [153] has highlighted the impact of inorganics on biomass pyrolysis. He did not explain the explicit catalytic reaction mechanism rather included the impact of inorganics in his model bio-FLASHCHAIN using a calibration procedure and predicted the pyrolysis product yield in the presence of potassium.

Mechanistic models of the pyrolysis of biomass model compounds in the presence of inorganics have also been developed by many researchers at the molecular level. Mayes et al. [154] studied the effect of sodium and calcium ions on glucose present in plant biomass using quantum mechanics and molecular dynamics. It has been observed that sodium ion has very small effect on β-glucose, but it significantly affects the α-glucose anomeric and ring oxygens. Elementary steps involved in the conversion of α-glucose and β-glucose in the presence of NaCl have been discussed in detail by Mayes et al. [132] using quantum mechanics. The rate coefficients were increased in the presence of metal ions (Na^+) for most of the reactions, which was in agreement with the experimental data. The kinetic data determined for a range of isomerization and dehydration reactions can be used to predict the kinetics of other elementary steps. Effect of the presence of inorganic species on fast pyrolysis of glucose-based carbohydrates was studied by conducting research on the salt-added materials. It was hypothesized that inorganic species present in the feed do not affect the basic pyrolysis mechanism however it alters the kinetics and was validated later [155,156]. Figure 14 presents one of the schemes for the effect of NaCl on glucose pyrolysis [155].

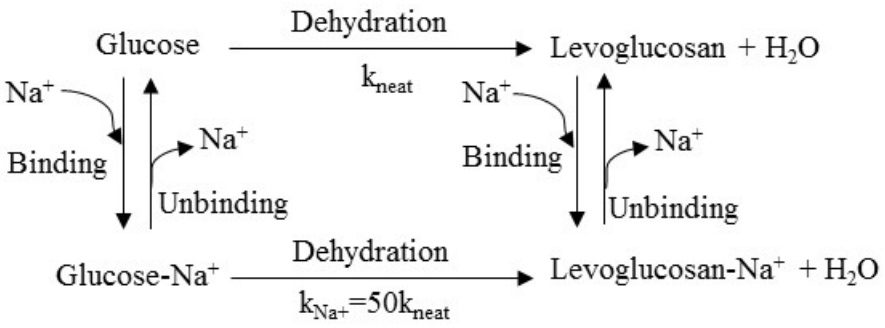

Figure 2.14. Modelling approach to study the effect of Na^+ on the product distribution of glucose pyrolysis [155].

This mechanistic model was developed and validated by Zhou et al. [155,156] to incorporate the catalytic effects of NaCl on the fast pyrolysis of glucose-based carbohydrates including glucose, cellobiose, maltohexose, cellulose and levoglucosan. Mechanistic model for pure cellulose deals with 103 number of species involving 342 reactions, while the number of species increases to 222 with 768 reactions in the presence of NaCl. All the reactions with the species formed for all the carbohydrates have been discussed in the work of Zhou et al. [155,156]. Inorganic species not only effect the product yield but also alter the amount of species formed due to catalytic effects, which will ultimately affect the product composition. Hence, to obtain a required composition of bio-oil, char and gases from biomass pyrolysis it is mandatory to control the amount of inorganics in the feedstock.

Classical kinetic models were unable to unravel the chemistry of catalytic effect of inorganic species. However, detailed kinetic model solved this problem to some extent. Among all the models, mechanistic models are able to provide the detailed chemistry of the reactions affected by the presence of inorganic species. From the experimental data discussed above as well as few studies on kinetic, network and mechanistic models including the inorganic species, it is confirmed that these species catalyse the pyrolysis reactions and affect the rate of reaction and the product yield. Detailed kinetic schemes and mechanistic models have contributed significantly to unravel the pyrolysis of model compounds in the presence of inorganic species. However, there are still significant challenges for researchers to model the influence of inorganic species during biomass pyrolysis.

2.3.2. Interactions Among the Biomass Constituents

The reaction rate of biomass pyrolysis is usually taken as the sum of the evolution rate of its basic constituents. However, studies on the interactions among the components of biomass dictate that this additive scheme may not always give the accurate product yield. Among the three components of biomass, the strongest interaction exists between cellulose and lignin, and interaction between hemicellulose and cellulose is quite weak, as verified experimentally [157]. The interactions among the different phases of pyrolysis products have also been studied for cellulose and lignin [158]. Solid/liquid phase interactions increased the amount of tar and reduced the amount of

char and water. However, the vapour phase interactions promoted the gas formation from volatiles produced from cellulose and reduced the char formation from the volatiles of lignin [158]. In many literature studies, biomass pyrolysis has been simulated using a synthetic mixture of its constituents. However, such a simulated mixture behaves differently from original whole biomass [159–161]. The experimental data reported dictates that interactions among the biomass constituents not only affect the temperature range for product distribution but also alter the product compositions. Hence, considering the interactions among the biomass constituents is another challenge for modelling the biomass pyrolysis. This requires in-depth understandings of the interactions among the pyrolysis of various biomass constituents.

2.3.3. Multi-scale Modelling for Biomass Pyrolysis

Three different scales are important for modelling of biomass pyrolysis: molecular, particle and reactor scale. Molecular level studies involve the primary and secondary pyrolysis reactions elaborating the mechanism of biomass pyrolysis [118]. A detailed review presented by Mushrif et al. [119] highlighted the difficulties involved in the molecular modelling of biomass pyrolysis. To investigate biomass pyrolysis using first-principles, it is necessary to have clear understanding of reaction mechanism and the interactions among biomass constituents at the molecular level. Most of the data available on molecular modelling of biomass pyrolysis considers the reactions in the gas phase only, without considering the condensed phase [119]. The key aspects of recent review articles on multi-phase, multi-scale modelling are discussed in Table 6. Particle scale models include the intra-particle transport phenomena [14,32,33]. Rate of heat and mass transfer inside the particle due to temperature gradients are addressed and particle shrinkage models are included to describe the change in particle size [162–164]. A single or multi-step kinetic model is directly implemented to the reactor scale neglecting the transport phenomena inside the biomass particles [165,166]. In this case, reactor hydrodynamics become dominant for the reacting particles and product yield is determined [167]. The reviews summarized in Table 6 provide detailed analysis of biomass pyrolysis modelling at different scales.

Table 2.6. Review articles on multiscale modelling of biomass pyrolysis [30,31,119].

Reference	Aspects covered	Year of publication	Duration of literature covered
Sharma et al. [30]	• Modelling of biomass pyrolysis focusing kinetic, particle and reactor level models • Effect of process parameters on pyrolysis • Catalytic pyrolysis	2015	1975-2012
Mushrif et al. [119]	• Multiscale molecular methods like CPMD and metadynamics • Using multiscale molecular modelling to elaborate the reaction chemistry of pyrolysis • Conversion of biomass in the presence of solvents as catalyst	2015	1996-2014
Anca-Couce [31]	• Recent developments in the fundamental reaction mechanisms for lignocellulosic biomass pyrolysis • Biomass pyrolysis as a sum of its constituents with its kinetic schemes and product compositions • Molecular, particle and reaction level modelling of pyrolysis	2016	1965-2015

2.3.4. Applications of Kinetic and Network Models to CFD Simulations

CFD simulation techniques are frequently used to understand biomass thermochemical conversion processes. This section discusses few studies in which the reactor has been modelled using kinetic mechanism. An overview on the application of CFD modelling of different biomass conversion processes has been presented by Wang and Yan. [168]. The authors discussed, the models for combustion, gasification, pyrolysis and carbonation including the fluid flow, reaction kinetics, heat and mass transport phenomena. In last few years, researchers have worked on coupling the particle scale model to reactor model using CFD simulations for biomass pyrolysis, which has focused on kinetic models however, there is limited literature available on using

network models in CFD. Multi-phase CFD modelling including both Eulerian-Eulerian and Eulerian-Lagrangian approaches has been used in this regard. Most of the studies available in the literature used lumped kinetic approach and predicted the pyrolysis product yield of tar, char and gases [166,169–173], while recently distributed kinetic model has been included in CFD to predict the detailed product yield [152]. The FG-DVC model was used for the determination of input parameters and then those were implemented into a CFD model for combustion of biomass in a drop-tube furnace [174]. A pyrolysis sub-model has also been proposed including the DAEM calculations for the implementation of FG-DVC model to biomass [175] and has been validated from experimental data available in literature. Hence, CFD simulations including detailed kinetic models and network models help in getting a detailed product distribution from the biomass pyrolysis using a pyrolysis reactor.

Biomass pyrolysis can be modelled at three different scales individually. However, when biomass pyrolysis is simulated at a reactor scale, global kinetic models are usually coupled with the reactor model to describe the biomass pyrolysis at a reactor scale as discussed above. There is a need to develop a robust model which includes the molecular level kinetics coupled with the reactor hydrodynamics to describe the biomass pyrolysis in depth and make it applicable for the industrial applications.

2.4. Comparison of Pyrolysis Reaction Models

Due to the complicated chemical structure of biomass, and underlying chemical reactions, the process of biomass pyrolysis is challenging to model. Several models have been proposed in the literature, and they all have certain assumptions with respect to operating conditions and the feedstock characteristics. Silva [176] compared different kinetic models: one single- order reaction model from Nunn [177], a model with parallel-competitive reactions from Thurner and Mann [50], another model from Wagennar [178] with parallel-competitive reaction scheme, a model of Gordon and Knight [177] and the model of Hong [179] including the secondary reaction and one network model CPD for biomass pyrolysis. The model results were compared with the experimental data obtained from Hong's drop-tube reactor [179]. There were discrepancies observed in the results for all the models. However, results from Nunn et al. [180] produced closest match with the experimental data. Further analysis were performed and results were compared with the Tognoti's reactor data [181]. The

models which showed agreement with the experimental data were further used for CFD based numerical simulations by the researcher.

2.4.1. Advantages and Disadvantages of Pyrolysis Models

Three types of models discussed in this review have their advantages and disadvantages. Kinetic models are most commonly used to determine the overall kinetics of pyrolysis reactions. Numerous experimental techniques have been developed for the determination of kinetic parameters. However, classical kinetic models cannot explain which components contribute to the formation of char, tar and volatiles. To understand the structural changes at macromolecular level, network models were developed. These models have the advantage of exploring bridge breaking and bonds forming mechanisms, but are unable to get generalized form, as the structural parameters and the functional groups are highly dependent on feedstock characterization. Determination of these parameters makes the network models complex and difficult to use. Moreover, each biomass component is considered individually with no interactions with the other components. Ashes and extractives have never been considered. Since biomass breaks down into hundreds of components during pyrolysis, it is more important to understand the formation mechanism of pyrolysis intermediates and final product. This leads to the development of mechanistic models, which have presented acceptable results for cellulose but other components have not been considered so far. Some key points on the advantages and disadvantages of these models are summarized in Table 2.7.

Table 2.7. Advantages and disadvantages of different biomass pyrolysis models.

Kinetic Models	
Advantages	**Disadvantages**
• Process is represented by an overall reaction rate to determine the lumped products yields. • Extensive structural data is not required. • Kinetic parameters required can be obtained experimentally, using simple analysis techniques, like TGA, FTIR, MS etc.	• Only classical lumped kinetic models cannot simulate the structural changes during biomass pyrolysis. • Less effective in predicting yields of tar, char and volatile gases. • More than one data points are determined at different operating conditions and then average values of the parameters are used. • Only applicable within a specific range of data.
Network Models	
Advantages	**Disadvantages**
• Suitable for predicting the yield of tar, char and light gases during pyrolysis. • Consider basic phenomena during pyrolysis, i.e., cross-linking, fragmentation. • Can determine structural changes, i.e. the labile bridges breaking, charred bridges stabilizing and the new bridges forming.	• Input data for these models is highly specific for different feedstocks. • Become complex if transport mechanisms are included. • Considers cellulose, hemicellulose and lignin only. The effect of inorganic species on pyrolysis is not addressed.
Mechanistic Models	
Advantages	**Disadvantages**
• Suitable to determine the mechanism of pyrolysis only on molecular level. • Suitable to study the effect of inorganic species on pyrolysis.	• Mainly focus on the gas phase reactions. • Mainly focus on the model compound. • Interactions between components are not considered. • The exact mechanism of cellulose pyrolysis is still unknown due to complex reactions.

2.4.2. Quantitative Comparison of Pyrolysis Models

Biomass pyrolysis is a complex network of reactions. Chemical structural changes that occur in biomass particle during pyrolysis depend on biomass composition, temperature, and heating rate. Qualitative and quantitative prediction of pyrolysis products depend on both, kinetic model and kinetic parameters. Comparisons can be made between the prediction of char, gas, and tar yield and profiles obtained from different pyrolysis models. This section compares the results of different models with the experimental data. Experimental data from TG-MS for rice straw (32 % cellulose, 35.7 % hemicellulose, 22.3 % lignin and 10.0% extractives) obtained from Worasuwannarak et al. [159] has been used as reference. Three models including multiple reaction schemes have been chosen to make a comparison between the experimental and modelling results: Shafizadeh and Bradbury model (SB-model) [11], Chemical Percolation Devolatilization model (CPD-model) [100] and the detailed kinetic scheme proposed by Ranzi et al. [182]. The total volatiles fraction obtained from three models and their comparison with the experimental data is presented in Figure 2.15.

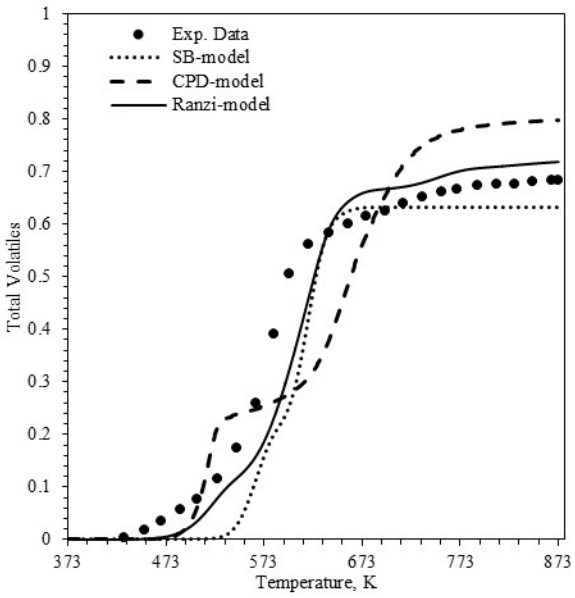

Figure 2.15. Comparison of total volatiles fraction obtained from experiments and biomass pyrolysis models.

As per Figure 2.15, trends of the total volatile formation from Shafizadeh and Bradbury model and Ranzi model are quite similar to the experimental data and fraction lies in the range of 0.6-0.7. However, CPD model over predicts the total

volatile yield and also does not predict the qualitative profile. The variation in the results can be attributed to use of CPD kinetic parameters obtained under experimental conditions of high heating rate (~1000 K/s) [100] which are not suitable to predict pyrolysis behaviour at a low heating rate. The yield of char, tar, and gases (CO, CO_2, H_2O, CH_4, and H_2) obtained using different models are also compared with experimental data in Figure 2.16.

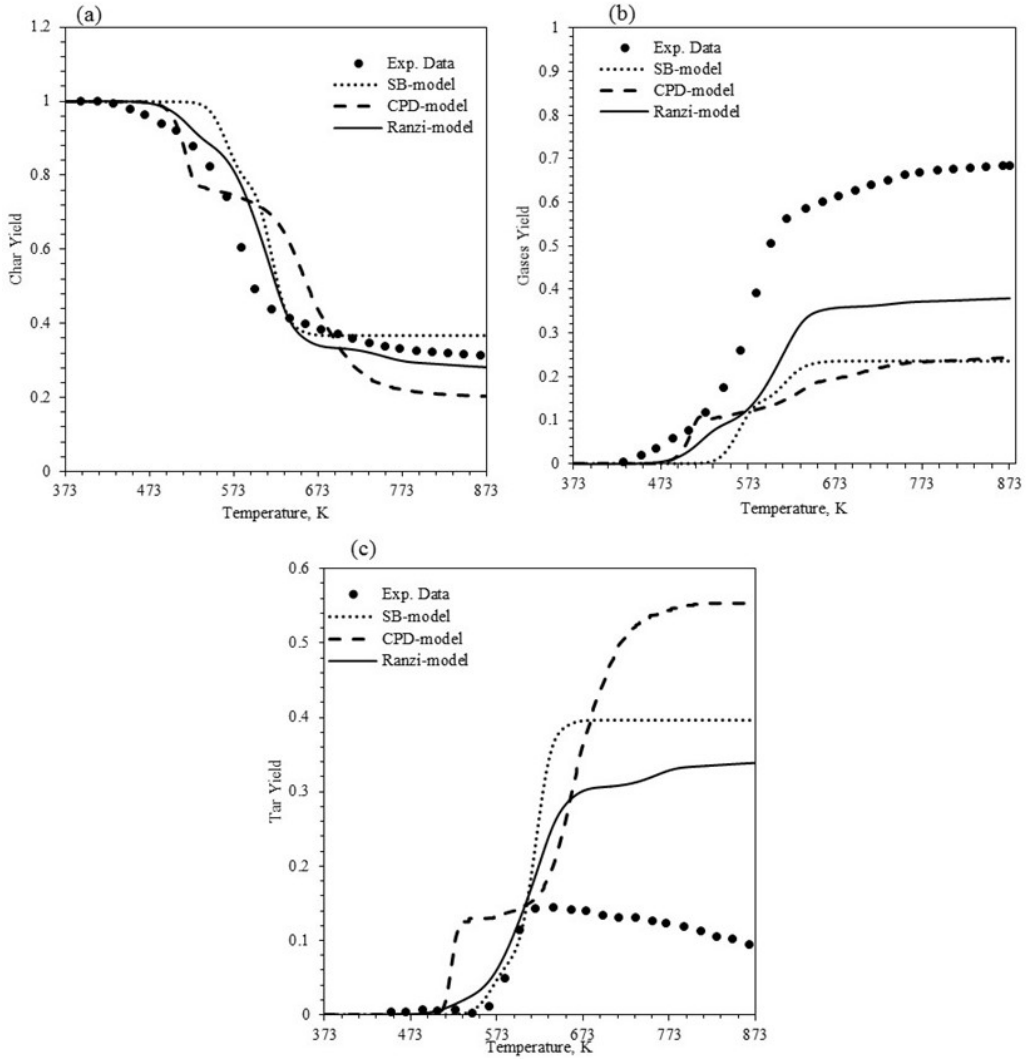

Figure 2.16. Char, gases and tar yield from different biomass pyrolysis models.

According to Figure 2.16, the high gas yield as compared to tar yield in the experimental data can either be attributed to tar cracking and/or co-production of gas with char. Char formation occurs through radical recombination or condensation reactions, and the latter produces gas or low molecular weight compounds [159]. Also, char yield predicted from all three models is comparable to the experimental data.

Although the experimental data in Figures 2.16 (b) and 2.16 (c) do not suffer from internal temperature gradients due to small particle size and very low heating rate, but vapour-solid interactions promote secondary reactions that favours gas formation. While all three models predicted less yield of gases as compared to tar because primary tar conversion reaction has not been considered in the SB model, it has been taken into consideration in CPD model however it exists as tar evaporation inside the particle.

To summarize, all models can fairly predict the total volatile evolution profile of biomass pyrolysis. However, depending on the model assumptions for reaction mechanism, prediction of lumped product yield may not be accurate. Kinetic parameters for simple lumped models would not be valid over a wide operating range because the reaction mechanism does not consider vital intermediates or conversion reactions. Although CPD and Ranzi model consider the details of pyrolysis reactions, the kinetic parameters require re-evaluation and also may not be valid over a wide range of heating rates. Careful experimentation based on the findings of Paulsen et.al. [183] and Krumm et.al. [184] should be devised to determine kinetic parameters for different models under a wide range of operating conditions.

2.5. Cellulose Pyrolysis Modelling

Cellulose is considered to be the most abundantly available biopolymer on earth [185–187]. Among all the biomass constituents, cellulose has majorly been used for energy production and other research developments. Since the time it is discovered, it has been used in its raw form as well as in the derived forms for different applications as it is considered harmless for the environment [188].The models discussed in the previous sections are applicable to cellulose pyrolysis. In a review presented by Serbanescu [67] different modelling schemes for cellulose pyrolysis have been discussed. The Broido-Shafizadeh model [52] is one of the most commonly used model for cellulose pyrolysis. Detailed kinetic models and mechanistic models have made great contribution in understanding the decomposition mechanism of cellulose pyrolysis. Mayes and Broadbelt [118] have used DFT to understand the cellulose pyrolysis mechanism and presented mechanism of glycosidic cleavage and levoglucosan formation. In many research studies, cellulose has been used as a base model for wood and biomass pyrolysis. In spite of extensive research on cellulose pyrolysis and its modelling, the decomposition process is not completely understood.

Cellulose has been selected for this study because of its easy and excessive availability and also because it is more practical to develop a model for cellulose and then extend it to other constituents of biomass.

2.6. Summary

Biomass pyrolysis process has been modelled using different modelling schemes. Kinetic models have been developed for decades and are helpful in specifying the reaction kinetics for biomass and cellulose pyrolysis. The kinetic models are important for reactor design as they are easy to use with other heat and mass transport models. Network models explain the pyrolysis mechanism well and the basis for their development is the structural deformation which may change with the feedstock type. However, the yield of char, tar and the volatiles can be determined accurately using network models. Among different network models available, the CPD model has received more attention, because the input parameters required are less than those for other models. In addition, CPD models are easy to use with other simulation software such as CFD simulations. CFD simulations can be a useful tool in integrating the pyrolysis reaction kinetics with the reactor hydrodynamics, to make them industrially applicable. Mechanistic models can explain the mechanism of pyrolysis well, but those models include the molecular dynamics, CPMD and Monte-Carlo techniques which are complex and time consuming. Currently, mechanistic models are mostly based upon theoretical studies and are used for model compounds such as cellulose, hemicellulose and lignin, however more attention is required to develop mechanistic models for biomass. The presence of inorganic species significantly affects the reaction kinetics and pyrolysis product yields.

2.7. Research Gaps and Research Direction

From the above literature review following observations could be made:

- Biomass contains cellulose, hemicellulose, lignin and other compounds such as inorganic species, which can have a profound effect on the distribution of products in biomass pyrolysis. The effect of inorganic species should also be accounted for, to determine the kinetics of pyrolysis.

- For network models especially CPD, the model should first implemented to individual components, and then the overall yield is taken as the weighted average of all the components.
- There has been only a moderate progress on integrating the network models with CFD simulations. To understand the cellulose pyrolysis reaction mechanism, and to couple the reaction kinetics with the reactor hydrodynamics, more detailed modelling is needed.
- A number of kinetic models have been developed for cellulosic materials but there is still a lack of generalized models that include the kinetics, heat and mass transfer effects at reactor level.

Based on the above observations, the key research gaps that need to be addressed in the current study are:

- To understand the catalytic effect of inorganic species, there is a need to determine the reaction kinetics of pyrolysis process in the presence of inorganic salts.
- While using different modelling schemes for biomass pyrolysis, whole biomass should be taken consider basic constituents, ash, moisture and extractives.
- A generalized model including the kinetics, heat and mass transfer effects is required to practically implement to pyrolysis at reactor level.

2.7.1. Research Objectives and Methodology

To address the identified research gaps for pyrolysis of cellulose will be modelled with the following objectives:

1. Determining the kinetics of cellulose pyrolysis in the absence and presence of inorganic species, and predicting the product yield to study the effect of inorganic species.
2. Understanding the mixing and segregation behaviour of cellulose in a fluidized bed both qualitatively and quantitatively.
3. Combining distributed activation energy model with CFD reactor model to predict the cellulose pyrolysis product yield for a range of activation energies in a fluidized bed reactor.

These are also schematically shown in Figure 2.17. In order to achieve these objectives, a number of experimental modelling methodologies have been used, which are explained in detail as follows:

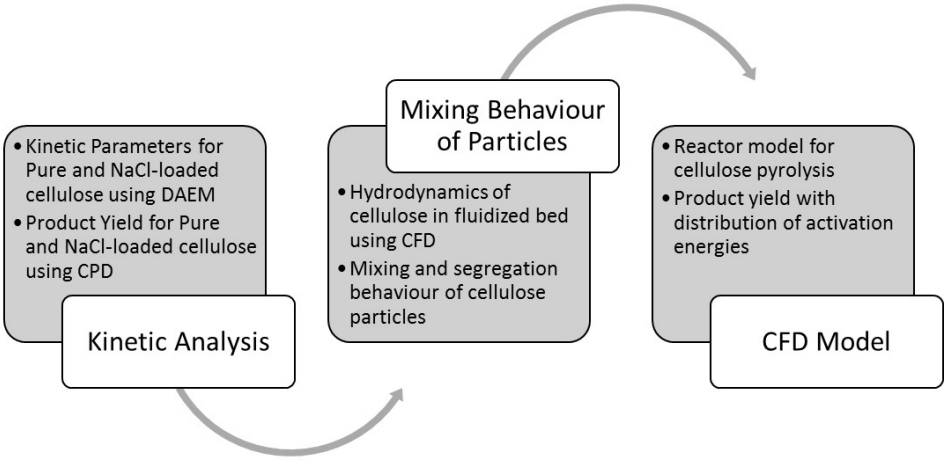

Figure 2.17. Main objectives of this research work.

Objective 1: Kinetic Analysis of Pure and NaCl-loaded cellulose

The effect of inorganic species on the kinetics of cellulosic pyrolysis is evaluated in Chapter 3. First thermogravimetric analysis were performed for pure cellulose at different heating rates and kinetic parameters were determined using 2-component distributed activation energy model. Once the model was validated for pure cellulose, it was then used to predict the kinetic parameters for NaCl-loaded cellulose. The optimized kinetic parameters were then substituted to chemical percolation devolatilization model to predict the pyrolysis product yield and the results compared to reported literature data to analyse the effect of NaCl on cellulose pyrolysis products.

Objective 2: Mixing and Segregation Behaviour of Cellulose Particles

In Chapter 4, the behaviour of cellulose particle in a bubbling fluidized bed of sand bed has been examined. A CFD model was developed, and validated using experimental data. After the model validation qualitative analysis of the mixing and segregation of cellulose particles was performed by observing the contour plots and volume fraction profiles of cellulose particles in the sand bed. Particle segregation number was used to quantify the extent of mixing and segregation. This study was extended by analysing the effect of operating parameters such as superficial gas velocity, particle size and density on mixing and segregation.

Objective 3: CFD Model for Cellulose Pyrolysis including Distribution of Activation Energies

In Chapter 5, a CFD model has been developed for cellulose pyrolysis in a fluidized bed reactor to include the heat and mass transfer effects and the reaction kinetics. The model was validated with the experimental data from a lab-scale fluidized bed reactor, and those available in the literature. Once the model was validated, it was further used to simulate the cellulose pyrolysis incorporating the effect of distribution of activation energies. Behaviour of cellulose pyrolysis was quantified by determining the lumped product yield of tar, char and gases.

The overall methodology for achieving these research objectives is illustrated in Figure 2.18. This gives a detailed overview of linkage between research objectives and the thesis structure.

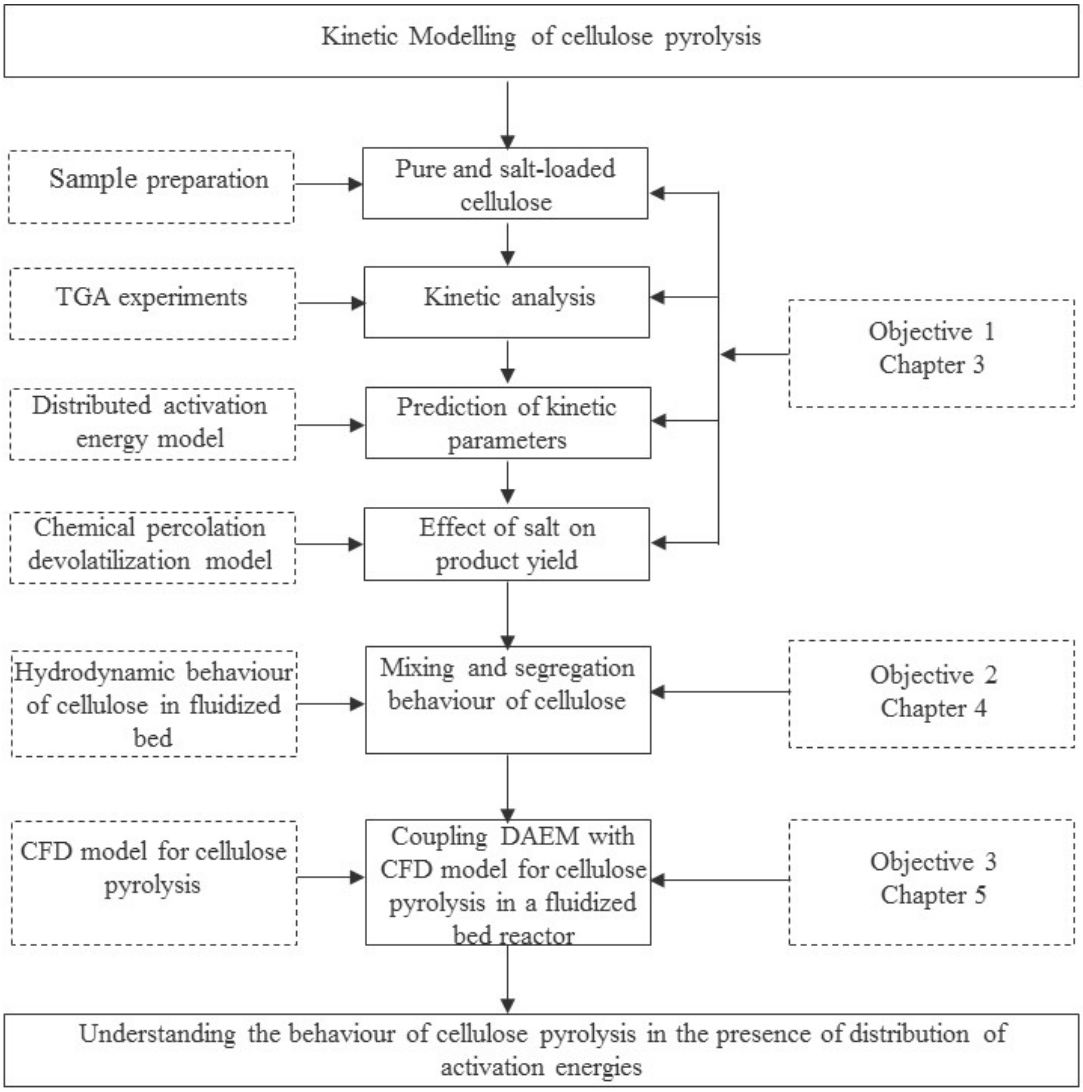

Figure 2.18. Research methodology linked with the research objectives.

CHAPTER 3 KINETIC MODELLING OF SALT-LOADED CELLULOSE PYROLYSIS

3.1. Introduction

Cellulose pyrolysis is a combination of parallel and series reactions. Despite of sufficient literature available addressing the mechanism and kinetics of cellulose pyrolysis, still there exist uncertainties for the complete understanding of the decomposition behaviour of this process [63,66,67,118]. The parameters which govern the kinetics of these reactions are activation energy and frequency factor. An overview of some of the kinetic models published for cellulose pyrolysis along with kinetic parameters has been presented by Cristina [67]. Among these models Broido-Shafizadeh [11] is the most frequently used model.

Distributed activation energy model assumes that solid decomposition is a combination of infinite parallel reactions which may be first or n^{th} order with different activation energies describing the variation in bond strengths of species, which can be determined using a probabilistic distribution function [189]. This model was proposed by Vand and was then used by Pitt [190] for coal devolatilization and later popularized by Anthony and Howard [191]. Different types of global kinetic models including first-order, nth-order, nucleation and sequential models along with several methods of energy distribution have been reviewed by Burnham and Braun [57]. There are two distinct methods of treating distributed reactivity: 1) fitting a set of parallel reactions to either a mathematical or arbitrary distribution and 2) the use of iso-conversional method which is an infinitely sequential method [192]. Friedman method is considered to be the most accurate among all the iso-conversional methods [193].

Chemical percolation devolatilization model is a network model which describes the devolatilization of biomass components on the basis of chemical structure. CPD model has been discussed in detail in Chapter 2 along with the reaction scheme and mechanism. This scheme has been selected for cellulose devolatilization in this part of the project because this is analogous to the most commonly used Broido-Shafizadeh scheme for cellulose pyrolysis. There are different versions of CPD model such as CPD-CP, CPD-heat [194] and CPD-nlg [195] CPD-heat is used in the current work which requires heating rate as input and calculates particle temperature at every step

using that heating rate. CPD model for biomass was run for its three components i.e. cellulose, hemicellulose, lignin individually and overall product yield was determined as weighted average of the yield of the components [100,196]. The model produced results comparable to experimental results, however, effect of inorganic species or ash content present in biomass on the pyrolysis product yield was not considered. Several researchers have studied the effect of presence of inorganic matter on biomass pyrolysis and have come across a general trend that it increases the char and volatiles yield at the expense of bio-oil yield [9,68,137,143,150]. Raveendran et al. [7], Varhegyi et al. [197], Mayer et al. [198] and Liu et al. [198] have studied the effect of added salts on cellulose pyrolysis as discussed in section 2.3.1 of Chapter 2. To reduce the complexity and better understand the effect of salt on pyrolysis reactions, this paper studies the kinetics of pure cellulose and NaCl-loaded cellulose. The first objective of this chapter is to propose a strategy to predict the kinetic parameters for CPD model by performing thermogravimetric analysis of the sample and using the DAEM. Secondly, using the CPD model for NaCl-loaded cellulose to predict pyrolysis product yield to highlight the significance of inorganics while implementing the CPD model to the whole biomass and setting a milestone for future research in this direction.

Flow diagram in Figure 3.1 represents the modelling and simulation strategy used in this paper.

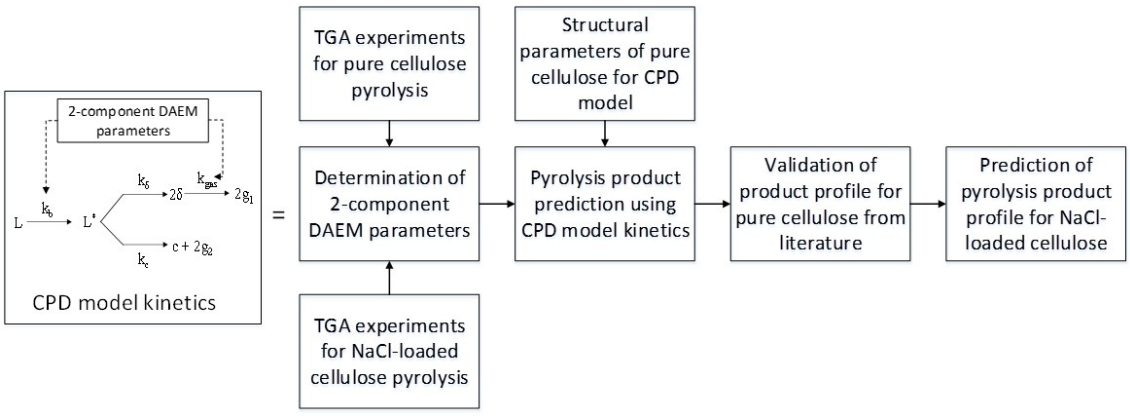

Figure 3.1. Strategy for using distributed activation energy model and CPD model to predict pyrolysis product composition for pure and NaCl-loaded cellulose.

In order to achieve these objectives, TGA experiments for pure and NaCl-loaded cellulose were carried out over a wide range of heating rate (5 to 250 K/min). The TGA data were processed and kinetic parameters were determined using a two

component distributed activation energy model (DAEM) for pure and NaCl-loaded cellulose. In the second part, the distributed activation energy and CPD models were coupled by substituting the rate constants (k_b and k_{gas}) calculated by DAEM into the CPD model. The substituted values and CPD-heat model algorithm were then used to predict the pyrolysis products of pure cellulose, and the results were compared with the literature to validate the coupled distributed activation energy model and CPD for pure cellulose. Once validated, kinetic parameters obtained for NaCl-loaded cellulose using distributed activation energy model were used to evaluate the effect of salts on pyrolysis product profile obtained using CPD-heat model.

3.2. Experiments

3.2.1. Materials

Microcrystalline cellulose (Avicel PH-101, Sigma Aldrich) was first sieved to obtain the particles in a size range of ≤ 45 μm, the results of particle size distribution obtained from Mastersizer 2000 are shown in Table 3.1.

Table 3.1. Particle size distribution for pure cellulose sample.

Sample	**Volume weighted mean, D[4,3] μm**	**D(v,0.1) μm**	**D(v,0.5) μm**	**D(v,0.9) μm**
Pure Cellulose	48.525	16.309	42.712	89.4213

The sample was then washed using deionized water at room temperature to remove any water soluble compounds which may be present in the sample and dried in the oven at 70 °C. Pure cellulose sample was also tested for ash since no ashes were found in the sample and all the calculations were made on dry, ash free bases (daf). Washed cellulose was then used for the preparation of salt-loaded cellulose. NaCl was selected for this study as inorganic specie and its effect on yield was observed. There are several methods in literature for sample preparation, while wet impregnation method was used in this study [199–201]. A specific amount of NaCl was dissolved in water to prepare salt solution, then 2.0 g of cellulose was added to the solution and stirred for 2 hours. This slurry was filtered and product was dried in the oven at 343 K. Salt concentration was varied between 0 to 2.0 wt. % and five different samples (with concentrations 0.25, 0.5, 1, 1.5 and 2 wt. %) were prepared.

3.2.2. Equipment and Experimental Procedure

Perkin Elmer thermogravimetric analyser (TGA-8000) was used for pyrolysis at a temperature ramp of 373-973 K, for different heating rates in the range of 5 to 250 K/min in the presence of argon (Ar) as an inert gas at a flow rate of 60 ml/min. The heating rates selected for experiments were : 5, 10, 20, 60, 100, 150, 200 and 250 K/min. Weight loss data was generated for lower heating rates such as 5, 20, 40 and 60 K/min as well as higher heating rates i.e. 100, 150, 200 and 250 K/min for both pure and NaCl-loaded cellulose. A weighed sample of 3.0-4.0 mg was put in the crucible and then temperature program, shown in Table 3.2, was run. Step no. 6 was used only in case of NaCl-induced cellulose to determine the organic fraction of solid residue remained after pyrolysis. The sample was cooled to room temperature before removing it from the TGA apparatus.

Table 3.2. Non-isothermal TGA program for pure and NaCl-loaded cellulose pyrolysis.

Step no.	Gas	Initial temperature (K)	Final temperature (K)	Heating rate / holding time
1	Argon (60 ml/min)	308	308	5 min
2		308	373	20 K/min
3		373	373	15 min
4		373	973	5, 20, 40, 60, 100, 150, 200 and 250 K/min
5		973	973	20 min
6	Oxygen (20 ml/min)	973	973	30 min

3.2.3. Modelling and Simulations

To estimate kinetic parameters using a distributed activation energy model there are two methods namely distribution-free method and distribution-fitting method. In this work, kinetic parameters have been determined through distribution-fitting method using first order reaction model written in Matlab because this method predicts reliable parameters using a set of heating rates. The basic steps involved for optimization of kinetic parameters are as follows:

1. Raw TGA data was used to calculate conversion (α) using Eq. 3.1.
2. TGA data smoothing using Sovitzky-Golay filter in Matlab to derive a smooth differential TGA (DTG) curve.

3. Choosing 60 equidistant points of TGA and DTG curves in the non-isothermal region of the data.
4. An initial guess for frequency factor (A) and mean activation energy (E_0) was taken from literature.
5. $f(E)$ was assumed to have a Gaussian distribution.
6. An objective function (Eq. 3.4) was constructed to simultaneously minimize the error between experimental and predicted conversion values obtained for multiple heating rates.
7. Frequency factor (A) and E_0 were optimized by minimizing the objective function using fmincon in Matlab.

$$\alpha_i = \frac{M_{dry} - M_t}{M_{dry} - M_\infty} \tag{3.1}$$

where, M_{dry} and M_∞ are the initial dry weight of biomass and final weight of residue remaining after completion of pyrolysis reaction respectively. M_t is the mass of biomass remaining in the TGA pan at time't'.

$$\mathbf{J_1} = \sqrt{\sum_{j=1}^{n}\sum_{i=1}^{m}\frac{\left(\alpha_{expt,ij} - \alpha_{pred,ij}\right)^2}{n}} \tag{3.2}$$

$$\mathbf{J_2} = \sqrt{\sum_{j=1}^{n}\sum_{i=1}^{m}\frac{\left(\left(\frac{d\alpha}{dt}\right)_{expt,ij} - \left(\frac{d\alpha}{dt}\right)_{pred,ij}\right)^2}{u_j^2 n}} \tag{3.3}$$

$$\mathbf{J_3} = \frac{J_1 + J_2}{2} \tag{3.4}$$

where, n is the number of heating rates used simultaneously to fit the kinetic parameters, m is the number of points on each evaluated curve, u is the peak maximum for each DTG curve. The use of "u' is to normalize the objective function.

Weight loss data, in the non-isothermal region, collected from TGA was used to determine the kinetic parameters at low heating rates (5, 20, 40, 60 K/min) and high heating rates (100, 150, 200, 250 K/min) using distributed activation energy model.

Optimized kinetic parameters were then substituted as input parameters (k_b and k_{gas}) to the CPD model and overall volatiles yield was compared to the experimental data to validate the model. CPD-heat model was used for this work as it required particle heating rate as an input which was suitable for TGA data. The code for this model is available online [202]. Once the CPD model was validated for pure cellulose using

the optimized parameters from distributed activation energy, same strategy was used to predict pyrolysis product profile for NaCl-loaded cellulose.

3.3. Results and Discussion

3.3.1. TGA Results for Pure Cellulose

The first part of the analysis from TGA involved the selection of sample weight. Experiments were performed with different amounts of sample and results were compared. In the first run sample weight was taken in the range of 1.2-1.5 mg, while in the second run the weight was increased to 3.5-4.0 mg and weight loss data was collected at different heating rates. Figure 3.2 compares the results for the lowest heating rate of 5 K/min, an intermediate heating rate of 100 K/min and the highest heating rate of 250 K/min, which clearly confirms that difference for conversion "α" and derivative of conversion "dα/dt" is not significant for different weighed samples. As a result, 3.5-4.0 mg sample weight was selected for further experiments in this study.

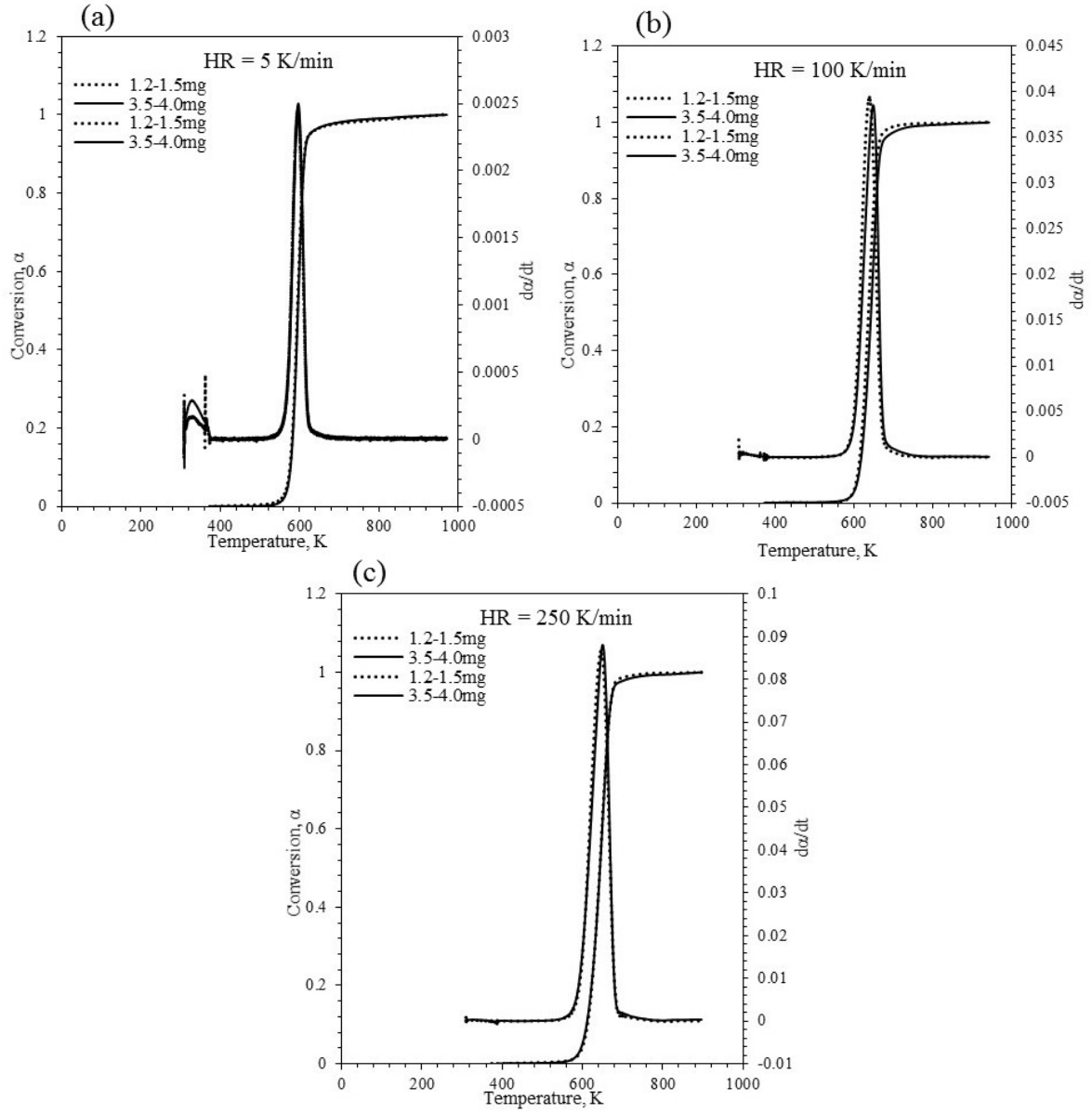

Figure 3.2. Comparison of weight loss data for different weighted samples of pure cellulose at different heating rates.

Conversion α, and derivative of conversion dα/dt was calculated using weight loss data from TGA. Trends of "α" and "dα/dt" for low heating rates 5, 20, 40, 60 K/min versus temperature are shown Figure 3.3 (a) and (b) respectively, while the same trends for higher heating rates 100, 150, 200, 250 K/min are shown in Figure 3.4 (a) and (b).

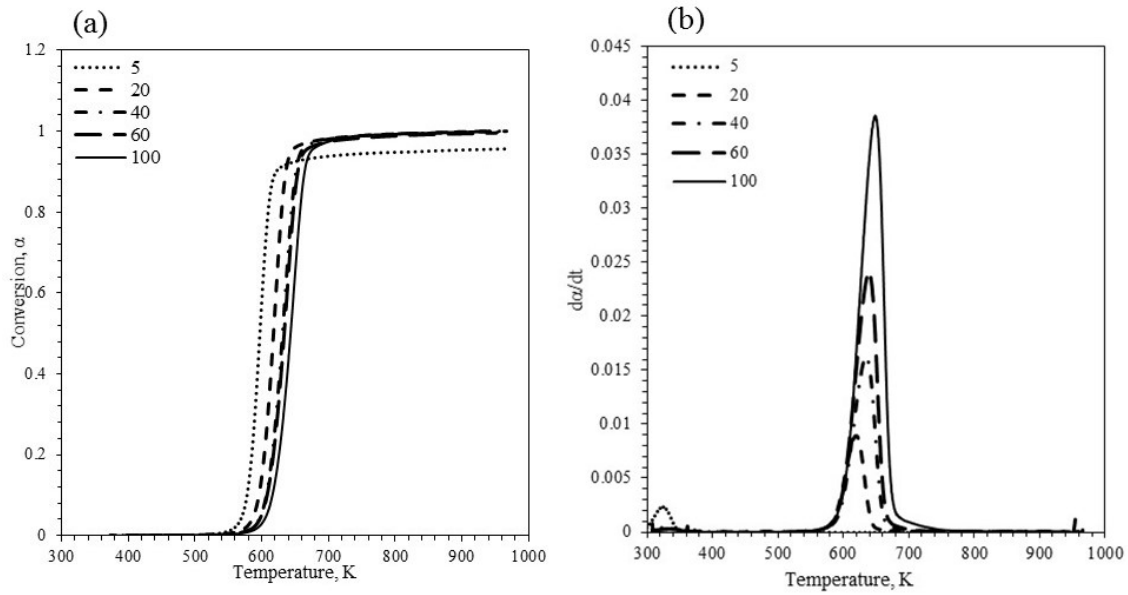

Figure 3.3. TGA results of pure cellulose (a) Conversion, α (b) Rate of conversion, dα/dt at low heating rates (5, 20, 40, 60 and 100 K/min).

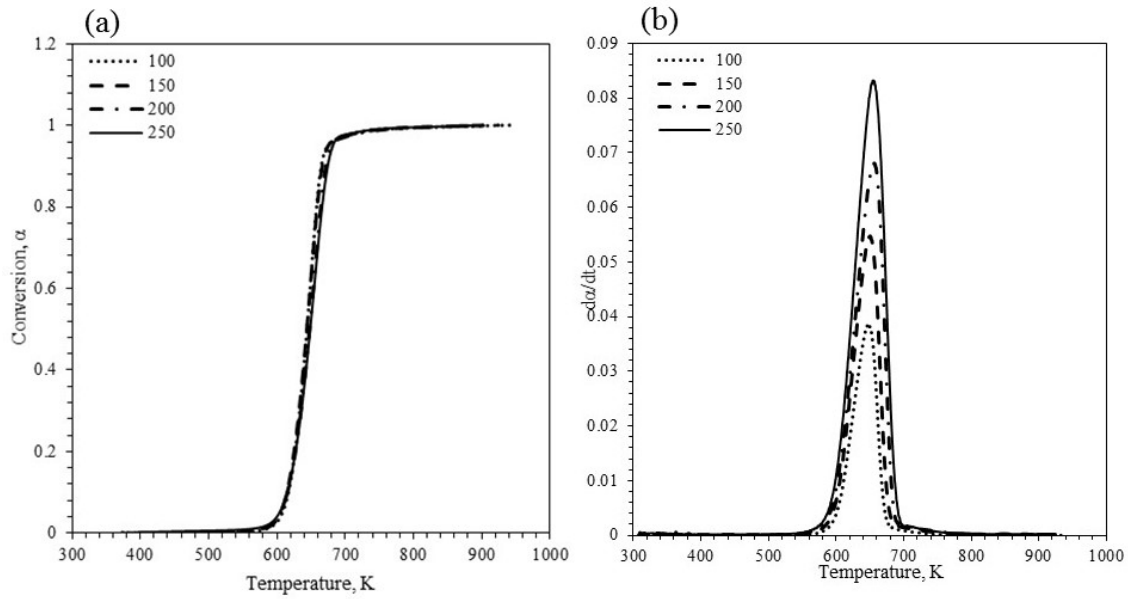

Figure 3.4. (a) Conversion, α (b) Rate of conversion, dα/dt for pure cellulose at low heating rates (100, 150, 200 and 250 K/min)..

Conversion increased with the increase in heating rate, which is more prominent from 5-60 K/min (Figure 3.3(a)), however above 100 K/min this increase is not significant (Figure 3.4(a)). Peak of conversion rate shifted to higher temperatures with increase in heating rate as presented in Figure 3.3(b) and 3.4(b). The results in terms of trends for conversion and conversion rate were same as reported in literature previously [203].

3.3.2. Kinetic Parameters for Pure Cellulose using Distributed Activation Energy Model

The weight loss data from TGA was further used to determine kinetic parameters using distributed activation energy model. Since there are four reactions in the CPD scheme and it is important to know the kinetics of these reactions. Specifying ρ as a constant which is the ratio of $^{k_\delta}/_{k_c}$, only k_b and k_g need to be determined. For this purpose two component modelling scheme was used. Initial guess for the parameters was taken from the literature [108] and then parameters were optimized. These optimized values and the literature values are shown in Table 3.3.

Table 3.3. Kinetic parameters for pure cellulose from literature [108] and this work.

Parameter	Literature Values	Optimized Values (this work)
Activation energy for bridge breaking, E_b (kJ/mol)	231.7	232.7
Frequency factor for bridge breaking, A_b (s^{-1})	2.0×10^{16}	8.52×10^{17}
Standard deviation in bridge breaking activation energy, σ_b (kJ/mol)	17.11	2.41
Activation energy for gas formation, E_{gas} (kJ/mol)	256	255.9
Frequency factor for gas formation, A_{gas} (s^{-1})	3×10^{15}	5.51×10^{15}
Standard deviation in gas release activation energy, σ_{gas} (kJ/mol)	33.8	33.9

Change in the values of activation energy, frequency factor and standard deviation of activation energy for bridge breaking reaction are prominent, however for the gas phase reaction, optimized values of these parameters are almost similar to the literature values. Conversion of cellulose obtained from distributed activation energy model was compared with experimental data available in literature [204] to validate the parameters. Figure 3.5 (a) and (b) represent the conversions obtained at two different heating rates of 5 and 100 K/min respectively. These results show good agreements with the literature data reported and confirm that these optimized parameters can be used for further analysis of cellulose pyrolysis in the range of low (5, 20, 40, 60 K/min) as well as high heating rates (100, 150, 200, 250 K/min).

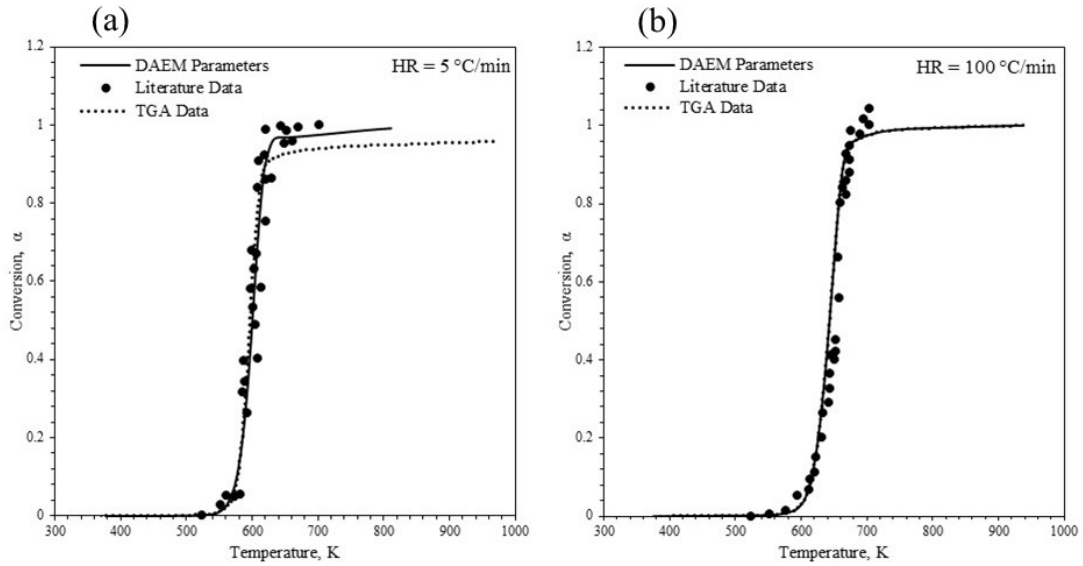

Figure 3.5. Comparison of conversion of cellulose using predicted parameters using distributed activation energy model and parameters available in literature [204] and from TGA experiments.

3.3.3. Product Yield from CPD for Pure Cellulose

Kinetic parameters obtained from two component distributed activation energy model dictate the two basic reactions of CPD mechanism i.e. bridge breaking and gas formation. These were used as input to the CPD model to determine the volatiles, tar and char yield and the yield of bridge population reactions. Other than kinetic parameters, structural parameters used as input to CPD model are shown in Table 3.4.

Table 3.4. Structural parameters for cellulose [100].

Parameters	Values for Cellulose
Molecular weight per cluster, MW_{cl}	81
Molecular weight per side chain, M_δ	22.7
Percent intact bridges, p_o	1.0
Number of bridges per cluster, $\sigma+1$	3.0

The total volatiles fraction from CPD and its comparison with experimental and literature data are shown in Figure 3.6 (a) and (b). These are represented as: data points are from experimental work of Dufour et al. [204], dotted line is the one obtained using already reported kinetic parameters [108] and the solid line is for optimized parameters from distributed activation energy model at heating rates of 5 and 100 K/min from present work. At low heating rate of 5 K/min, the curves show that result of DAEM

parameters is in well agreement with the experimental data points, however the literature parameters have more shift towards higher temperature. At higher heating rate of 100 K/min, the experimental data points are in between the curves of literature and DAEM parameters giving a better match to the solid curve. The maximum fraction obtained by the end was 1.0 because of the constant value of $\rho = {}^{k_\delta}/_{k_c} = 100$. This value was kept same as reported in the literature to minimize char formation and maximize total volatiles fraction [108]. Also, it was observed from low heating rate experimental data in the literature that char residue was very low [205].

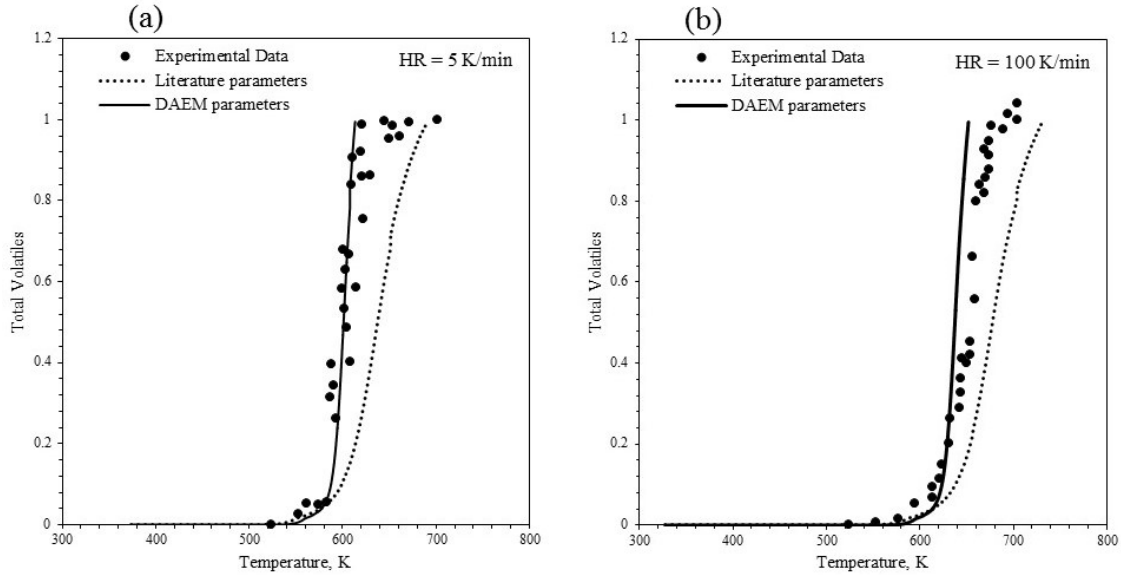

Figure 3.6. Validation of our predicted distributed activation energy model parameters for CPD model with our TGA experimental data and parameters available in literature at two different heating rates.[204,205]

For the validation of optimized parameters, other than total volatiles, fraction of tar and gases produced was also determined and compared with the literature data [159]. The comparison of these fractions obtained from literature and from CPD model is shown in Figure 3.7 (a) and (b). Tar fraction data predicted from distributed activation energy model parameters gave an accurate fit with the experimental data, however some discrepancies were observed in the trends of gas fraction. The fraction of the gases shows a maxima at around 600 K because the labile bridges break and form intermediate which is immediately converted into other products through two parallel reactions and the gas formation increases. After a certain time as the intermediate is consumed a decline in the gas fraction is observed, which increases again due to the formation of gases through gas formation reaction which has higher activation energy

as compared to bride breaking reaction. The final yield of three products char, tar and gases were in acceptable range when compared with the experimental data and are represented in Table 3.5.

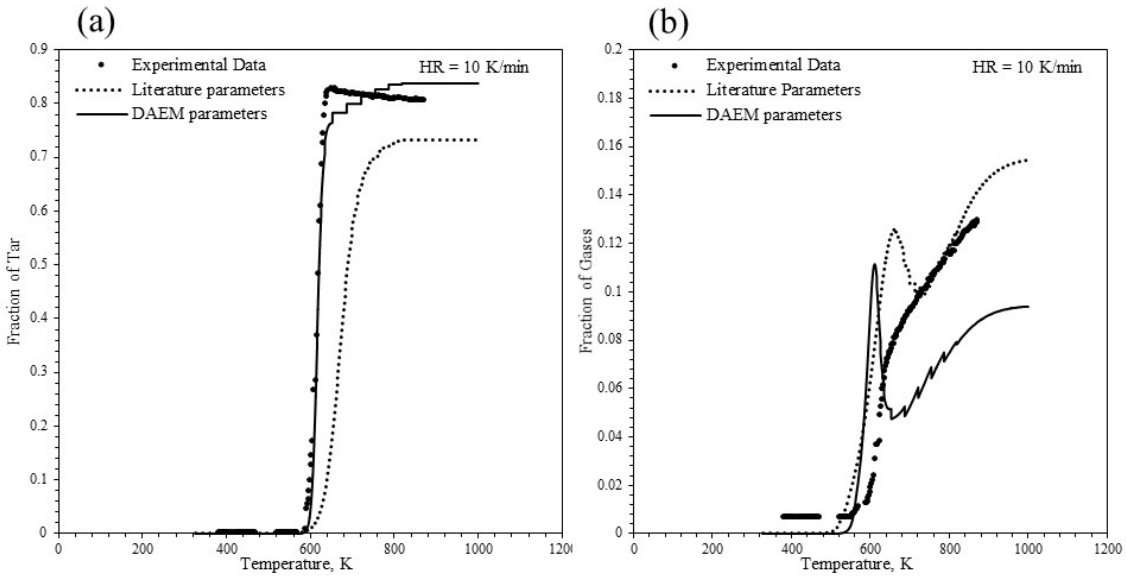

Figure 3.7. Comparison of fraction of (a) tar and (b) gases obtained from our TGA experiments, CPD model using DAEM parameters and CPD model using literature parameters [159].

Table 3.5. Comparison of product yield predicted from distributed activation energy model with experimental values [159].

Yield (%)	**Char**	**Tar**	**Gases**
Experimental	6.467	80.44	12.93
Predicted from CPD using parameters from distributed activation energy model	6.82	83.79	9.39

3.3.4. TGA Results for NaCl-loaded Cellulose

Thermogravimetric analysis can be useful to obtain weight loss data for salt-loaded cellulose as well. NaCl-loaded samples of cellulose were run in the TGA using the same temperature program as explained in section 3.3.2 of this chapter. Weight loss data was collected for the heating rates 5, 20, 40 and 60 K/min for all five concentrations of NaCl in cellulose. The conversion, "α" and derivative of conversion, "dα/dt" are shown in Figure 3.8 and 3.9 respectively. Conversion of cellulose is supressed in the presence of NaCl (Figure 3.8). At heating rate of 5 K/min, final conversion of NaCl-loaded cellulose surpasses the pure cellulose (Figure 3.8 (a)). For

all other heating rates 20, 40 and 60 K/min, the final conversion of NaCl-loaded cellulose lies below the pure cellulose curve (Figure 3.8 (b), 3.8 (c), 3.8 (d)).

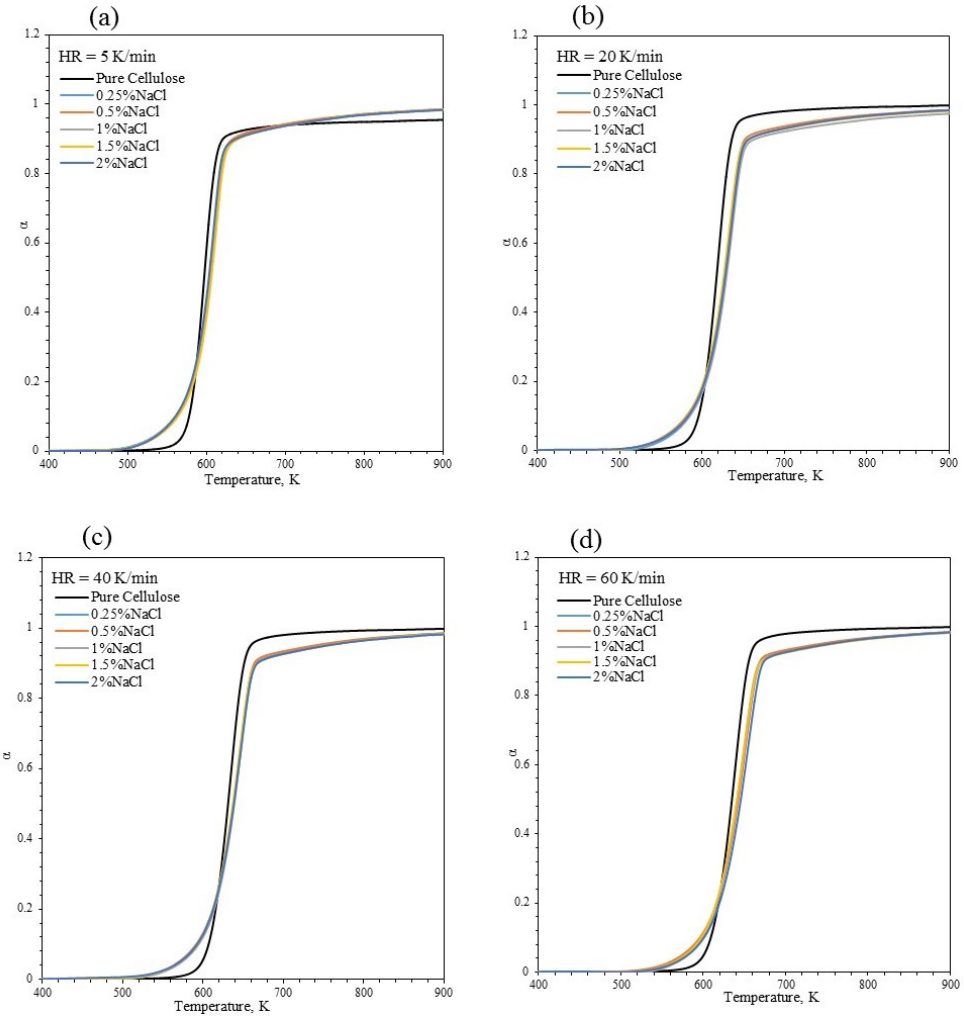

Figure 3.8. TGA experimental results for Conversion of cellulose and NaCl-loaded cellulose for different heating rates (a) 5 K/min (b) 20 K/min (c) 40 K/min (d) 60 K/min.

This is very clear from the Figure 3.9 that the presence of NaCl has also reduced the rate of conversion for cellulose. The maxima of pure cellulose rate curve is higher than the maxima of NaCl-loaded curves, this difference is small at a heating rate of 5 °C/min and increases for the heating rates 20, 40 and 60 K/min, while increase in salt concentration shows negligible shift in the curve.

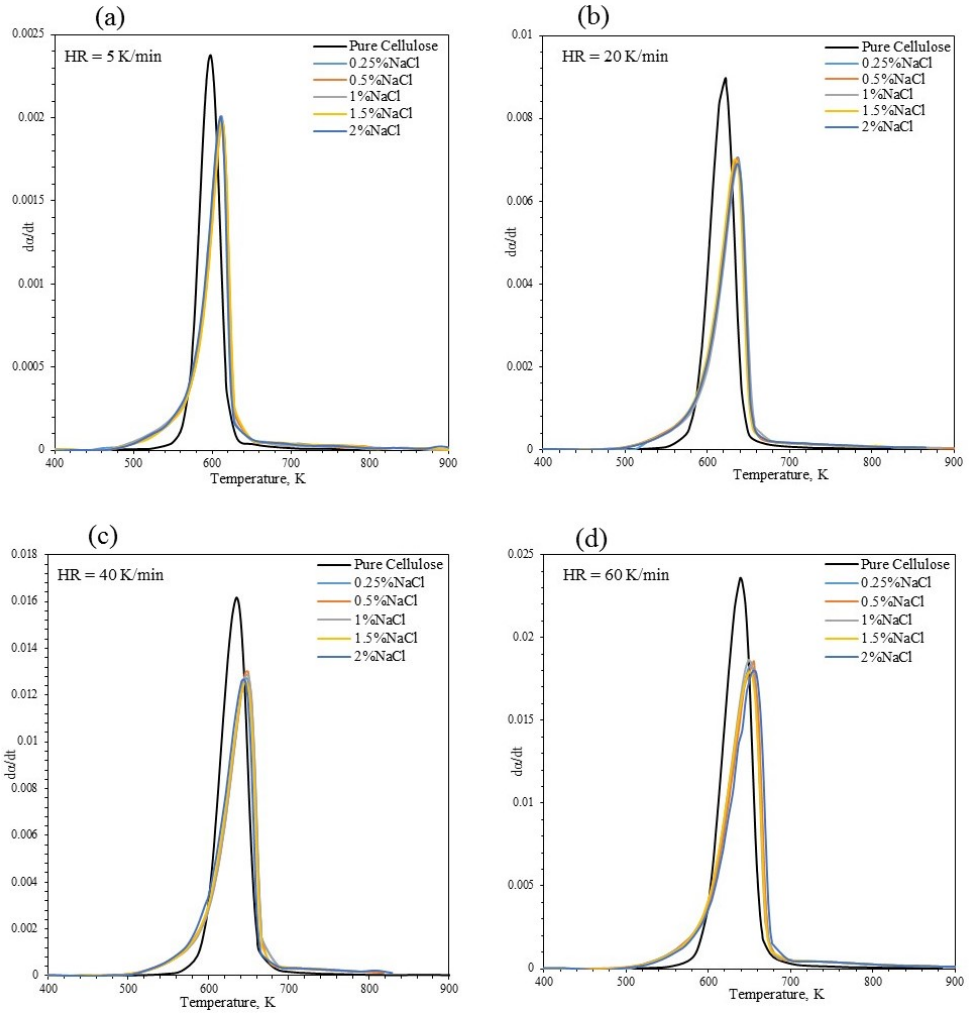

Figure 3.9. Rate of conversion for pure cellulose and for different concentrations of NaCl in cellulose for different heating rates (a) 5 K/min (b) 20 K/min (c) 40 K/min (d) 60 K/min.

In pyrolysis of NaCl-loaded cellulose, Na^+ has major contribution towards binding with the original cellulose matrix and neutral species to from Na^+-complexes while chloride will volatilize and become a part of gaseous phase. The catalytic effect of Na^+ on the reactions as well as product species has already been reported in literature in detail using mechanistic model [155,156]. Mechanistic studies showed that same chemical species were produced in the pyrolysis of pure cellulose and NaCl-loaded cellulose but the kinetics were different. Fraction of char produced at the end of pyrolysis has been calculated to study the effect of presence of NaCl in cellulose. Char yield determined for pure cellulose was around 3-4 %, while addition of NaCl increased the char yield up to 14-16 % which is consistent with already reported data in literature [143,206]. Figure 3.10 shows that increase in heating rate decreases the char yield produced for different NaCl-loaded cellulose samples (0.25-2.0 %).

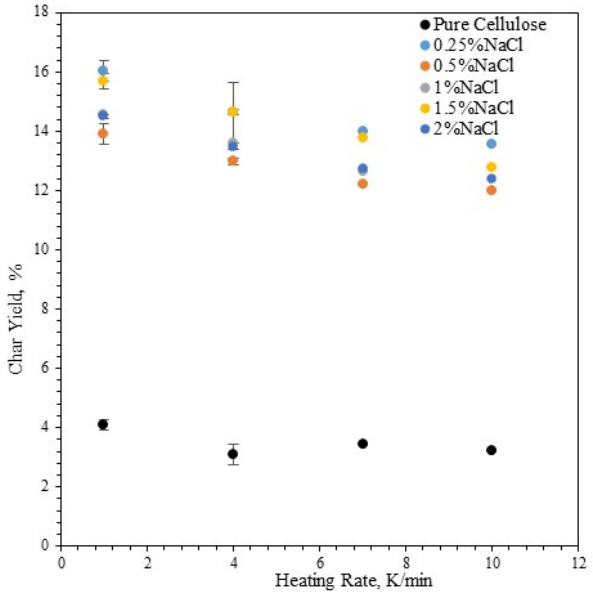

Figure 3.10. Effect of presence of NaCl on char yield determined on dry, ash free basis (daf).

Effect of increase in salt concentration on the char yield did not follow an increasing or decreasing pattern. At low concentrations i.e. 0.25% NaCl in cellulose the char yield was maximum and for all the other concentrations it may increase or decrease. Detailed product analysis of cellulose pyrolysis in the presence of inorganic salts performed by Patwardhan et al. [207] explained that increase in salt concentration decreases the formation of certain products such as levoglucosan and 5-hydroxymethyl furfural, while yield of other products such as formic acid, glycoaldehyde, acetol and 2-furaldehyde first increases and then decreases. But this is also shown that the product yield does not change significantly after a certain amount and effect of salt concentration becomes constant. Yield of char and total volatiles for pure and NaCl-loaded cellulose obtained at different heating rates is presented in Table 3.6.

Table 3.6. Pyrolysis product yield for pure cellulose and different concentrations of NaCl in cellulose at different heating rates.

Sample	**Pyrolysis product yield**							
Heating Rate	5 K/min		20 K/min		40 K/min		60 K/min	
Products	Volatiles	Char	Volatiles	Char	Volatiles	Char	Volatiles	Char
Pure Cellulose	95.93	4.06	96.91	3.09	96.56	3.44	96.78	3.22
Cellulose+0.25%NaCl	83.97	16.03	85.36	14.64	85.99	14.01	86.45	13.55
Cellulose+0.5%NaCl	86.10	13.90	87.03	12.97	87.81	12.19	87.99	12.01
Cellulose+1.0%NaCl	85.44	14.56	86.40	13.60	87.37	12.63	87.85	12.15
Cellulose+1.5%NaCl	84.32	15.68	85.37	14.63	86.22	13.78	87.24	12.76
Cellulose+2.0%NaCl	85.50	14.50	86.43	13.57	87.25	12.75	87.64	12.36

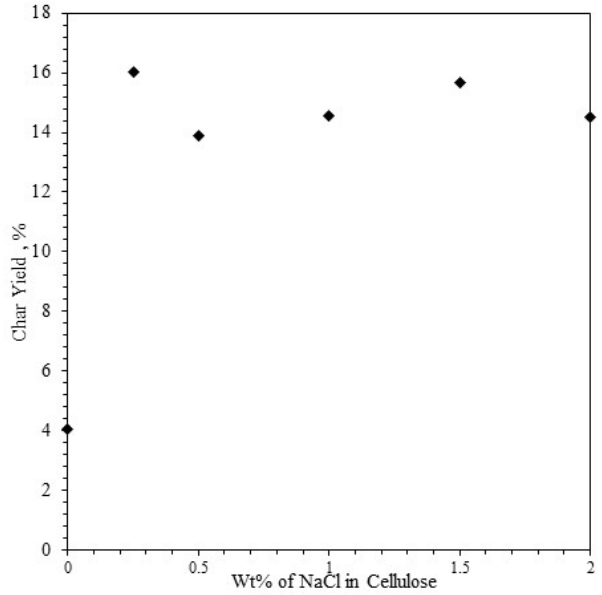

Figure 3.11. Char yield for different NaCl concentrations in cellulose (daf) at heating rates (5-60K/min).

Figure 3.11 is representing a sharp increase in char yield for NaCl concentrations as 0-0.25 % at a heating rate of 5 K/min, while the average of the yield remains constant in between 0.5-2.0 % of NaCl.

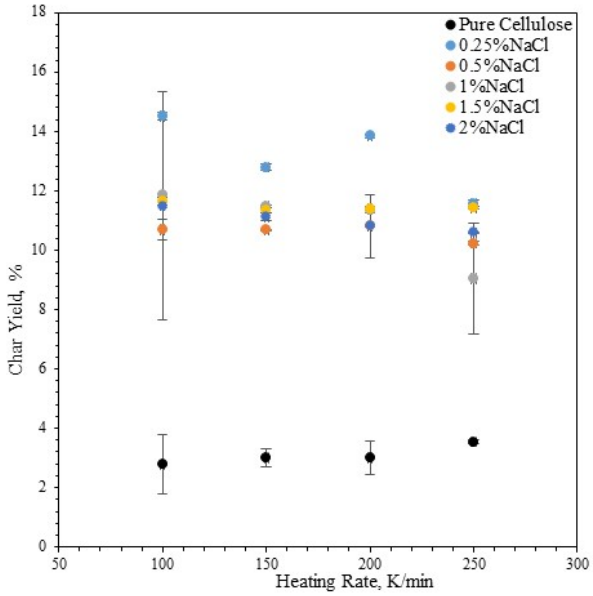

Figure 3.12. Char yield (daf) for different NaCl concentrations in cellulose at heating rates (100-250 K/min).

Char yield determined for pure and NaCl-loaded cellulose at high heating rates (100, 150, 200, 250 K/min) is shown in Figure 3.12, which shows the similar behaviour as at low heating rates that addition of small quantity of salt increases the char yield to 13-14%.

3.3.5. Kinetic Parameters from DAEM for NaCl-loaded Cellulose

Inorganic species added to cellulose do not change the cellulose structure or reaction mechanism, however they effect the reaction kinetics [155,156]. Two component distributed activation energy model was used to predict the kinetic parameters for NaCl-loaded cellulose samples. Initial guess was taken from the values of pure cellulose and then optimized for different concentrations of NaCl. The parameters obtained are presented in Table 3.7.

Table 3.7. Predicted kinetic parameters using distributed activation energy model for different mixtures of cellulose and NaCl.

Kinetic Parameters	Pure Cellulose	0.25 wt. % NaCl	0.5 wt. % NaCl	1 wt. % NaCl	1.5 wt. % NaCl	2 wt. % NaCl
E_b (kJ/mol)	232.7	228.6	225.8	231.0	230.3	230.9
A_b (s^{-1})	8.52×10^{17}	1.71×10^{17}	1.06×10^{17}	2.80×10^{17}	2.55×10^{17}	2.89×10^{17}
σ_b (kJ/mol)	2.41	2.70	3.32	2.26	2.30	2.98
E_{gas} (kJ/mol)	255.9	249.2	254.5	248.9	250.0	250.0
A_{gas} (s^{-1})	5.51×10^{15}	1.97×10^{19}	1.5×10^{19}	1.56×10^{19}	1.59×10^{19}	1.32×10^{19}
σ_{gas} (kJ/mol)	33.9	25.9	34.0	22.2	21.9	23.7
w_c	0.968	0.763	0.832	0.704	0.710	0.730

For bridge breaking reaction, there is a decrease in activation energy, E_b as well frequency factor, A_b with the addition of NaCl to pure cellulose, while the values then increase with the increase in NaCl concentration. The value of standard deviation of bridge breaking, σ_b does not follow any increasing or decreasing trend. For gas formation reaction, activation energy, E_{gas}, frequency factor, A_{gas} and the standard deviation of gas formation, σ_{gas} decrease for NaCl-loaded cellulose as compared to the pure cellulose however, this trend is not linear with increase in salt concentration.

3.3.6. Product Yield from CPD for NaCl-loaded Cellulose

The parameters obtained from distributed activation energy model were used to predict the product yield. Structural parameters were kept same as that of pure cellulose (Table 3.3) making an assumption that NaCl loaded to cellulose does not alter the structural configuration of cellulose [108]. While kinetic parameters were predicted using distributed activation energy model. Among the four reactions of CPD scheme, kinetics of bridge breaking and gas forming reactions were predicted and the compositional ratio, ρ was also optimized. ρ was taken as 100 for pure cellulose which will not be true for the NaCl-loaded cellulose [108]. So, a value of "ρ" other than the maximum value was required to determine product yield. When finding an optimum of "ρ", it was observed that it had a very little effect when above 3-100 but showed significant effect when the value was below 1.0, hence an optimized value of 2.0 was selected for this work. Results for this analysis are compared in Figure 3.13.

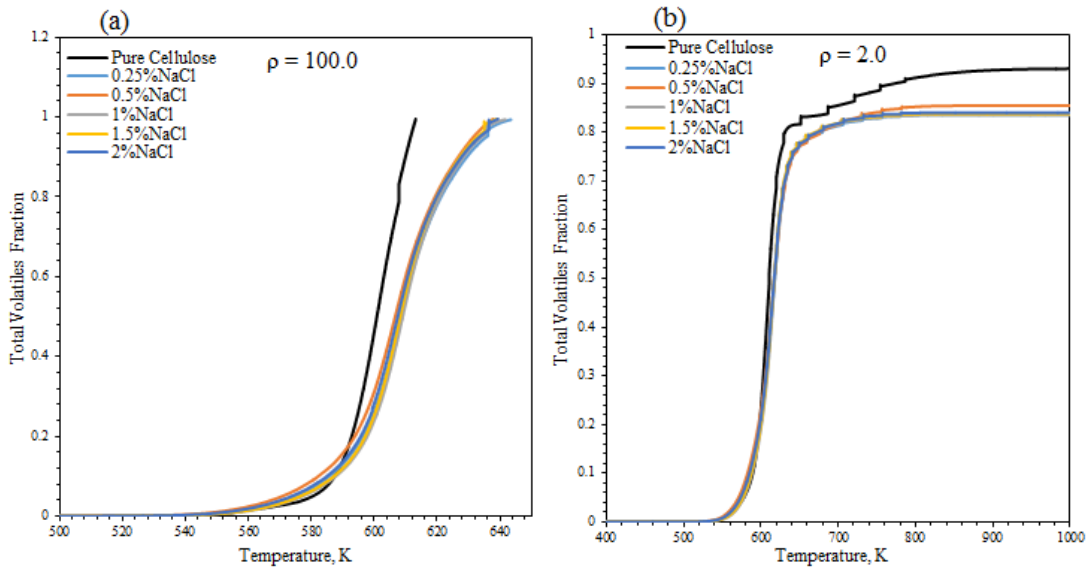

Figure 3.13. Comparison of total volatiles fraction at two different values of ρ.

The graph (a) of Figure 3.13 shows that, at maximum value of ρ = 100 the maximum amount of volatiles will be produced reducing the char to a minimum value. For pure cellulose, the curve is approaching to one which remains same for all other samples having NaCl. For NaCl-loaded cellulose, the curve shifts significantly towards higher temperatures and reache maximum fraction of 1.0 at around 640 K. Change in the value of ρ, changes the product distribution. For a value of ρ = 2, fraction of total volatiles from pure cellulose was maximum around 0.9 however, it decreased to 0.835 with 0.25% of NaCl. The fractions of three products of cellulose pyrolysis were also determined which are shown in Figure 3.14.

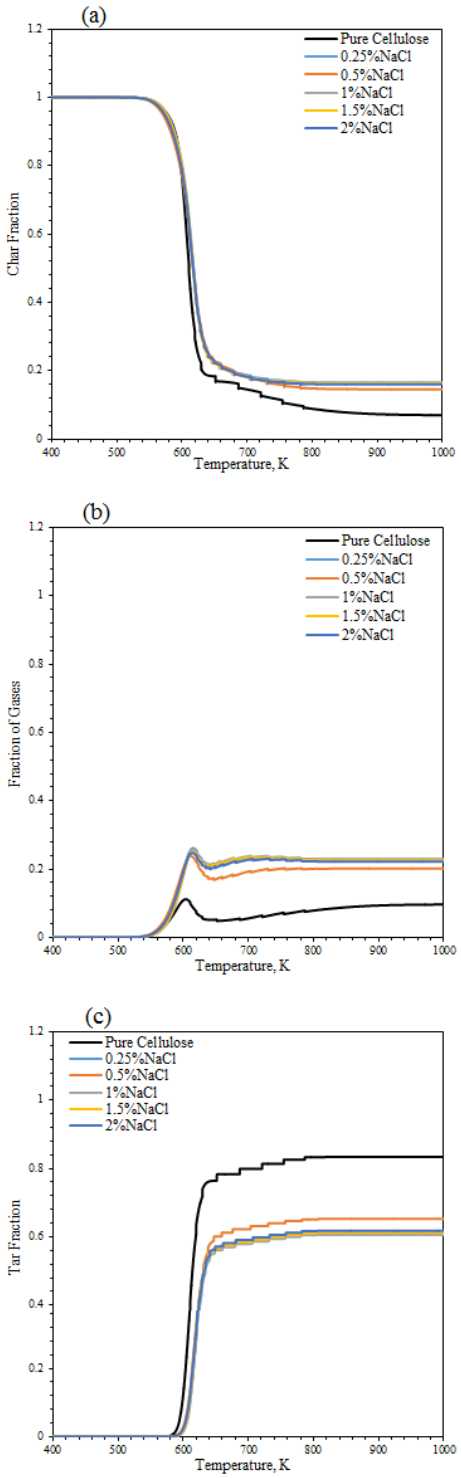

Figure 3.14. Char, gas and tar fraction from CPD using optimized parameters.

The amount of char residue at the end of the simulation for pure cellulose was 6.97% and this amount increased to 16.45% for 0.25% NaCl in cellulose. The amount of char for all the other salt concentrations is shown in Table 3.8. The amount of gases produced as a result of pure cellulose pyrolysis was 9.63% and this amount increased

with addition of NaCl to 22.85% and then further increases with increase in NaCl concentration which is presented in Table 3.8. Amount of tar produced for pure cellulose was 83.4% and this amount reduced to 60.7% with addition of 0.25%NaCl. For all other NaCl-loaded samples, the amount of tar produced in the presence of different salt concentrations is shown in Table 3.8.

Table 3.8. Pyrolysis product yield for pure and NaCl-loaded cellulose.

Sample	**Pyrolysis Product Yield (%)**		
Heating Rate	10 K/min		
	Tar	Gases	Char
Pure Cellulose	83.40	9.63	6.97
Cellulose+0.25%NaCl	60.70	22.85	16.45
Cellulose+0.5%NaCl	65.26	20.20	14.54
Cellulose+1.0%NaCl	60.62	22.90	16.48
Cellulose+1.5%NaCl	61.19	22.57	16.24
Cellulose+2.0%NaCl	61.79	22.22	15.99

These result correlate to data available in literature stating that the presence of NaCl accelerates the cellulose decomposition and favours the formation of gases and char [155]. Patwardhan et al. [137] performed experiments for pure and salt impregnated cellulose in a micro-pyrolyser at heating rates of >2000 K/min and the results obtained are shown in Table 3.9. Char yield for pure cellulose is comparable however the char yield for NaCl-loaded cellulose in TGA experiments is higher because at low heating rate the sample will spend more time in the reactor and will promote charring reactions. Even at higher heating rates the amount of char produced is significant which indicates that the inorganic species have a profound effect on the cellulose pyrolysis at lower and higher heating rates and should be taken into consideration while modelling the cellulose pyrolysis.

Table 3.9. Literature data for char yield for pure and NaCl-loaded cellulose samples [207]

Sample	**Pyrolysis Product Yield (%)**
	Char
Cellulose	5.35±3.54
Cellulose+0.1%NaCl	6.76
Cellulose+1.0%NaCl	9.77

3.4. Conclusions

Kinetic parameters to be used as input data for CPD model have been determined using thermogravimetric analysis (TGA) and distributed activation energy model. The parameters obtained for pure cellulose have a reasonable consistency with the literature data. Once validated, the same methodology was used to determine the kinetics of NaCl-loaded cellulose. The effect of inorganic species specifically NaCl on the pyrolysis of cellulose was studied by producing NaCl-loaded cellulose using wet impregnation method. Presence of inorganic salts supresses the volatiles formation by increasing the char and gases yield which has been confirmed from weight loss data collected from TGA. For pure cellulose, char yield at the end of pyrolysis was 3-4 %, however this percentage increased to 14-16 % for NaCl-loaded cellulose. Activation energy, frequency factor and standard deviation of activation energy were optimized for bridge breaking and gas forming reactions of chemical percolation devolatilization, CPD scheme for pure and NaCl-loaded cellulose. These optimized parameters were then implemented to CPD model and char, tar and gases yield were predicted which showed an increase in the char and fraction of gases and decrease in tar yield in the presence of NaCl. This leads to the conclusion that while modelling biomass pyrolysis, inorganics should not be neglected as they have a significant effect on the product yield and future work must incorporate these species and the mutual interaction among the constituents of biomass.

CHAPTER 4 MIXING AND SEGREGATION BEHAVIOUR OF CELLULOSE IN FLUIDIZED BED

4.1. Introduction

Uniform fluidization is of critical importance for optimal performance of fluidized bed reactors, which among other applications, are widely used for biomass pyrolysis. In fluidized bed pyrolysis, the mixing and segregation of biomass with other particles is considered as the measure of fluidization behaviour, which is strongly affected by parameters such as mixture composition, size, shape and density of particles. Level of mixing/segregation in a fluidized bed reactor can be determined using three different quantities: mixing index (MI), segregation rate (SR) and particle segregation number (PSN). These are based upon the fraction of light particles which usually float over the surface of the fluidized bed and heavy particles which prefer to settle down in a fluidized bed reactor. These light and heavy particles are more commonly termed as flotsam and jetsam [208]. Rowe and his research group used mixing index as a measure of quantifying the level of mixing or segregation in a mixture. Goldschmidt et al. [209] explored the segregation dynamics in dense gas-fluidized beds of mono-disperse systems and binary mixtures using the digital image analysis techniques. Extensive experimental data has been generated to validate the hydrodynamic models. Fluidization, mixing and segregation behaviour of biomass-sand mixture in a 3D gas-fluidized bed has also been investigated experimentally. Effect of three variables: fluidization time, the initial packing state and mixing ratio of biomass to sand on the segregation have been studied using segregation index [210]. Lu et al. [211] proposed a model based on the kinetic theory of granular flow to evaluate the influence of particle size distribution on the segregation behaviour of same density particles in a binary mixture. A CFD model for bubbling fluidized bed was developed by Lu et al. [212] for binary mixtures having same density particles but different diameters. Segregation behaviour of the binary mixtures was mainly influenced by the particle size, mass fraction of small particles and the gas velocity. Unlike the previous models where only one mixture granular temperature equation was used for multi-phase systems, a new model including separate equations for granular temperature of each phase was proposed by Lu and Gidaspow [213]. The model for binary mixtures was further extended to ternary mixtures by Iddir et al. [214] to investigate the behaviour

of particles having different densities and diameters. Qiaoqun et al. [215] investigated the behaviour of mixing of rice-husk in an inert sand bed of bubbling fluidized bed reactor. The level of particle mixing in a binary system has been quantified using the particle segregation number and a method called the cube analysis, which was developed by Keller et al. [216]. A fluidizing media usually sand is needed for uniform mixing of biomass particles. There are several studies investigating the mixing and segregation behaviour of biomass in the presence of bed material which acts as catalyst. For example, Sharma et al. [217] conducted CFD simulations to study the hydrodynamics of a mixture of biomass and biochar in a bubbling fluidized bed. Bai et al. [218] studied the mixing and segregation behaviour of ground walnut shell particles (GWS) in the bed of glass beads (GB) as inert media. Finally, Gera et al. [219] provided a modified particle-particle drag model to predict the mixing at higher velocities and segregation at relatively low velocities for multi-fluid mixtures.

The objective of the present work is to study the mixing and segregation behaviour of cellulose and sand in a bubbling fluidized bed. Simulations have been carried out in a cold flow environment. Since fluidization velocity is one of the crucial parameters for defining the bubbling bed dynamics, the effect of superficial gas velocity on the mixing and segregation behaviour of cellulose particles in an inert sand bed has been studied. The other relevant parameters such as composition of mixture and size of particles have also been considered.

4.1.1. Mathematical Model

Among the two simulation methodologies available, Eulerian-Eulerian modelling approach has been specified in this case for the mixture of cellulose and sand. Gas phase and solid particles are considered as an interpenetrating continua and flow is considered to be incompressible. The governing equations of conservation of mass and momentum for each phase in multi-fluid Eulerian model have been solved using kinetic theory of granular flow (KTGF). The fluctuating kinetic energy of solid phases and other basic laws have been specified using the following models in ANSYS FLUENT [220].

For the gas phase the continuity equation can be defined as:

$$\frac{\partial}{\partial t}\left(\alpha_g \rho_g\right) + \nabla.\left(\alpha_g \rho_g \vec{v}_g\right) = 0 \tag{4.1}$$

For each *sth* solid phase, in a system of *n* solid phases the conservation of mass has been defined as:

$$\frac{\partial}{\partial t}(\alpha_s \rho_s) + \nabla.(\alpha_s \rho_s \vec{v}_s) = 0 \quad (4.2)$$

Here,

ρ_g = Density of gas phase

ρ_s = Density of *sth* solid phase

$\vec{v}_g$ = Velocity of gas phase

$\vec{v}_s$ = Velocity of *sth* solid phase

The sum of the volume fractions of two phases α_g and α_s should be one.

$$\boldsymbol{\alpha_g + \sum_{s=1}^{n} \alpha_s = 1} \quad (4.3)$$

Navier-Stokes equation has been used to specify the momentum conservation for gas phase

$$\boldsymbol{\frac{\partial(\alpha_g \rho_g \vec{v}_g)}{\partial t} + \nabla(\alpha_g \rho_g \vec{v}_g \vec{v}_g) = -\alpha_g \nabla P_g + \nabla \vec{\tau}_g + \alpha_g \rho_g \vec{g} + \sum_{s=1}^{n} \vec{R}_{gs}} \quad (4.4)$$

$$\boldsymbol{\vec{R}_{gs} = K_{gs}(\vec{v}_g - \vec{v}_s)} \quad (4.5)$$

K_{gs} = Gas-solid momentum exchange co-efficient

This gas-solid momentum exchange coefficient represents the drag force between these phases and is modelled using Gidaspow model [221] for the dense fluidized beds.

When $\alpha_g > 0.8$, the momentum exchange co-efficient is of the form:

$$\boldsymbol{K_{gs} = \frac{3}{4} C_D \frac{\alpha_s \alpha_g \rho_g |\vec{v}_s - \vec{v}_g|}{d_s} \alpha_g^{-2.65}} \quad (4.6)$$

$$\boldsymbol{C_D = \begin{cases} \frac{24}{\alpha_g Re_s}\left[1 + 0.15(\alpha_g Re_s)^{0.687}\right], & Re_s < 1000 \\ 0.44, & Re_s > 1000 \end{cases}} \quad (4.7)$$

The Reynolds number for solid particles is given by:

$$\boldsymbol{Re_s} = \frac{\boldsymbol{\rho_g d_s |\vec{v}_s - \vec{v}_g|}}{\boldsymbol{\mu_g}} \quad (4.8)$$

When $\alpha_g < 0.8$, the momentum exchange co-efficient is calculated using the following equation:

$$\boldsymbol{K_{gs}} = \mathbf{150}\frac{\boldsymbol{\alpha_s(1-\alpha_g)\mu_g}}{\boldsymbol{\alpha_g d_s^2}} + \mathbf{1.75}\frac{\boldsymbol{\rho_g \alpha_s |\vec{v}_s - \vec{v}_g|}}{\boldsymbol{d_s}} \quad (4.9)$$

Stress-strain tensor for gas phase will be:

$$\bar{\bar{\boldsymbol{\tau}}}_{\boldsymbol{g}} = \boldsymbol{\alpha_g \mu_g}\left[\boldsymbol{\nabla \vec{v}_g} + \boldsymbol{\nabla \vec{v}_g^T}\right] + \boldsymbol{\alpha_g}\left(\boldsymbol{\lambda_g} - \frac{\mathbf{2}}{\mathbf{3}}\boldsymbol{\mu_g}\right)\boldsymbol{\nabla . \vec{v}_g \bar{\bar{I}}} \quad (4.10)$$

Momentum conservation equation for *sth* solid phase is:

$$\frac{\boldsymbol{\partial(\alpha_s \rho_s \vec{v}_s)}}{\boldsymbol{\partial t}} + \boldsymbol{\nabla(\alpha_s \rho_s \vec{v}_s \vec{v}_s)} = \boldsymbol{-\alpha_s \nabla p - \nabla p_s + \nabla \vec{\tau}_s + \alpha_s \rho_s \vec{g} + \sum_{l=1}^{N} \vec{R}_{ls}} \quad (4.11)$$

$$\boldsymbol{\vec{R}_{ls}} = \boldsymbol{K_{ls}(\vec{v}_l - \vec{v}_s)} \quad (4.12)$$

K_{ls} = Momentum exchange co-efficient between the *lth*-fluid and *sth*-solid phase

Syamlal-O'brien symmetric model [222] has been used to specify the drag force between and the two solid phases. The model is of form:

$$\boldsymbol{K_{ls}} = \frac{\mathbf{3(1+e_{ls})}\left((\pi/2) + \boldsymbol{C_{fr,ls}}\left(\pi^2/8\right)\right)\boldsymbol{\alpha_s \rho_s \alpha_l \rho_l (d_l + d_s)^2 g_{0,ls}}}{\mathbf{2\pi}\left(\boldsymbol{\rho_l d_l^3 + \rho_s d_s^3}\right)}\boldsymbol{|\vec{v}_l - \vec{v}_s|} \quad (4.13)$$

Stress-strain tensor for solid phase

$$\bar{\bar{\boldsymbol{\tau}}}_{\boldsymbol{s}} = \boldsymbol{\alpha_s \mu_s}[\boldsymbol{\nabla \vec{v}_s} + \boldsymbol{\nabla \vec{v}_s^T}] + \boldsymbol{\alpha_s}\left(\boldsymbol{\lambda_s} - \frac{\mathbf{2}}{\mathbf{3}}\boldsymbol{\mu_s}\right)\boldsymbol{\nabla . \vec{v}_s \bar{\bar{I}}} \quad (4.14)$$

In granular systems of moving particles, the granular temperature is defined in the same manner as that for ideal gases using kinetic theory of granular flow [223]. The granular temperature, θ_s needs to be specified for the *sth* solid phase which represents the kinetic energy of fluctuating particles and is proportional to the one-third of the mean square of the fluctuating velocity of solid particles ($\theta_s = v_s^2/3$) [220]. The transport equation of this granular temperature from kinetic theory is as:

$$\frac{3}{2}\left[\frac{\partial(\alpha_s\rho_s\theta_s)}{\partial t}+\nabla(\alpha_s\rho_s\vec{v}_s\theta_s)\right]=-\left(p_s\bar{\bar{I}}+\bar{\bar{\tau}}_s\right):\nabla\vec{v}_s+\nabla(k_{\theta s}\nabla\theta_s)-\gamma_{\theta s}+\Phi_{ls} \quad (4.15)$$

This equation is a combination of different forms of energy. These terms may be defined as:

$(\alpha_s\rho_s\vec{v}_s\theta_s)$ = Convective granular energy

$-\left(p_s\bar{\bar{I}}+\bar{\bar{\tau}}_s\right):\nabla\vec{v}_s$ = Generation of fluctuating energy due to solid stress tensor

$k_{\theta s}\nabla\theta_s$ = Diffusive granular energy

$\gamma_{\theta s}$ = Energy dissipation due to collisions among particles

Φ_{ls} = Exchange of fluctuation energy between the *lth*-fluid or solid phase and *sth*-solid phase

$$\Phi_{ls}=-3k_{ls}\theta_s \quad (4.16)$$

According to Syamlal et al. [224] the algebraic form of granular temperature can be obtained by neglecting the convection and diffusion terms and considering only dissipation and generation of fluctuating energy terms.

The rate of energy dissipation due to collisions between the solid particles specified by Lun et al. [225] is given as:

$$\gamma_{\theta s}=\frac{12(1-e_{ss}^2)g_{0,ss}}{d_s\sqrt{\pi}}\rho_s\alpha_s^2\theta_s^{3/2} \quad (4.17)$$

Some other constitutive equations are also required for studying the multi-phase model in Fluent which include the shear and bulk viscosities, solids pressure, radial distribution function and frictional model. Solid shear viscosity is obtained by adding the kinetic, collisional and frictional viscosities, such as:

$$\mu_s=\mu_{s,kin}+\mu_{s,col}+\mu_{s,fr} \quad (4.18)$$

Syamlal-O'brien model [224] has been used to define these viscosities which results in the expressions as:

$$\mu_{s,kin}=\frac{\alpha_s d_s\rho_s\sqrt{\theta_s\pi}}{6(3-e_{ss})}\left[1+\frac{2}{5}(1+e_{ss})(3e_{ss}-1)\alpha_s g_{0,ss}\right] \quad (4.19)$$

$$\mu_{s,col}=\frac{4}{5}\alpha_s d_s\rho_s g_{0,ss}(1+e_{ss})\left(\frac{\theta_s}{\pi}\right)^2\alpha_s \quad (4.20)$$

Schaffer's relation [226] has been used to incorporate frictional stress for the solid phase near the packing limit:

$$\boldsymbol{\mu_{s,fr}} = \frac{\boldsymbol{p_s \sin \emptyset}}{\boldsymbol{2\sqrt{I_{2D}}}} \tag{4.21}$$

Where p_s is the solids pressure, $\emptyset$ is the angle of internal friction and I_{2D} is the second invariant of deviatoric stress tensor. To specify frictional pressure the model based on kinetic theory of granular flow (KTGF) has been used.

Additional to shear viscosity, there is solid bulk viscosity which includes the resistance of the granular particles to compression and expansion. The expression is given by Lun et al. [225]:

$$\boldsymbol{\lambda_s} = \frac{\boldsymbol{4}}{\boldsymbol{3}}\boldsymbol{\alpha_s d_s \rho_s g_{0,ss}}(\boldsymbol{1 + e_{ss}})\left(\frac{\boldsymbol{\theta_s}}{\boldsymbol{\pi}}\right)^{\boldsymbol{1/2}} \tag{4.22}$$

The pressure for the *sth* solid phase has been defined using the model given by Lun et al. [225] which is the sum of the kinetic term and the pressure because of collisions among particles.

$$\boldsymbol{p_s} = \boldsymbol{\alpha_s \rho_s \theta_s} + \boldsymbol{2\rho_s}(\boldsymbol{1 + e_{ss}})\boldsymbol{\alpha_s^2 g_{0,ss} \theta_s} \tag{4.23}$$

In the particles collision term there are two important parameters: e_{ss} is known as restitution coefficient and $g_{0,ss}$ is the radial distribution function.

For multiphase systems having N number of phases, the same equation (equation 4.20) has been modified as:

$$\boldsymbol{p_l} = \boldsymbol{\alpha_l \rho_l \theta_l} + \sum_{\boldsymbol{l=1}}^{\boldsymbol{N}} \boldsymbol{2}\frac{\boldsymbol{d_{ls}^3}}{\boldsymbol{d_l^3}}(\boldsymbol{1 + e_{ls}})\boldsymbol{g_{0,ls}\alpha_l \alpha_s \rho_l \theta_l} \tag{4.24}$$

The radial distribution is calculated according to Syamlal-O'brien [224]:

$$\boldsymbol{g_{0,kl}} = \frac{\boldsymbol{1}}{\boldsymbol{(1-\alpha_s)}} + \frac{\boldsymbol{3}\left(\sum_{\boldsymbol{k=1}}^{\boldsymbol{N}} \boldsymbol{\alpha_k}/\boldsymbol{d_k}\right)}{\boldsymbol{(1-\alpha_s)^2(d_s+d_l)}}\boldsymbol{d_s d_l}$$

(4.25)

In this study the fluid flow is considered to be laminar with respect to vessel since the Reynolds number calculated for the gas phase based on column diameter is 1000. The contribution of solid phase and interaction among particles has been dealt as proposed by Sinclair and Jackson [227], according to which the solid-phase stresses can be described by particle motion arising due to the particle collisions and thermal motion

of gas molecules. Kinetic energy of these fluctuations is described by granular temperature. Since no turbulence model has been selected for simulations therefore the sub-grid scale viscous effects were neglected.

4.2. Computational Details

4.2.1. Material and Reactor Configuration

Biomass comprises of several components, mainly cellulose, hemicellulose and lignin. Since cellulose is considered as the model compound for biomass, it has been selected for the present study. A mixture of cellulose and sand as bed material has been fluidized using air as fluidizing media. Physical properties of materials are provided in Table 4.1.

Table 4.1. Physical properties of both materials.

Material	**Cellulose**	**Sand**	**Air**
Density (kg/m^3)	1500	2560	1.225
Particle Diameter (μm)	250-900	440	---

Fluidized bed configuration used for this study is shown in Figure 4.1, which is taken from the work of Bai et al. [218]. Bai et al. [218] had used this experimental data for the validation of his model. Keller [228] had performed cold flow experiments using ground walnut shells (GWS) and glass beads (GB) for different reactor configurations and operating parameters. These experiments were performed considering a well-mixed bed in the fluidized bed. The bed was fluidized for a specific time and then collapsed and this was continued for 60 seconds. And then X-ray computed tomography scans were used to visually observe and investigate the mixing or segregation behaviour in a 3D reactor.

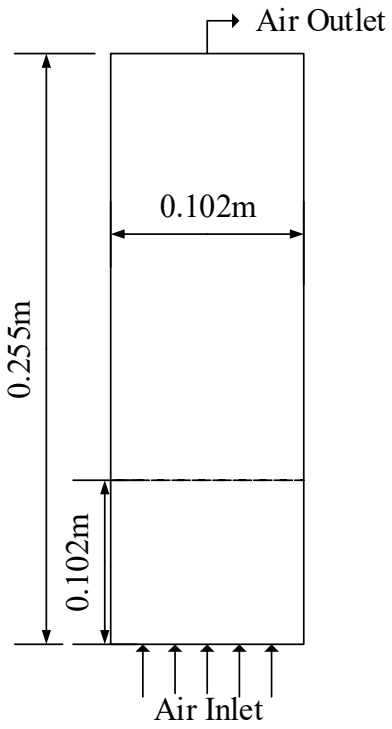

Figure 4.1. Dimensions of fluidized bed reactor [218].

4.2.2. Numerical Simulations and Calculations

Simulations have been carried out in a 2-D geometry as shown in Figure 4.1 using ANSYS Fluent. Four sets of grids were used in these simulations and mesh size with the total number of cells along the bed width and height are represented in Table 4.2.

Table 4.2. Different grid sizes and number of cells.

Grid Size (m)	No. of cells in x-direction	No. of cells in y-direction
0.0102 × 0.0102	10	25
0.0051 × 0.0051	20	50
0.0041 × 0.0041	25	62
0.0034 × 0.0034	30	75

For boundary conditions, the velocity of inlet air was specified at the bottom of the reactor with assumption of one-dimensional plug flow, and a pressure boundary condition was specified at top of the reactor. As initial conditions, the bed material, consisting of cellulose and sand, were assigned a velocity of zero as they were static in the bed initially. For the bed material, different mixture compositions were used to study the effect of this parameter. Material characteristics and relevant operating parameters are shown in Table 4.3.

Table 4.3. Operating parameters.

	Cellulose	**Sand**
Particle Diameter (μm)	250-900	440
Restitution coefficient	0.97	0.97
Angle of internal friction	35	
Ratio of volume fraction α_C : α_S	0.1-1.0	
U_{mf} (sand) (m/s)	0.145	
U_g/U_{mf}	1-3	

The restitution coefficient for the cellulose as well as sand was specified as 0.97. For boundary conditions of walls, no slip was specified for the gas phase while for the solid phase partial slip condition was used. Equations were solved using second-order upwind scheme with a time step size of 10^{-4} sec. All simulations were run for a real time of 60 seconds. This time was selected for the simulations as it is the time used in the experiments as mentioned above.

To quantify the mixing and segregation behaviour, particle segregation number was used. This number is defined as [218]:

$$\boldsymbol{PSN = 2\left(\Delta h_{floatsam} - \Delta h_{jetsam}\right) \times 100\%} \tag{4.26}$$

In this study, flotsam represents the fraction of cellulose while jetsam represents the sand particles. The value of PSN varies between 0 and 100%. If PSN is 0%, that means the particles are in perfectly mixed state and 100% shows the complete segregation in the mixture. Δh, represents the dimensionless average height of solid phase and can be determined using the formula:

$$\boldsymbol{\Delta h = \frac{\sum_k^N \alpha_{s,k} h_k h'_{kk} V_k}{H \sum_k^N \alpha_{s,k} V_k}} \tag{4.27}$$

where,

$\alpha_{s,k}$ = Volume fraction of individual solid phase (either cellulose or sand) in cell k

h_k = Height of the centre of any grid cell k from the distributor

h'_{kk} = Correction factor to account for collapsed bed condition

V_k = Volume of cell k

H = Static bed height

And the correction factor is:

$$\boldsymbol{h_k' = \frac{V_{g,0}}{V_{g,k}}} \tag{4.28}$$

$V_{g,0}$ = Gas phase volume in any grid cell where void fraction is known

$V_{g,k}$ = Gas phase volume in the grid cell k, which can be determined as: $V_{g,k} = \alpha_{g,k} V_k$

4.3. Results and Discussion

4.3.1. Model Validation

Bai et al. [218] used multi-fluid model based on kinetic theory of granular flow developed in multiphase flow with interphase exchange (MFIX). They conducted simulations for the mixture of glass beads (GB) and ground walnut shells (GWS) and compared the simulation results with the experimental data. The initial simulations for the current study were conducted to benchmark our results with those of Bai et al. [218], for which the mixture composition of 50% of GWS particles of size 256 μm and 50% of GB having particle size of 550 μm, was used. Based on the diameter and density of particles, minimum fluidization velocity for each phase was calculated using the Ergun Equation [229]. Four different grid sizes (as shown in Table 4.3) were used for each of the simulations. The particle segregation number was calculated for all the four cases and plotted as a function of time. The model formulated in ANSYS fluent was first validated by comparing the results of the current simulations with the experimental data, obtained from 3D X-ray computed tomography measurements [218], as shown in Figure 4.2. This Figure represents the comparison of experimentally determined PSN and those obtained from simulations for three different superficial gas velocities in the range of 1-3 times of minimum fluidization velocity.

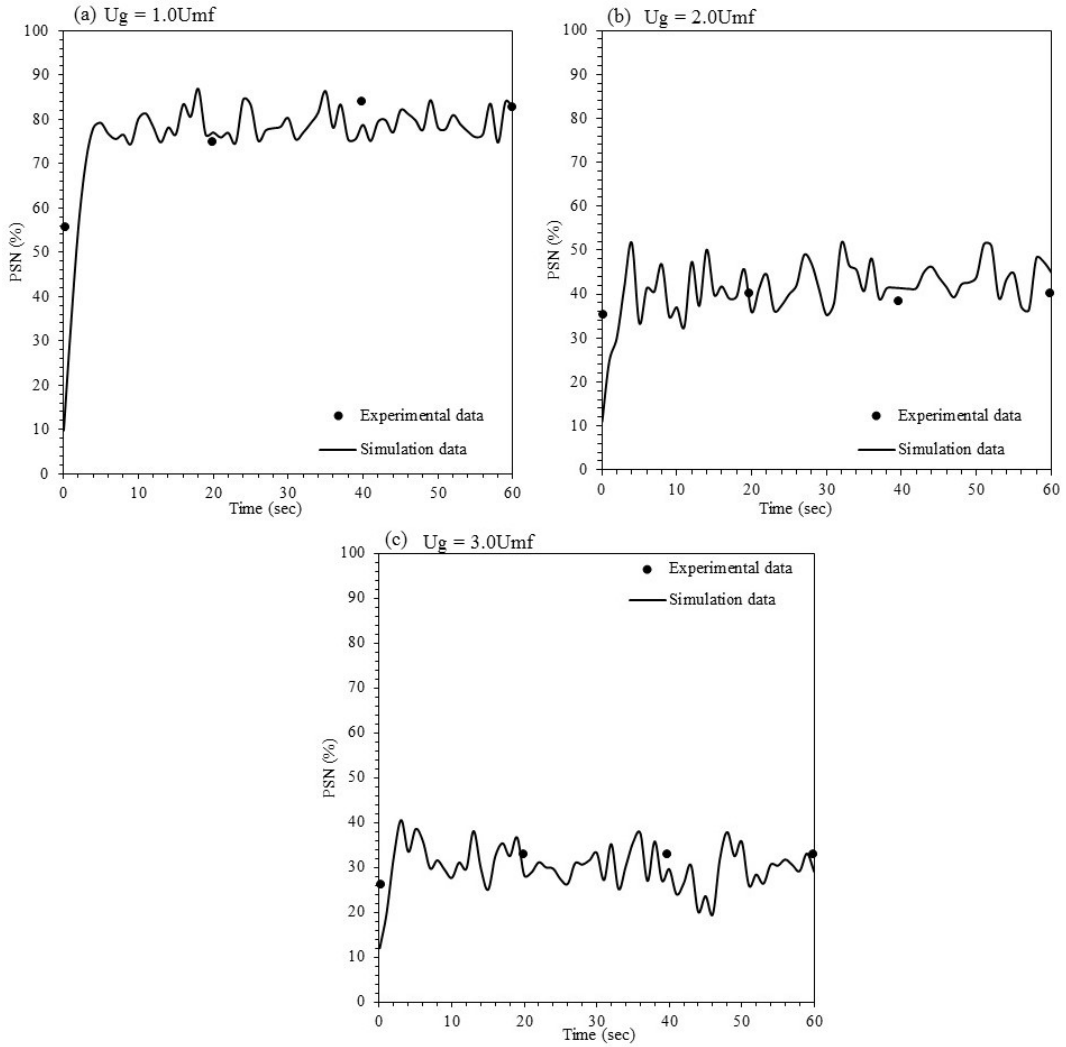

Figure 4.2. Comparison of PSN for GWS and GB from experimental data and current simulations data at three different gas velocities.

PSN values calculated from simulations are in good agreement with the experimental data. The PSN values from experimental data at lower gas velocity i.e. $U_g = U_{mf}$ (Figure 4.2(a)) are in the range of 55-82 % and simulated values are in the range of 70-80 %. Increase in velocity promotes mixing and hence PSN values decrease which is evident from experimental data as well as simulation results. At higher superficial gas velocity $U_g = 2U_{mf}$ (Figure 4.2(b)), the experimental data values of PSN lie in the range of 35-40%, however the PSN values from simulation data are in the range of 10-52 % which on average is consistent with the experimental results. Further increase in gas velocity $U_g = 3U_{mf}$, reduced the experimentally determined PSN to 26-33 % as well the results of simulations to the range of 10-38 % (Figure 4.2(c)). The three cases

of simulations compared with the experimental data at three different superficial gas velocities validate the model to be used for further investigations.

The model was further validated by making a comparison between the current study and the simulated data reported in the literature for the volume fractions of all the phases of multi-fluid models using different grid sizes (Figure 4.3).

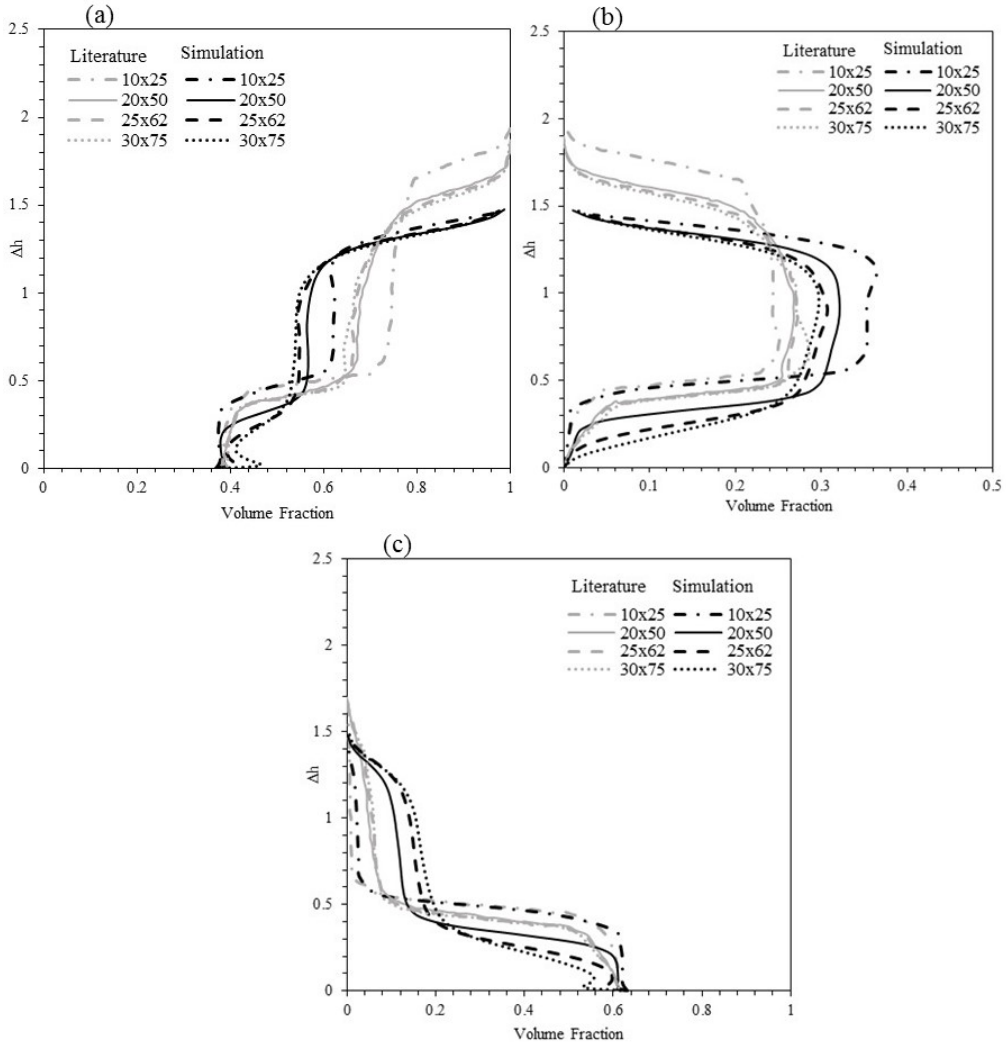

Figure 4.3. Time-averaged volume fraction profiles for (a) air (b) GWS and (c) GB from current simulations and literature data (U_g=1U_{mf}, α_{GB}: α_{GWS}=0.5:0.5, d_{GWS}=256 µm, d_{GB}=550 µm) [218].

The time-averaged volume fractions along the bed height, obtained for different grid sizes from literature showed a deviation for the coarse mesh i.e. 10×25, while for all the three other grid sizes (20×50, 25×62, 30×75) the trends of the air, GWS and GB volume fraction were consistent. Qualitatively, behaviour of volume fractions obtained from the simulations of same materials using same grid sizes was similar to the

literature data, however, values of volume fractions have been under predicted along the bed height. Grid size 10×25 showed major difference for all three phases, however the difference started to reduce with the refinement of the mesh. For gas volume fraction, the results of the last three grids were closer at volume fractions above 0.5 and showed some deviation below this value. For GWS and glass beads the volume fraction profiles of grid size 25×62 and 30×75 were closest and had some consistency with the grid size 20×50 above the bed height. Hence the trends for the two grids (25×62 and 30×75) have shown the consistent behaviour for all the three phases.

Contour plots of volume fraction of ground walnut shells and glass beads at different times are shown in Figure 4.4 and Figure 4.5 respectively. These contours represent the transition of two phases from mixing state to segregation. Contours of GWS represent flotsam, which was initially mixed in the bed and then was segregating towards the top of the bed with the passage of time. GB contours represent the behaviour of jetsam, which as expected, settled down to the bottom of the bed with respect to time.

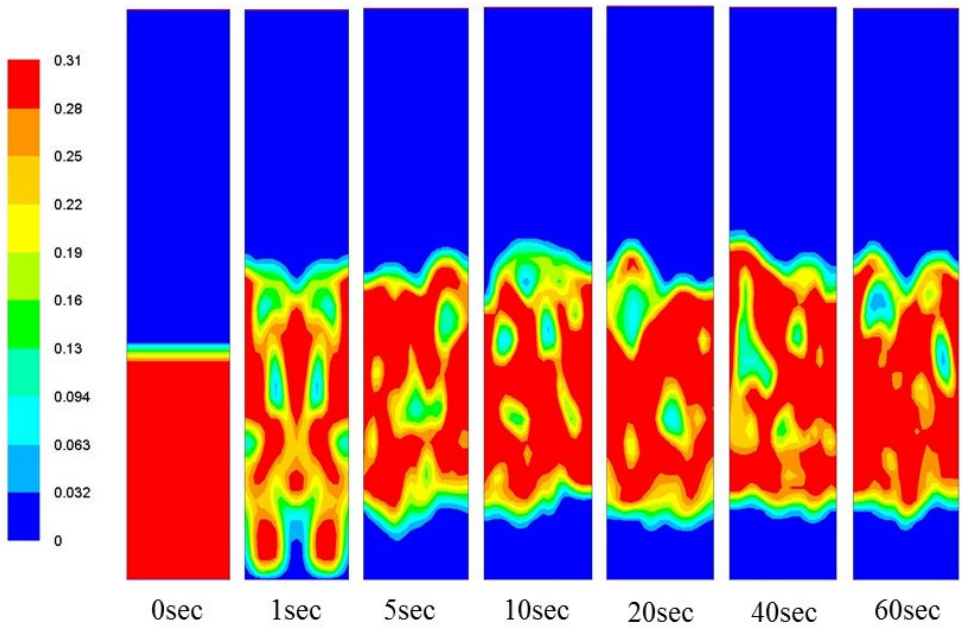

Figure 4.4. Contours of volume fraction for GWS (U_g=1U_{mf}, α_{GB}: α_{GWS}=0.5:0.5, d_{GWS}=256 µm, d_{GB}=550 µm).

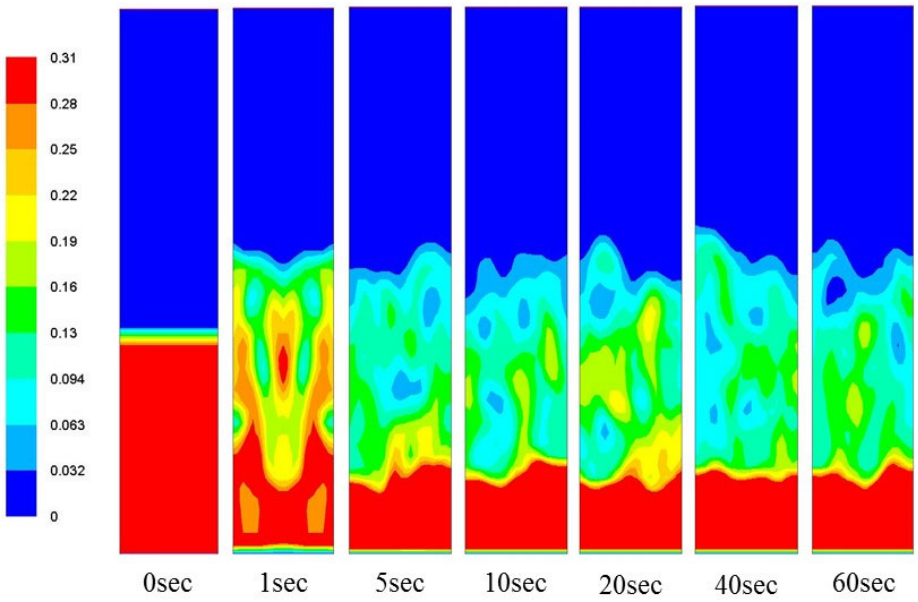

Figure 4.5. Contours of volume fraction for GB (U_g=1U_{mf}, α_{GB}: α_{GWS}=0.5:0.5, d_{GWS}=256 µm, d_{GB}=550 µm).

4.3.2. Simulations of Cellulose and Sand Mixture

Once the model was validated, it was used to simulate the fluidization behaviour of cellulose and sand mixture. Simulations were carried out again for four different grid sizes (shown in Table 4.2). The mixture contained 50 % of cellulose particles of size 250 µm and 50 % of sand particles having particle size of 440 µm. The superficial gas velocity was 0.145 m/sec, which was equivalent to the minimum fluidization velocity when calculated on the sand basis. Initially, the mixture was well mixed and then start to segregate with the time. The simulations run time was 60 seconds. The plots of volume fraction of air, cellulose and sand in the fluidized bed for all four grid sizes are shown in Figure 4.6 (a), (b) and (c) respectively. Volume fraction of air along the bed height has shown some differences for grid size 10×25, and for rest of three grid sizes the change in volume fraction is minimum. Cellulose volume fraction profiles have also shown maximum deviation for the grid size 10×25, however there were less discrepancies in the trends of grid size 20×50 and 25×62. For the sand volume fractions grid size 10×25 and 30×75 showed deviations, while the curves of other two grid sizes were closest to one another.

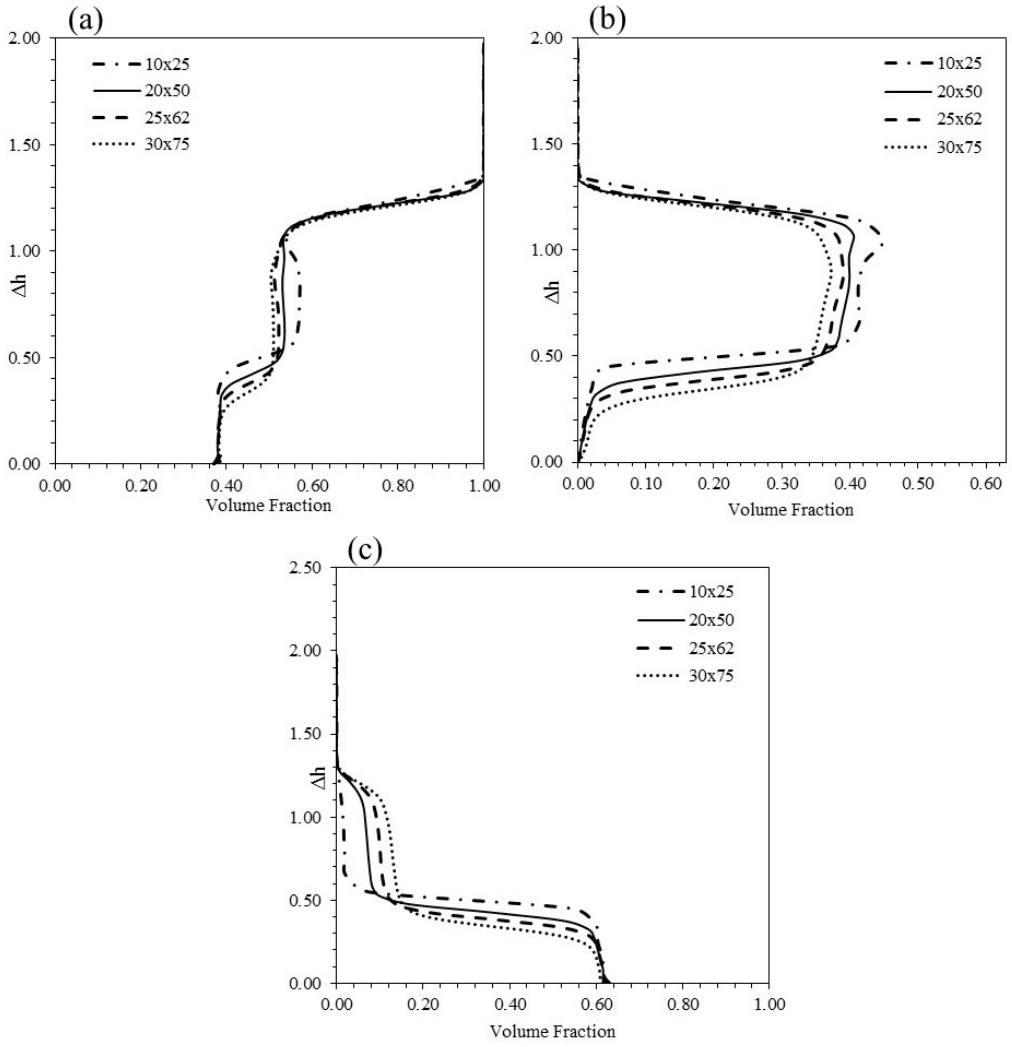

Figure 4.6. Time-averaged volume fraction profiles for (a) air (b) cellulose and (c) sand (U_g=1U_{mf}, α_c: α_s=0.5:0.5, d_c=250 μm, d_s=440 μm).

Contour plots of volume fraction of cellulose and sand at different time intervals are shown in Figure 4.7 and Figure 4.8 respectively. Fraction of flotsam and jetsam can be clearly seen in the contours. Perfect separation for the mixture was not achieved for any of the cases.

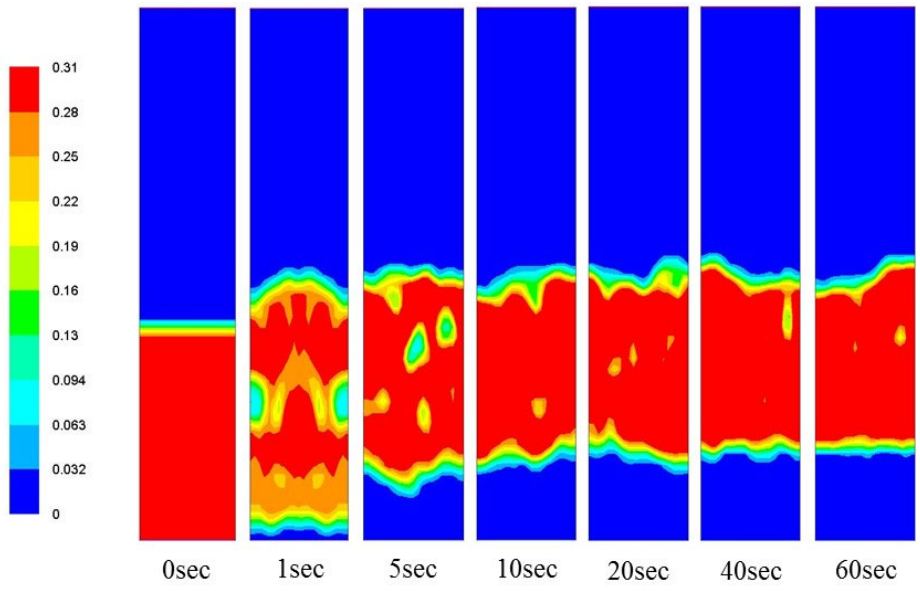

Figure 4.7. Contours of volume fraction of cellulose (U_g=1U_{mf}, α_c: α_s=0.5:0.5, d_c=250 µm, d_s=440 µm).

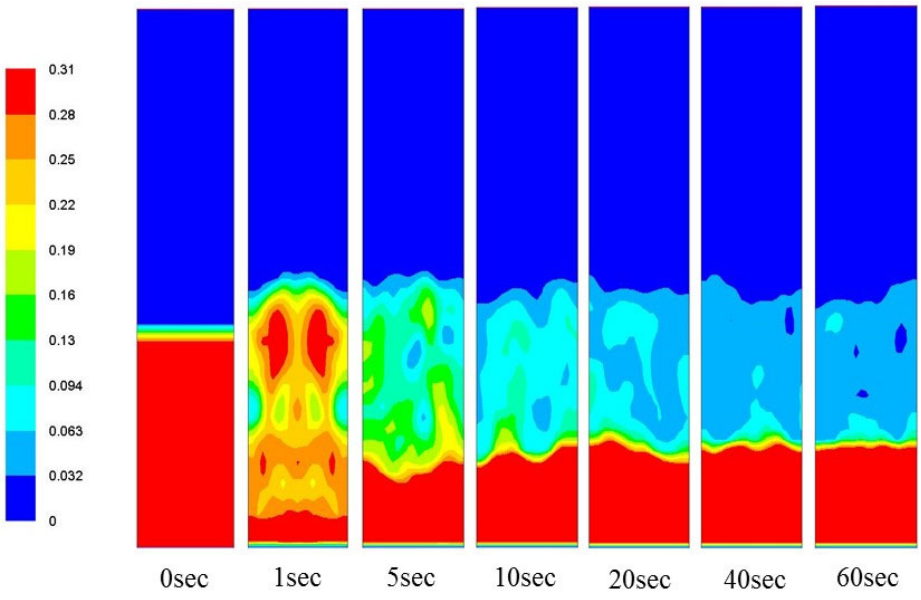

Figure 4.8. Contours of volume fraction of sand (U_g=1U_{mf}, α_c: α_s=0.5:0.5, d_c=250 µm, d_s=440 µm).

PSN was also calculated for all grid sizes and their trends can be seen in Figure 4.9. It was maximum for the grid size 10×25 and reduced with the finer meshes. PSN for 10×25 grid size shows that mixture segregated quickly, just in 5 seconds and obtained an average value of 71%. For the grid sizes 20×50 and 25×62 PSN stabilized in less than 10 seconds and the values were in the range of 59-66%.The PSN values for grid size 30×75 started to stabilize after 10 seconds and the values are below 60 %. Despite of some deviations in 20×50 and 25×62 at longer times, these two grid sizes have

closest values for the first 30 seconds of simulations, which is consistent with the behaviour of phase volume fractions. Grid size 20×50 has been selected for this study, since this grid size and the 25×62 remained consistent for all three phases.

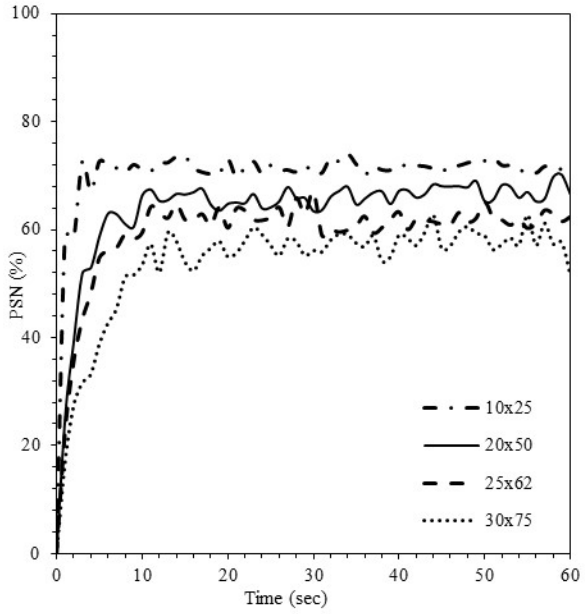

Figure 4.9. PSN calculated for cellulose and sand (U_g=1U_{mf}, α_c: α_s=0.5:0.5, d_c=250 μm, d_s=440 μm).

4.3.3. Effect of Superficial Gas Velocity

Superficial gas velocity is one of the key parameters affecting the fluidization behaviour in a fluidized bed. In this case, four different gas velocities were taken in the range of 1-3 times the minimum fluidization velocity. A 50:50 mixture of cellulose and sand particles with diameter as 440 μm was taken in the bed. Figure 4.10 shows the effect of increase in superficial gas velocity on mixing behaviour in the form of contour plots of cellulose volume fraction. These are time-averaged contours of volume fraction of cellulose in the bed over a 30-second period. It is clear that the mixing of different phases improved with increase in the superficial gas velocity. For example, at minimum fluidization velocity, mixture segregated after 30 seconds, while at higher gas velocities, the mixture stayed in the mixed state for much longer.

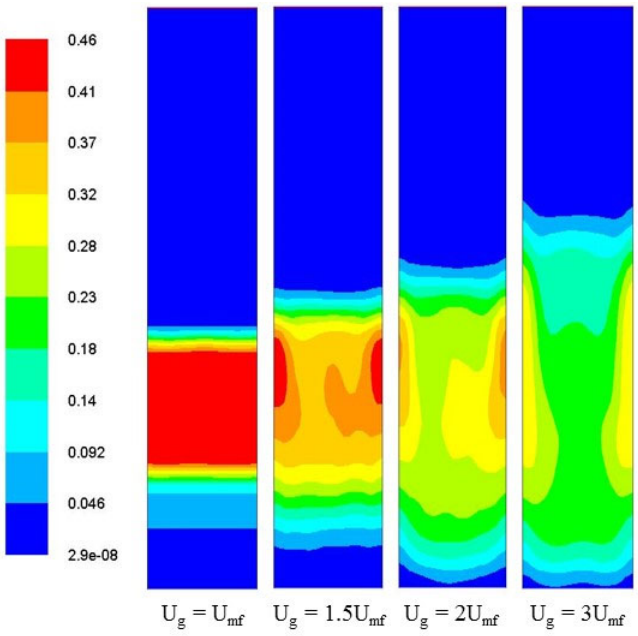

Figure 4.10. Time-averaged contours for volume fraction of cellulose at different velocities after 30 seconds.

Quantitatively, the results of Figure 4.10 are plotted as particle segregation numbers in Figure 4.11, where it is clear that an increase in superficial gas velocity increased the mixing of particles. For U_g=1.0U_{mf} (Fig. 4.11(a)), the mixture, which was in mixed state at the start of simulations, rapidly got segregated with PSN values increasing rapidly and stabilising after about 10 seconds to a range of 80-85 %. Increasing U_g to 1.5U_{mf} (Fig. 4.11(b)) decreased this PSN range to about 60-70 %. Doubling the U_{mf} (Fig. 4.11(c)) not only led to a further reduction in the "stable" PSN range but also showed a greater variation with the range being 20-40%. At U_g=3.0U_{mf}, the stable PSN range became 20-30%, thus indicating greatest mixing state.

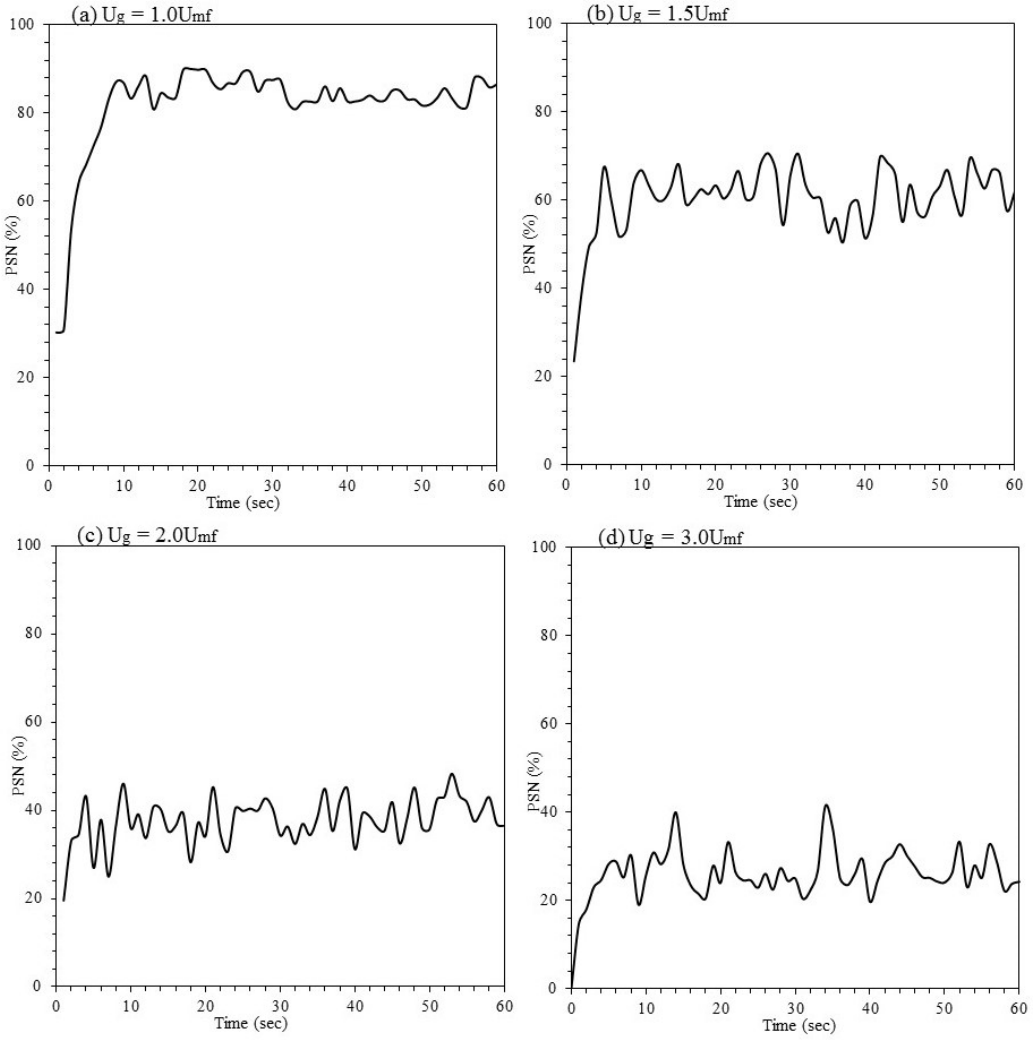

Figure 4.11. PSN for different gas velocities (a) U_g=1U_{mf} (b) U_g=1.5U_{mf} (c) U_g=2U_{mf} (d) U_g=3U_{mf}.

4.3.4. Velocity Distribution

Figure 4.12 represents the vectors of time-averaged velocity magnitude for cellulose in the fluidized bed. The vectors have been plotted for a 50:50 mixture of cellulose and sand particles – both with a diameter of 440 μm with gas velocity varying between 1.5-3.0 times of U_{mf}. It is clear that the cellulose particles experienced widespread recirculation patterns in the bed with particles moving in the upward direction in the centre of the column and in downward direction near the walls. The recirculation became more vigorous with increase in the gas velocity which enhances the mixing between the particles.

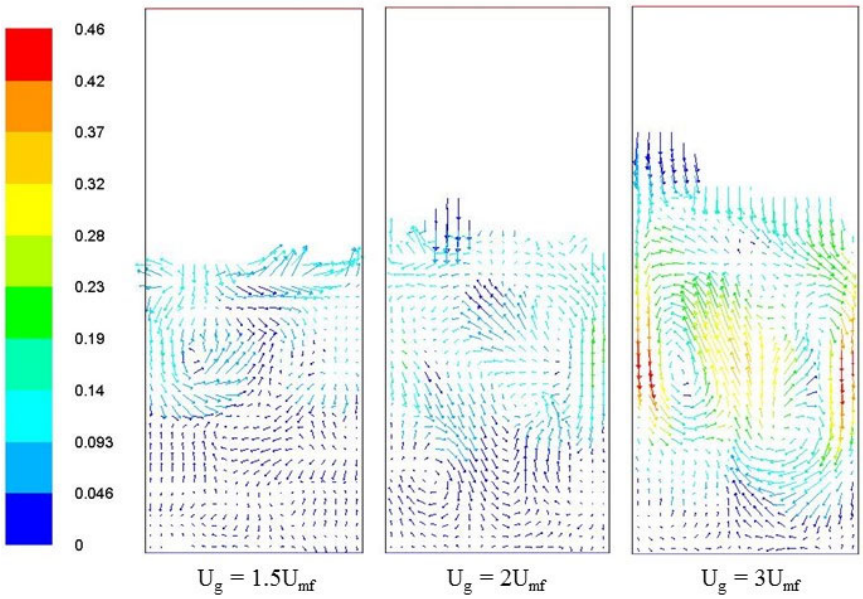

Figure 4.12. Time-averaged velocity magnitude for cellulose at different gas velocities (α_c: α_s=0.5:0.5, d_c=d_s=440μm).

Figure 4.13 shows the vertical velocity of cellulose and sand particles at a dimensionless bed height of 0.5 at three superficial gas velocities. It is evident that the velocity of particles had positive value around the centre of the bed, which progressively decreased before attaining negative value near the walls – thus achieving the core-annulus flow pattern. Both the peak positive velocity value at the centre and negative velocity near the wall increased in the magnitude with increasing superficial gas velocity. The velocity of cellulose particles (shown in darker colour) was numerically higher than the sand particles. This difference in the cellulose and sand particle velocities was greatest at the centre of the bed for superficial velocities greater than $2U_{mf}$. However, for the lower superficial velocities ($1.5U_{mf}$), an opposite trend was apparent, with this difference being greatest near the walls. Finally, the average numerical difference in the cellulose and sand particle velocities was higher for lower superficial gas velocities, which perhaps explains the greater segregation of particles at lower superficial velocities in Figures 4.10 and 4.11.

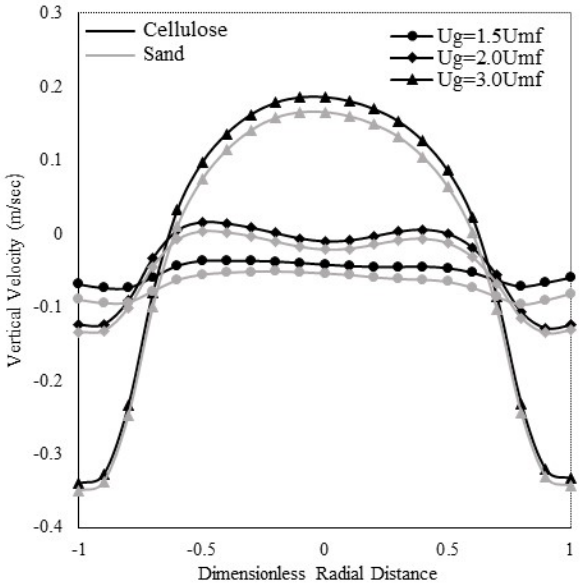

Figure 4.13. Vertical velocity distribution for cellulose and sand particles.

4.3.5. Effect of Particle Size

The effect of particle size on the segregation behaviour was studied by considering cellulose particles of three different diameters i.e. 250, 440 and 900 μm. Fluidization behaviour of cellulose and sand particles in a ratio 0.5:0.5 were simulated using a superficial velocity 3 times the minimum fluidization velocity (0.435 m/s), and by keeping the sand particle diameter at constant value of 440 μm. The calculated PSN for all three cases are shown in Figure 4.14. It is clear that the extent of segregation decreased as the particle size was increased. Particles of cellulose with diameter 250 μm did not mix well with the sand particles of diameter 440 μm, and hence had larger values of PSN (Figure 4.14a). However, as shown in Figure 4.14 (c), larger particles of cellulose with diameter 900 μm mixed well with 440 μm sand particles with PSN being in the range of 10-30 %. In addition, the variations in PSN values for 900 μm cellulose particle were lower than both of the other cases. The reason for this could be the height difference between flotsam and jetsam in the bed, which was more in the case of smaller cellulose particles giving rise to higher fluctuations in PSN values and was less for larger cellulose particles resulting in comparatively smooth values for PSN.

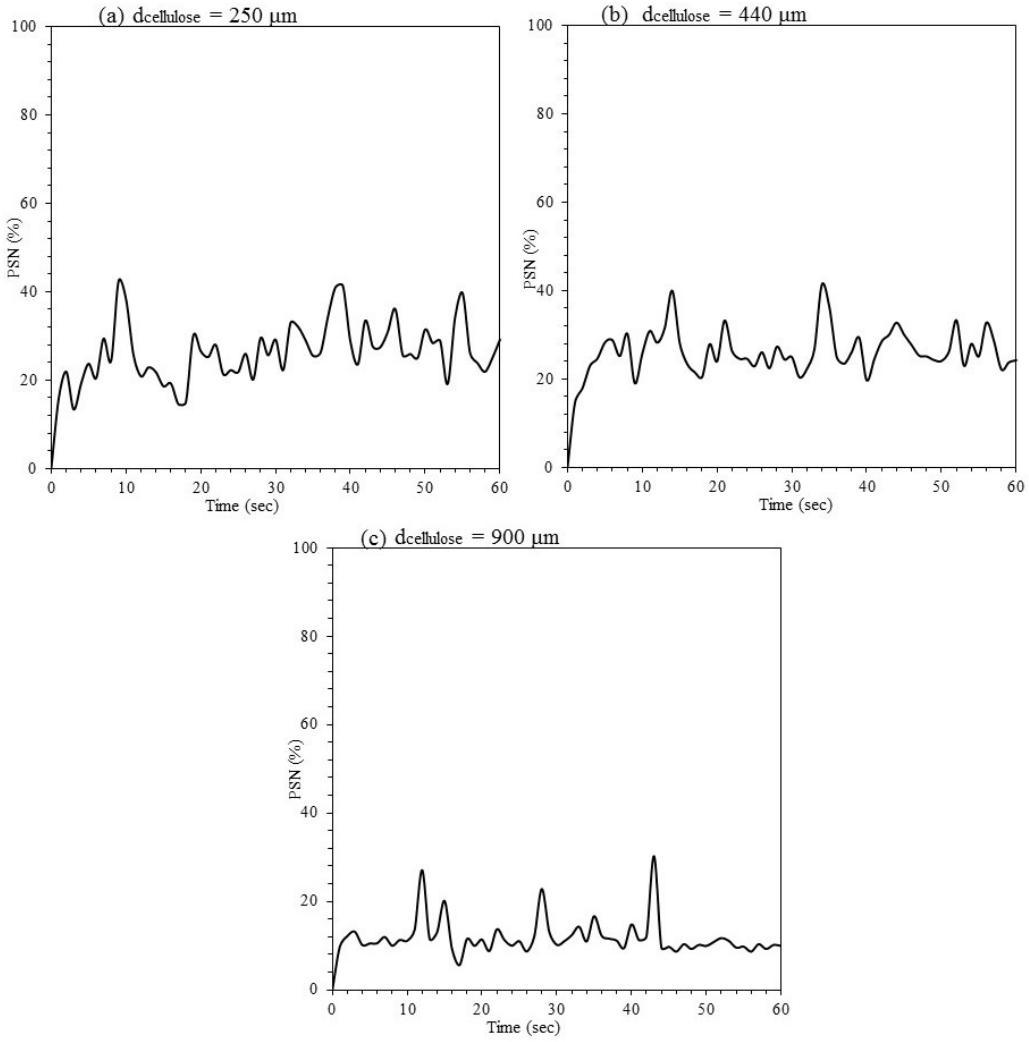

Figure 4.14. PSN for cellulose with different diameters (U_g=3.0U_{mf}, α_c: α_s=0.5:0.5) (a) d_c=250 µm, d_s=440µm (b) d_c=d_s=440µm (c) d_c=900 µm, d_s=440µm.

Figure 4.15 shows the time-averaged granular temperature for a binary mixture of sand and cellulose with the volume fraction as 0.5:0.5 and the particle diameter of 440 µm for both solid phases. The granular temperature has been calculated across the bed at a dimensionless height of 0.003 m. Since granular temperature is the fluctuating kinetic energy of the particles in the fluidized bed, it is higher where there is great motion of particles (as shown in graph). Sand is having higher granular temperature as compared to cellulose in this particular case because of the density difference. Density of sand is more than cellulose and mass of an individual sand particle will be greater than the cellulose particle and thus sand particles will have more kinetic energy of fluctuations.

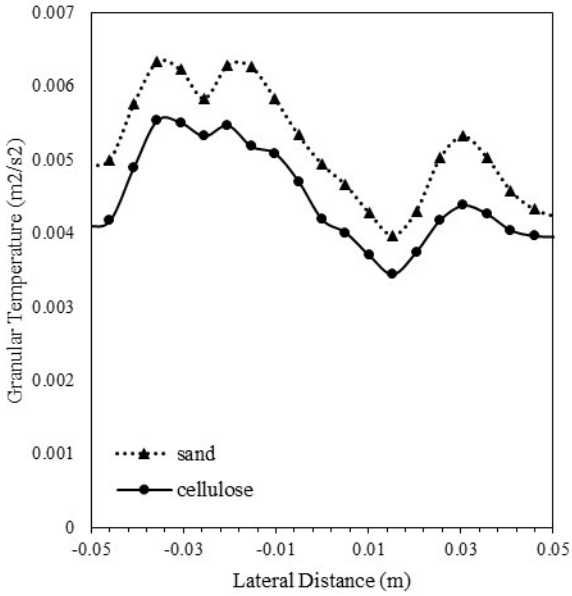

Figure 4.15. Time-averaged granular temperature of sand and cellulose having same particle diameters d_c=d_s=440μm.

Another graph representing the time-averaged granular temperature for a binary mixture of sand and cellulose having particle diameter of 440 and 900 μm respectively is shown in Figure 4.16. In this case cellulose is having higher granular temperature as compared to sand because of the different particle diameters. Mass of an individual cellulose particle will be more than the sand particle and hence will have more kinetic energy of fluctuations.

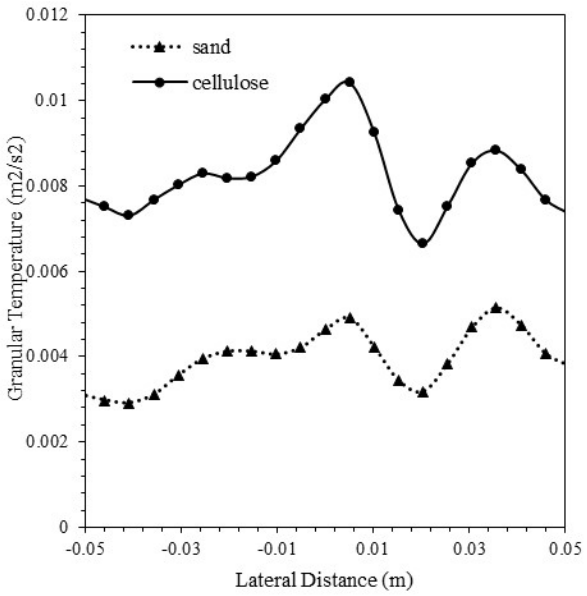

Figure 4.16. Time-averaged granular temperature for sand and cellulose having different particle diameters d_c=900 μm, d_s=440μm.

4.3.6. Effect of Mixture Composition

In this section, three different mixture compositions with cellulose to sand ratios as 0.1:0.9, 0.25:0.75, and 0.5:0.5 were simulated.

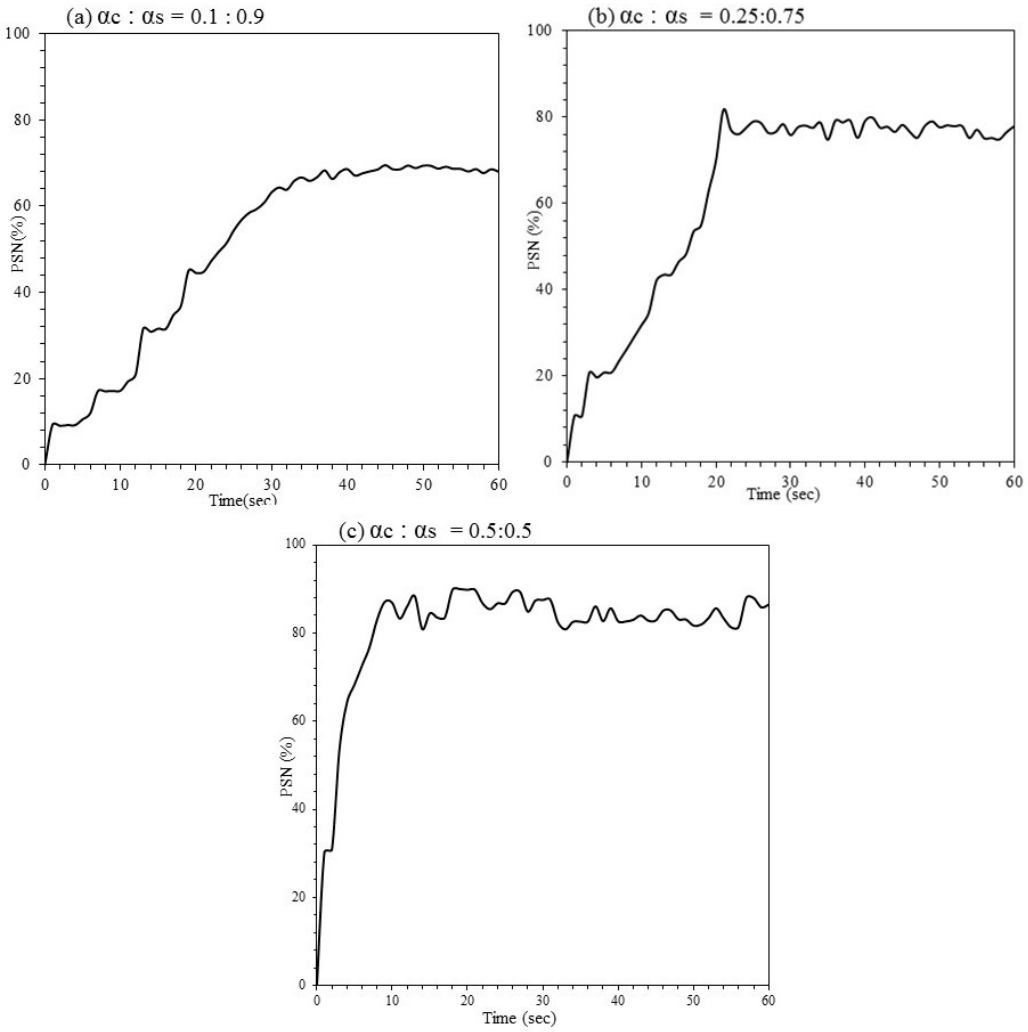

Figure 4.17. PSN for cellulose & sand mixtures with different compositions (U_g=1U_{mf}, d_c=d_s=440 μm).

It is clear from Figure 4.17 that at the start of simulations both sand and cellulose particles were in the mixed state but gradually started to segregate as a function of time. It could also be observed that as the cellulose fraction was increased not only it increased the extent of final segregation but also accelerated the onset of the segregation. For example, at lower cellulose fraction (0.1 cellulose), PSN increased gradually and then became constant after 40 seconds at around 70%. On increasing the cellulose fraction to 0.25, the PSN increased relatively rapidly and became stagnant after 20 seconds at a value of 80%. Using the mixture ratio as 50:50, the segregation

onset occurred even more very rapidly that within 10 seconds of fluidization, the PSN values reached to 90%.

4.3.7. Comparison of 2D and 3D Simulations with Cellulose and Sand Mixture

A set of 3D simulations were also conducted for the same fluidized bed. The configuration used for 3D simulations with meshed surface is shown in Figure 4.18. The initial height for the sand bed was kept as 0.102 m. Cellulose particles of diameter 250 μm and sand particles of diameter 440 μm were used and the mixture composition was specified as 50:50 with the initial volume fraction of cellulose and sand as 0.315. The superficial gas velocity used for this case was 0.435 m/sec which is equivalent to $3U_{mf}$. The results of volume fraction profiles as well as PSN calculated for 3D configuration have been compared to the results of the 2D configuration, calculated using same parameters.

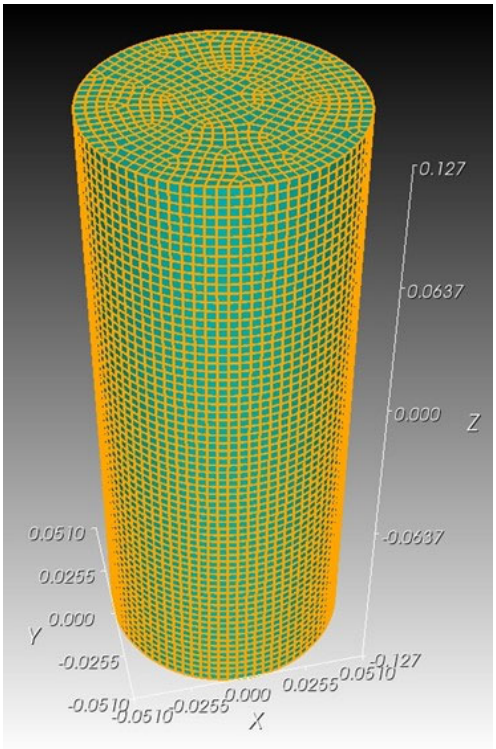

Figure 4.18. Schematic of 3D configuration.

The time-averaged volume fraction profiles obtained from the 3D configuration after 60 seconds of simulation have been compared with the profiles of 2D configuration along the dimensionless bed height (Δh) in Figure 4.19. The profiles of the three phases air (Figure 4.19a), cellulose (Figure 4.19b) and sand (Figure 4.19c) show consistent

behaviour for both configurations in the lower part of the column and some discrepancies are observed at the top of the column above the inert bed height.

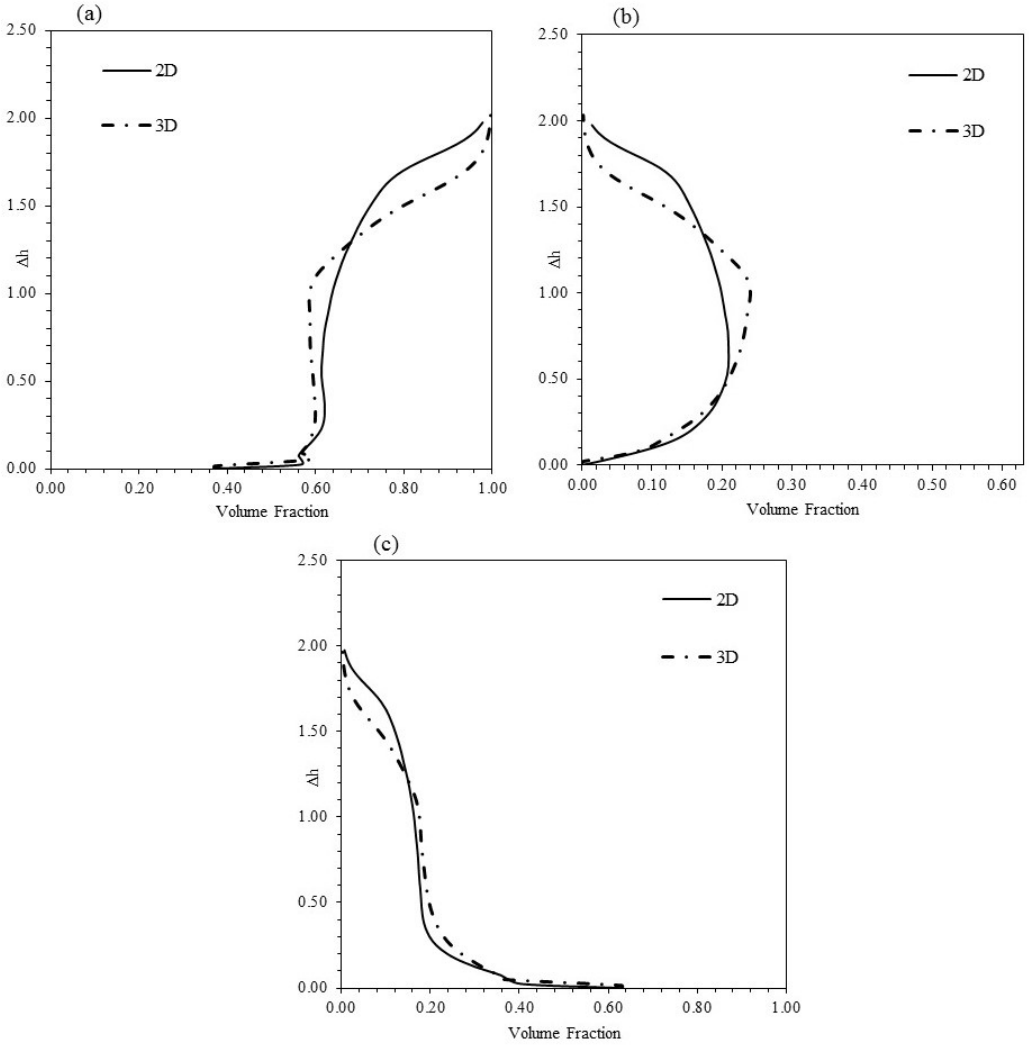

Figure 4.19. Time-averaged volume fraction profiles of 2D vs 3D configuration for (a) air (b) cellulose and (c) sand (U_g=3U_{mf}, α_c: α_s=0.5:0.5, d_c=250 μm, d_s=440 μm)**.**

The fluidization behaviour of the two phases (cellulose and sand) inside the cylindrical tube can be observed through the contour plots of volume fractions of the both phases inside the reactor. The contours for cellulose and sand after 60 seconds of simulations have been shown in Figure 4.20.

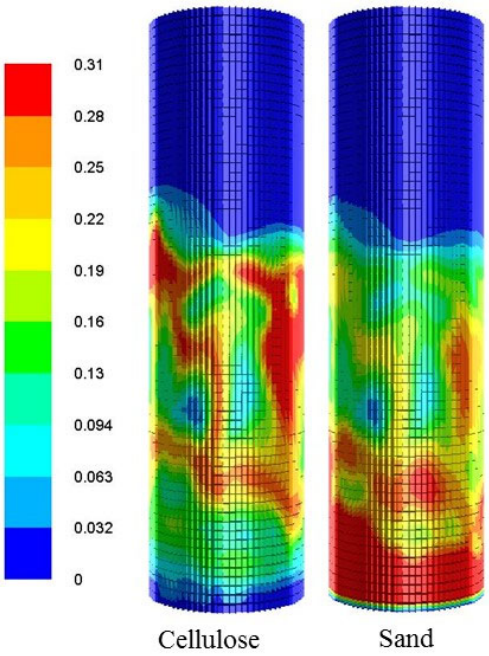

Figure 4.20. Contour plots of cellulose and sand in the interior of 3D-configuration.

Further, to make a comparison of fluidization behaviour of cellulose and sand in 2D and 3D, contour plots of volume fractions of cellulose and sand at different time intervals have been presented in Figure 4.21 and 4.22 respectively. For 3D-configuration a plane has been plotted along the bed height in the middle of the reactor, to observe the volume fraction contours. At the start of fluidization both phases are in mixed state and start to segregate with the passage of time which is almost similar in 2D and 3D results. After certain time cellulose starts to segregate towards the top of the bed as flotsam and sand settles down at the bottom of the bed as jetsam, however the phases are not completely segregated because of the high gas velocity. Hence, the behaviour of the flotsam and jetsam as well as the bed expansion are not effected significantly due to the configuration.

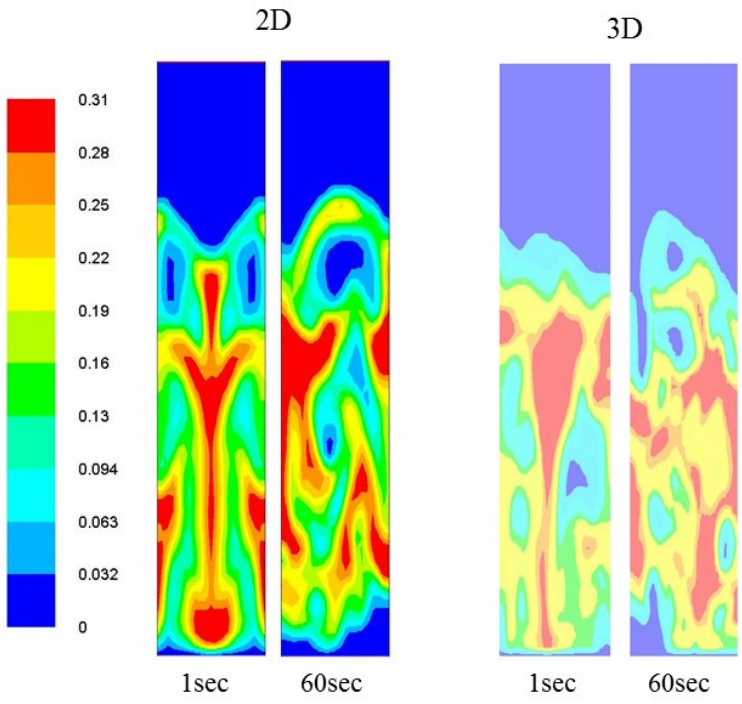

(a) Instantaneous volume fraction of cellulose

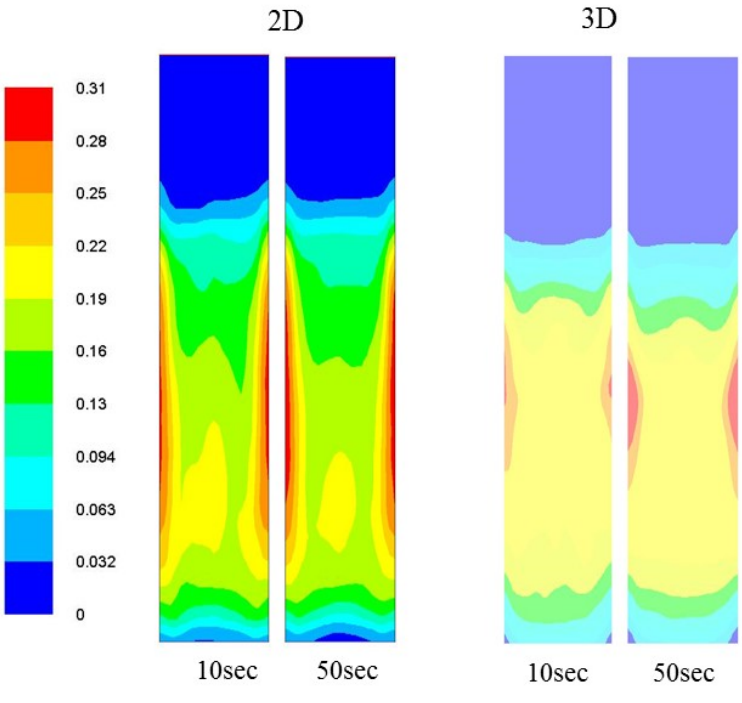

(b) Time-averaged volume fraction of cellulose

Figure 4.21. Contours of (a) instantaneous and (b) time-averaged volume fraction of cellulose.

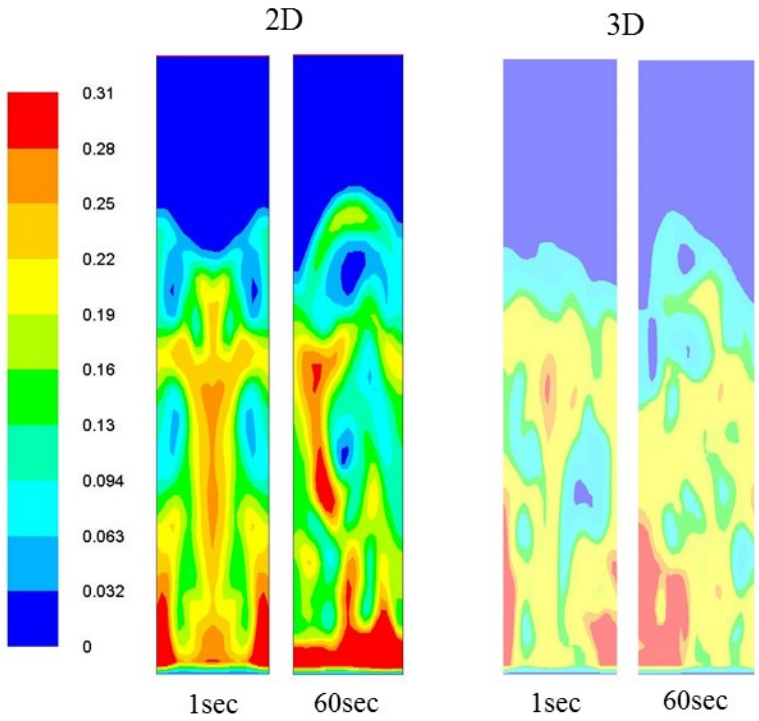

(a) Instantaneous volume fraction of sand

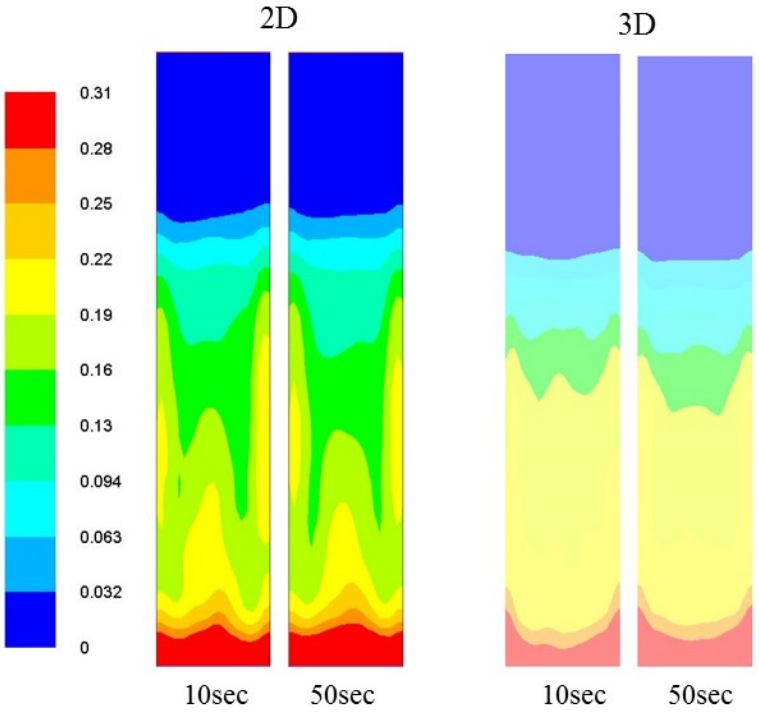

(b) Time-averaged volume fraction of sand

Figure 4.22. Contours of (a) instantaneous and (b) time-averaged volume fraction of sand.

The results of 2D and 3D have also been analysed quantitatively using the PSN. PSN calculated for the 3D configuration has been compared with the PSN calculated for the

same particle size and superficial gas velocity of $U_g = 3U_{mf}$. These are shown in Figure 4.23. The values are in the range 18-40 % because of the higher gas velocity, promoting the mixing behaviour. More precisely PSN values for 2D-cofiguration are in the range 14-41 % and PSN values for 3D-configuration are in range 9-27 %. The values are overlapping at the start of the simulations and with the passage of time the PSN for 3D configuration has low values as well as less fluctuations.

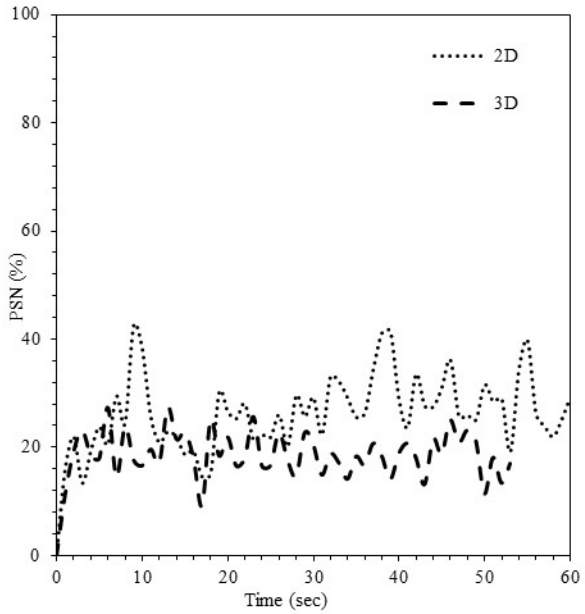

Figure 4.23. PSN calculated for 2D vs 3D configuration.

4.4. Conclusions

In the present work, the effect of different operating parameters on the hydrodynamics particularly mixing and segregation behaviour of cellulose and sand particles in a fluidized bed was studied. The model was validated using experimental and simulations data for the same configuration available in literature for different type of solids. The validated model was then used to study the effect of superficial gas velocity, particle size and mixture composition on the mixing and segregation behaviour. Increase in the gas velocity promoted the mixing between cellulose and sand particles. This was apparent not only from the velocity distribution of particles inside the bed but also the PSN values, which decreased rapidly with an increase in the gas velocity from $1.0U_{mf}$ to $3.0U_{mf}$. It was observed that the cellulose particles with larger diameters mixed well with smaller and heavier particles of sand. PSN values were also calculated for different mixture compositions of cellulose and sand. On

increasing the fraction of lighter cellulose particles, the extent of segregation increased with an acceleration in the onset of segregation. Qualitative as well as quantitative analysis was also made for 3D-configuration and then compared to the results of 2D-configuration.

CHAPTER 5 DISTRIBUTED ACTIVATION ENERGY MODELLING OF CELLULOSE PYROLYSIS IN A FLUIDIZED BED REACTOR

5.1. Introduction

To model the whole process of pyrolysis in fluidized bed systems, a multiphase fluid model has to be integrated with reaction kinetics using computational fluid dynamics (CFD). Several research articles [164,171,235,170,236,169] are available in the literature discussing the coupling of biomass pyrolysis models with CFD. Xue et al. [169] developed a multi-fluid model for bagasse and cellulose pyrolysis using CFD simulations and predicted the key features of the fast pyrolysis in a fluidized bed reactor [169]. The model was validated with the experimental data from a lab-scale bubbling fluidized bed reactor. The product yield of pure cellulose pyrolysis from simulations was in good agreement with the experimental results [170]. Furthermore, the results for red oak and switchgrass pyrolysis were also compared. Recently, a model was developed by Jalalifar et al. [231] using Eulerian-Eulerian approach for pure cellulose pyrolysis in a bubbling fluidized bed reactor. The model [232] was later used for biomass pyrolysis in a bubbling fluidized bed reactor to investigate the impact of different operating parameters on the product yield.

Since cellulose is the major component of lignocellulose biomass, there are several kinetic schemes reported in the literature which are used to understand the cellulose pyrolysis but not all of them have been used for the numerical simulation of the pyrolysis. Broido-Shafizadeh scheme is the most commonly used for cellulose pyrolysis modelling. This scheme only includes a single value of activation energy for each reaction. Since cellulose pyrolysis involves multiple reactions with different kinetic energies, it is essential to include the range of activation energies. In addition, as reported by Burnham et al. [117] first-order reaction constants derived from single heating rate do not always give true values of frequency factor, A and activation energy, E and specially in case of cellulose, the product yield is affected because of the high values of A. The distributed activation energy model (DAEM) as discussed in Chapter 3, includes the activation energies with a distribution (σ) and has gained researcher's attention in recent years. It has been implemented to better understand the

thermal decomposition of biomass [233–236]. DAEM has been discussed in detail in chapters 2 and 3. Xue et al. [170] performed experiments using a lab-scale fluidized bed reactor with different biomass and cellulose as feed material. A CFD model was also developed to better understand the biomass pyrolysis in a bubbling fluidized bed reactor and was simulated using MFIX [169]. The model was validated first and then used for studying the effect of operating parameters [169,170]. Xiong et al. [237] simulated a laboratory-scale bubbling fluidized bed reactor to predict the product yield of biomass pyrolysis and the fluctuations in the tar yield with hydrodynamics of bubbling bed. The model was further extended and coupled with DAEM to study the influence of distribution of activation energy [238]. The researchers focused on the comparison of two different distribution schemes (Gaussian and Logistic) and their effect on the exit tar yield. Also, the effect of variation in activation energy was accounted for by using coefficient of variation, skewness and kurtosis. Morphological changes in the cellulose structure during the pyrolysis process have revealed that the process involves several reactions which have different activation energies. Hence, using DAEM for cellulose pyrolysis indeed gives accurate product yield when compared with single activation energy value.

The objective of the present work is to develop an integrated model of the cellulose pyrolysis in a fluidized bed reactor encompassing both CFD and DAEM. Broido-Shafizadeh scheme for cellulose decomposition has been selected and the kinetics obtained from TGA (discussed in Chapter 3). Activation energies of the respective reactions have been specified using a distribution function, and the effect of this distributed activation energy on the pyrolysis product yield (yield of tar, char and gases) has been determined. This study is divided into two parts: first part includes the model validation for pure cellulose using CFD and second part focuses on the coupling of DAEM to multiphase model.

5.2. Mathematical Modelling Description

Multiphase reactive CFD models are formulated by coupling the kinetics of devolatilization of cellulose particles with the hydrodynamics of fluidizing bed in the reactor.

5.2.1. Kinetic Model

The kinetic scheme used in this work is shown in Figure 5.1. This is the Broido-Shafizadeh scheme and was first proposed by Shafizadeh and Bradbury [11,239,240] as a set of three reactions and was later modified to include the tar decomposition. According to this scheme, cellulose (Cell) is converted to some intermediate named as "active cellulose" (A.Cell) in the first reaction. The intermediate (A.Cell) then immediately decomposes to other products tar (T), char (C) and gases (G) following two parallel reaction schemes. Tar (T) produced as a result of second reaction undergoes decomposition to produce gases (G). Cellulose, active cellulose and char are included in the solid phase (s1) while tar vapors and the gases are considered as the gas phase (g) along with the inert gas nitrogen (N_2). Sand particles (s2) make the secondary solid phase, this phase does not react and act as an inert fluidizing media in the reactor.

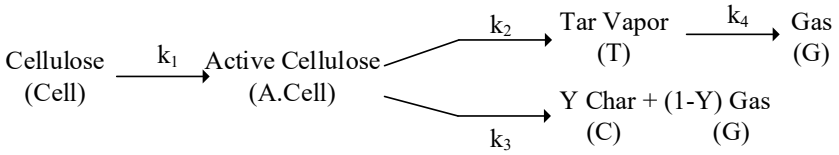

Figure 5.1. Cellulose reaction scheme [11]

The rate of generation and consumption of the solid phase (s1) and gas phase (g) species can be defined as:

Cellulose,

$$\boldsymbol{R_{s1,Cell} = -k_1 \alpha_{s1} \rho_{s1} X_{s1,Cell}} \tag{5.1}$$

Active Cellulose,

$$\boldsymbol{R_{s1,A.Cell} = k_1 \alpha_{s1} \rho_{s1} X_{s1,Cell} - (k_2 + k_3) \alpha_{s1} \rho_{s1} X_{s1,A.Cell}} \tag{5.2}$$

Tar Vapors,

$$\boldsymbol{R_{g,T} = k_2 \alpha_{s1} \rho_{s1} X_{s1,A.Cell} - k_4 \alpha_g \rho_g X_g} \tag{5.3}$$

Gas,

$$R_{g,G} = k_3 \alpha_{s1} \rho_{s1} X_{s1,A.Cell}(1 - Y) + k_4 \alpha_g \rho_g X_g + \left[\alpha_{s1} \rho_{s1} X_{s1,A.Cell}(k_2 + k_3)\right] \frac{\rho_g}{\rho_b} + \left[\alpha_{s1} \rho_{s1} X_{s1,A.Cell} k_3 Y\right] \frac{\rho_g}{\rho_c} \quad (5.4)$$

Char,

$$R_{s1,C} = \alpha_{s1} \rho_{s1} X_{s1,A.Cell} k_3 Y \quad (5.5)$$

All the reactions in this scheme are considered first-order and the reaction kinetics are determined according to Arrhenius law depending on pre-exponential factor A, activation energy E, and the temperature T, as:

$$k = A e^{-E/RT} \quad (5.6)$$

"Y" represents the ratio of char formed in the third reaction, which is 0.35 [241] in this case. The values of kinetic parameters are provided in Table 5.1. The heat of reaction data is given in Table 5.2:

Table 5.1. Kinetic data.

Reaction constant	Pre-exponential factor, A (sec^{-1})	Activation energy, E (kJ/mol)	Reference
k_1	2.8×10^{19}	242.4	[241]
k_2	3.28×10^{14}	196.5	[241]
k_3	1.3×10^{10}	150.5	[241]
k_4	4.25×10^{6}	108.0	[241]

Table 5.2. Heat of reaction data.

Reaction	Heat of reaction (kJ/kg)	Reference
Δh_1	0	[12]
Δh_2	255	[12]
Δh_3	-20	[12]
Δh_4	-42	[242]

Thermo-physical properties of species involved in the pyrolysis of cellulose are presented in Table 5.3.

Table 5.3. Thermo-physical properties of species.

Species	Density, ρ (kg/m^3)	Particle Diameter, d_s (m)	Molecular Weight, M.W (kg/kmol)	Heat Capacity, C_p (J/kg.K)	Dynamic Viscosity, μ (kg/ms)	Thermal Conductivity, k (J/kg.K)
Cellulose	400	5.0×10^{-5}	342.297	2300	---	0.18
Active Cellulose	400	5.0×10^{-5}	342.297	2300	---	0.18
Tar	---	---	100	950	1.3×10^{-5}	1.32
Char	2330	5.0×10^{-5}	12.01	1100	---	0.0878
Gases	---	---	23	4545.09	1.32×10^{-5}	0.0582
Nitrogen	---	---	28.04	1040.7	3.49×10^{-5}	0.0242
Sand	2649	5.2×10^{-4}	60.08	860	---	0.2

5.2.2. Distributed Activation Energy Model

Distributed activation energy model is comprised of a large number of independent parallel reactions with different activation energies, represented by a continuous distribution function [55]. This distribution function may be Weibull, Logistic or Gaussian. In this work Gaussian distribution function has been used which can be represented by the following equation:

$$\boldsymbol{f(E) = \frac{1}{\sigma\sqrt{2\pi}} exp\left[-\frac{(E-E_0)^2}{2\sigma^2}\right]} \quad (5.7)$$

where E_0 is the mean activation energy and "σ" is the standard deviation. DAEM has widely been applied to better understand the complexity of biomass pyrolysis and predict the reaction kinetics for different lignocellulosic biomass material [48,203,243].

5.2.3. Multi-fluid Model

The multiphase model used in this study describes the gas and solid phases as inter-penetrating continua in Eulerian-Eulerian framework. During the pyrolysis in a fluidized bed reactor there exist three different phases: gas phase as primary phase and the two solid phases as the secondary phases. Primary phase is a gas-mixture which contains tar vapors, gases from two different reactions and inert fluidizing gas, nitrogen. One of the secondary phase comprises of cellulose, active cellulose and char

with sand making the second solid phase which is an inert bed of particles. The two solid phases are differentiated based upon their physical and thermal properties. Conservation of mass, momentum, energy and the other basic laws is specified using the models described below [220]. In addition to basic conservation laws, some other correlations necessary for the implementation of multi-fluid model are also discussed in the following sections:

5.2.3.1 Gas Phase

For the gas-mixture phase the conservation of mass, momentum and energy equations are formulated. The continuity equation can be defined as:

$$\frac{\partial}{\partial t}(\alpha_g \rho_g) + \nabla.(\alpha_g \rho_g \vec{v}_g) = R_g \tag{5.8}$$

ρ_g, α_g and $\vec{v}_g$ are the density, volume fraction and velocity of the gas-mixture phase. R_g represents the source term for the consumption/generation of the gas phase species in the reactor. This source term defines the interphase mass transfer taking place at the solid-fluid interphase due to the chemical reactions and is the sum of the reaction rates of all the species in the gas phase, which can be defined as:

$$R_g = R_{g,T} + R_{g,G} \tag{5.9}$$

For ith specie in the gas phase, the conservation equation is given as:

$$\frac{\partial}{\partial t}(\alpha_g \rho_g X_{g,i}) + \nabla.(\alpha_g \rho_g \vec{v}_g X_{g,i}) = -\nabla.(\alpha_g \rho_g D_{g,i} \nabla X_{g,i}) + R_{g,i} \tag{5.10}$$

Where $R_{g,i}$ represents the reaction rate term for the ith specie and $X_{g,i}$ and $D_{g,i}$ are the mass fraction and diffusion coefficient respectively.

The momentum balance for the gas phase can be defined using Navier-Stokes equation as:

$$\frac{\partial(\alpha_g \rho_g \vec{v}_g)}{\partial t} + \nabla(\alpha_g \rho_g \vec{v}_g \vec{v}_g) = -\alpha_g \nabla P + \nabla.\vec{\tau}_g + \alpha_g \rho_g \vec{g} + \sum_{s=1}^{n}(\vec{R}_{gs} + \vec{v}_{sg}\dot{m}_{sg} - \vec{v}_{gs}\dot{m}_{gs}) \tag{5.11}$$

In the first term on the right side of the equation, P represents the pressure shared by all the phases. The second term, $\vec{\tau}_g$ is the stress-strain tensor and the acceleration due to gravity is represented by $\vec{g}$. $\vec{R}_{gs}$ is the interaction force between the gas phase and

the solid phases due to momentum transfer happening because of the drag force between the different phases and the last two terms are representing the mass transfer between the phases due to thermal degradation of particles.

For gas phase the energy conservation equation is given as:

$$\frac{\partial(\alpha_g \rho_g H_g)}{\partial t} + \nabla.\left(\alpha_g \rho_g \vec{v}_g H_g\right) = -\nabla.\vec{q}_g + \Delta H_{rg} + \sum_{s=1}^{n} H_{sg} \quad (5.12)$$

Where, H_g is the specific heat of the gas phase and $\vec{q}_g$ is the conductive heat flux. Enthalpy change occurring due to chemical reactions is included using source term ΔH_g and the inter-phase heat transfer between the gas and the solid phase is given byH_{sg}. These terms can be defined as:

$$H_g = \int C_{p,g} dT_g \quad (5.13)$$

$$H_{sg} = h_{sg}\left(T_{sn} - T_g\right) \quad (5.14)$$

$C_{p,g}$ = Specific heat of the gas phase at constant pressure

h_{sg} = Convective heat transfer coefficient

T_{sn} = Temperature of nth solid phase

T_g = Gas phase temperature

5.2.3.2 Solid Phase

For each *sth* solid phase, in a system of *n* solid phases the equations of continuity, momentum and energy are formulated and discussed in this section. Continuity equation for solid phase has been defined as:

$$\frac{\partial}{\partial t}(\alpha_{sn}\rho_{sn}) + \nabla.(\alpha_{sn}\rho_{sn}\vec{v}_{sn}) = R_{sn} \quad (5.15)$$

ρ_{sn}, α_{sn} and $\vec{v}_{sn}$ are the bulk density, volume fraction and velocity of the nth solid phase respectively. The source term for solid phase R_{sn} is the sum of the reaction rates of all the species in the solid phase including cellulose, active cellulose and char.

$$R_{sn} = R_{s1,Cell} + R_{s1,A.cell} + R_{s1,C} \quad (5.16)$$

For ith specie in the gas phase, the conservation equation is given as:

$$\frac{\partial}{\partial t}\left(\alpha_{sn}\rho_{sn}X_{sn,i}\right)+\nabla.\left(\alpha_{sn}\rho_{sn}\vec{v}_{sn}X_{sn,i}\right)=-\nabla.\left(\alpha_{sn}\rho_{sn}D_{sn,i}\nabla X_{sn,i}\right)+R_{sn,i} \quad (5.17)$$

Momentum equation for *sth* solid phase is:

$$\frac{\partial(\alpha_{sn}\rho_{sn}\vec{v}_{sn})}{\partial t}+\nabla(\alpha_{sn}\rho_{sn}\vec{v}_{sn}\vec{v}_{sn})=-\alpha_{sn}\nabla p-\nabla p_{sn}+\nabla.\vec{\tau}_{sn}+\alpha_{sn}\rho_{sn}\vec{g}+\sum_{l=1}^{N}\left(R_{ln}+\vec{v}_{sg}\dot{m}_{sg}-\vec{v}_{gs}\dot{m}_{gs}\right) \quad (5.18)$$

In the momentum transport equation, p_{sn} represents of nth solid phase. $\vec{\tau}_{sn}$ is the stress-strain tensor for nth solid phase and the acceleration due to gravity is represented by $\vec{g}$. $\vec{R}_{ln}$ is the interaction force between lth gas phase or sth solid phase and nth solid phases including momentum transfer due to the drag force between the gas and the solid phase. The last two terms are representing the mass transfer between the phases same as explained for gas phase in equation 4.

The energy conservation equation for nth solid phase will be:

$$\frac{\partial(\alpha_{sn}\rho_{sn}H_{sn})}{\partial t}+\nabla.(\alpha_{sn}\rho_{sn}\vec{v}_{sn}H_{sn})=-\nabla.\vec{q}_{sn}+\Delta H_{rsn}+\sum_{s=1}^{n}H_{gs} \quad (5.19)$$

Where, H_{sn} and $\vec{q}_{sn}$ are the specific heat and conductive heat flux of the nth solid phase. ΔH_{rsn} is the source term which incorporates the enthalpy change due to chemical reactions in the solid phase. However, the inter-phase heat transfer between the gas and solid phases is given by H_{gs}. Since there is no radiative heat transfer in the system hence the terms including radiative heat transfer have been neglected. These terms can be defined as:

$$H_{sn}=\int C_{p,sn}dT_{g} \quad (5.20)$$

$$H_{gs}=h_{gs}\left(T_{g}-T_{sn}\right) \quad (5.21)$$

$C_{p,g}$ = Specific heat of the gas phase at constant pressure

h_{gs} = Convective heat transfer coefficient between the gas phase and nth solid phase

According to kinetic theory of granular flow (KTGF) kinetic energy of fluctuating particles needs to be defined for a multi-phase system. This kinetic energy is usually specified using granular temperature of the nth solid phase, θ_{sn}. Granular temperature

is proportional to the mean square of the fluctuating velocity of solid particles. The algebraic form of this fluctuating energy is given as:

$$\frac{3}{2}\frac{\partial(\alpha_{sn}\rho_{sn}\theta_{sn})}{\partial t} = -\left(p_{sn}\bar{\bar{I}} + \bar{\bar{\tau}}_{sn}\right):\nabla\vec{v}_{sn} + -\gamma_{\theta sn} + \Phi_{ln} \quad (5.22)$$

This equation is a combination of different forms of energy. These terms may be defined as:

$-\left(p_s\bar{\bar{I}} + \bar{\bar{\tau}}_s\right):\nabla\vec{v}_s$ = Energy produced due to solid stress tensor

$\gamma_{\theta s}$ = Energy dissipation due to collisions for nth solid phase

Φ_{ls} = Energy exchange between the *lth* gas or *sth* solid phase and nth solid phase

Other than basic conservation laws, the constitutive relations for gas-solid interaction in a multiphase system are required which have been described in detail in Appendix A. This includes the stress-strain tensor relations for gas and solid phase, solids pressure and drag models. Fourier's law has been used to calculate the conductive heat flux and for convective heat transfer coefficient Nusselt number correlation by Gunn [244] has been used.

5.3. CFD Simulation Strategy

The governing equations of momentum, pressure and volume fractions were solved using phase coupled SIMPLE algorithm in ANSYS FLUENT version 17.2. The coupled algorithm solves the momentum and pressure-based continuity equations together and pressure correction equation coefficients are calculated based on the momentum equations. According to this scheme the coupled per phase velocities are solved in a segregated manner [220]. However, the algorithm is coupled with iterative time advancement scheme in which all the equations are solved through iterations until the convergence occurs.

5.3.1. Solution Procedure with Initial and Boundary Conditions

The configuration used for this part of work is same as the one used in experiments and simulations of Xue et al. [169,170]. The computational domain for this system is a 2-dimensional (2-D) reactor which has been divided into fixed number of control volumes through specific number of grid cells in horizontal and vertical direction. The

2-D reactor is shown in Figure 5.2 with the reactor configuration data presented in Table 5.4.

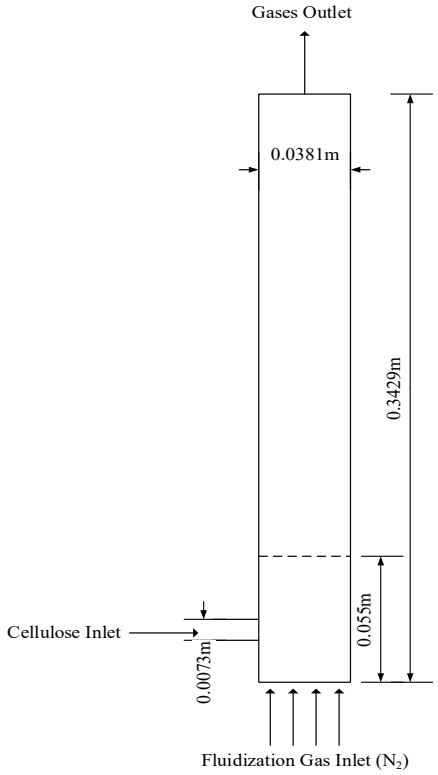

Figure 5.2. Fluidized bed reactor for cellulose pyrolysis.

Table 5.4. Reactor dimensions and computational domain data.

Parameter	**Value**
Reactor Height, H	0.3429 m
Reactor Diameter, D	0.0381 m
Bed Height, h	0.055 m
Biomass inlet Diameter, d	0.0073 m
Grid Cells in horizontal direction	10
Grid Cells in vertical direction	91

Sand being used as an inert fluidizing material in the bed was patched to the height of 0.055 m with the volume fraction of 0.59 and with an initial temperature of 773 K. The inlet velocity of the bed material was zero. Cellulose was entered to the reactor at a

flow rate of 2.77×10^{-5} kg/sec through the side inlet in a continuous manner at a temperature of 300 K. The gas phase entered through the gas inlet at the bottom of the reactor with the superficial gas velocity of $U_g = 3.5U_{mf}$ and a temperature of 773 K. At the outlet of the reactor pressure boundary condition was specified. The walls were kept isothermal with a constant temperature of 773 K. The value of co-efficient of restitution was taken as 0.97 and the angle of internal friction was 55. For boundary conditions of walls, no slip was specified for the gas phase while for the solid phase partial slip condition was used.

Energy conservation and species transport models were used to account for the pyrolysis reactions. The reaction terms have been integrated using a stiff ODE (Ordinary Differential Equations) solver. For time discretization, second order implicit method was used with the time step of 10^{-4} sec. QUICK algorithm has been used to calculate the volume fraction of each phase. Conservation equations for momentum, energy and the species transport equations have been solved using second order (upwind) method. All simulations were run for the simulation time of 150 seconds when pseudo-steady state was achieved in the system.

5.4. Results and Discussion

5.4.1. Model Validation

In this study, the CFD model was validated using the experimental data of Xue et al. [170], and the same model has been used to calculate the pyrolysis product yield with distributed activation energy model which will be discussed in the next section in detail. In this part of the research, all operating parameters and material properties have been kept same as of experimental data. The product yield (η) was calculated using the equation:

$$\eta(t) = \frac{\int_0^t \int_{outlet} (\rho \alpha v X) dA dt + \int_{reactor} (\rho \alpha X) dV}{M_{cell\_feed}} \quad (5.23)$$

The comparison of the product yield obtained from simulations with the experimental data is presented in Table 5.5.

Table 5.5. Pyrolysis product yield (wt. %) comparison between experiment and simulations for pure cellulose

Data	Bio-oil (wt.%)	Char (wt.%)	Gases (wt.%)
Experimental data [170]	82.1	2.2	12.4
Current Model	79.6	2.1	18.4

The comparison of the present simulation results with the experimental data shows that the predicted bio-oil yield was comparable to the experimental data reported in literature. Char yield predicted was especially in good agreement with the experimentally determined value. The non-condensable gases yield, however, was slightly over-predicted by the simulation when compared with the experimental results. Nevertheless, it is reasonable to conclude that the product yields predicted by the model were in close agreement with the experimental data, thus validating the CFD model.

5.4.2. Implementation of DAEM to CFD

After model validation, the main objective of this study was to predict the pyrolysis product yield using distribution of activation energies, for which DAEM has to be integrated with CFD. Xiong at al. [238] have previously carried out this integration, and concluded that if the integration interval and their spaces are chosen optimally, then this coupling does not increase the computational power prohibitively. However, in their work, the kinetic parameters used did not include the standard deviation, and only a small range was chosen. Kinetic parameters used in this study were obtained using thermogravimetric analysis and DAEM as discussed in chapter 3. The predicted kinetic parameters with the mean activation energy and the standard deviation for pure cellulose are summarized in Table 5.6. Kinetic parameters for reaction 1 and 4 were specified with standard deviations of activation energy; however; for reactions 2 and 3 only single values of activation energy were used.

Table 5.6. Optimized kinetic parameters for pure cellulose obtained in Chapter 3.

Reaction No.	Parameter	Value
Reaction 1	Activation energy, E_1 (kJ/mol)	232.7
	Frequency factor, A_1 (s^{-1})	8.52×10^{17}
	Standard deviation, σ_1 (kJ/mol)	2.41
Reaction 2	Activation energy, E_2 (kJ/mol)	196.5
	Frequency factor, A_2 (s^{-1})	3.28×10^{14}
	Standard deviation, σ_2 (kJ/mol)	0
Reaction 3	Activation energy, E_3 (kJ/mol)	150.5
	Frequency factor, A_3 (s^{-1})	1.3×10^{10}
	Standard deviation, σ_3 (kJ/mol)	0
Reaction 4	Activation energy, E_4 (kJ/mol)	255.9
	Frequency factor, A_4 (s^{-1})	5.51×10^{15}
	Standard deviation, σ_4 (kJ/mol)	33.9

These kinetic parameters have been used to understand the pyrolysis behaviour following the same reaction scheme as described in Figure 5.1, in a fluidized bed reactor using CFD simulations. The integration space chosen for this case had $(E_0 - 3\sigma\ ,\ E_0 + 3\sigma)$ 60 equal intervals. Mean activation energies and pre-exponential factor were calculated using the Gaussian distribution function to incorporate the probability function. Reaction terms along with the transport equations was solved in ANSYS FLUENT. The yield of bio-oil, char and gases is presented in Table 5.5.

A comparison of product yields from experimental data and simulation results using Broido-Shafizadeh scheme, with and without DAEM and with DAEM, is show in Table 5.7. It is clear that with DAEM the predicted bio-oil yield increased significantly. This observation is in agreement with those reported in the literature [238]. However, the yield of other pyrolysis product species was also affected due to standard deviation of activation energies. For example, the char yield was over-predicted and that for gases was under -predicted.

Table 5.7. Pyrolysis product yield for cellulose with and without using DAEM.

Data	**Bio-oil (wt.%)**	**Char (wt.%)**	**Gases (wt.%)**
Experimental data [170]	82.1	2.2	12.4
Without DAEM	77.8	3.4	18.9
With DAEM	82.1	9.9	8.0

These results show that the model including distributed activation energy predicted product yield more analogous to experimental data than those using a single value of activation energy. This is because cellulose pyrolysis is a combination of multiple reactions, using an averaged single value of activation energy may result in erroneous results if the difference between activation energies of reaction is significant. A small change in the value of activation energy may affect the rate of reaction exponentially because in CFD simulations rate of reaction is determined using Arrhenius law. Using a distribution of activation energies includes more number of reactions and helps in predicting better product yield. The prominent decrease in the gas yield may be attributed to the higher sigma value for the gas formation reaction.

Figure 5.3 (a) and (b) show the instantaneous volume fraction of gas and sand phase respectively. The bubbles start to develop near the biomass inlet due to decomposition of cellulose to volatiles. These bubbles combine with those produced in the bed due to fluidizing gas (N_2), and form big bubbles which move upward and then leave the surface of the bed (Figure 5.3(a)). This process continues and promotes the mixing behaviour of the particles. Similar behaviour can be observed while looking into the profiles of the sand phase (Figure 5.3(b)).

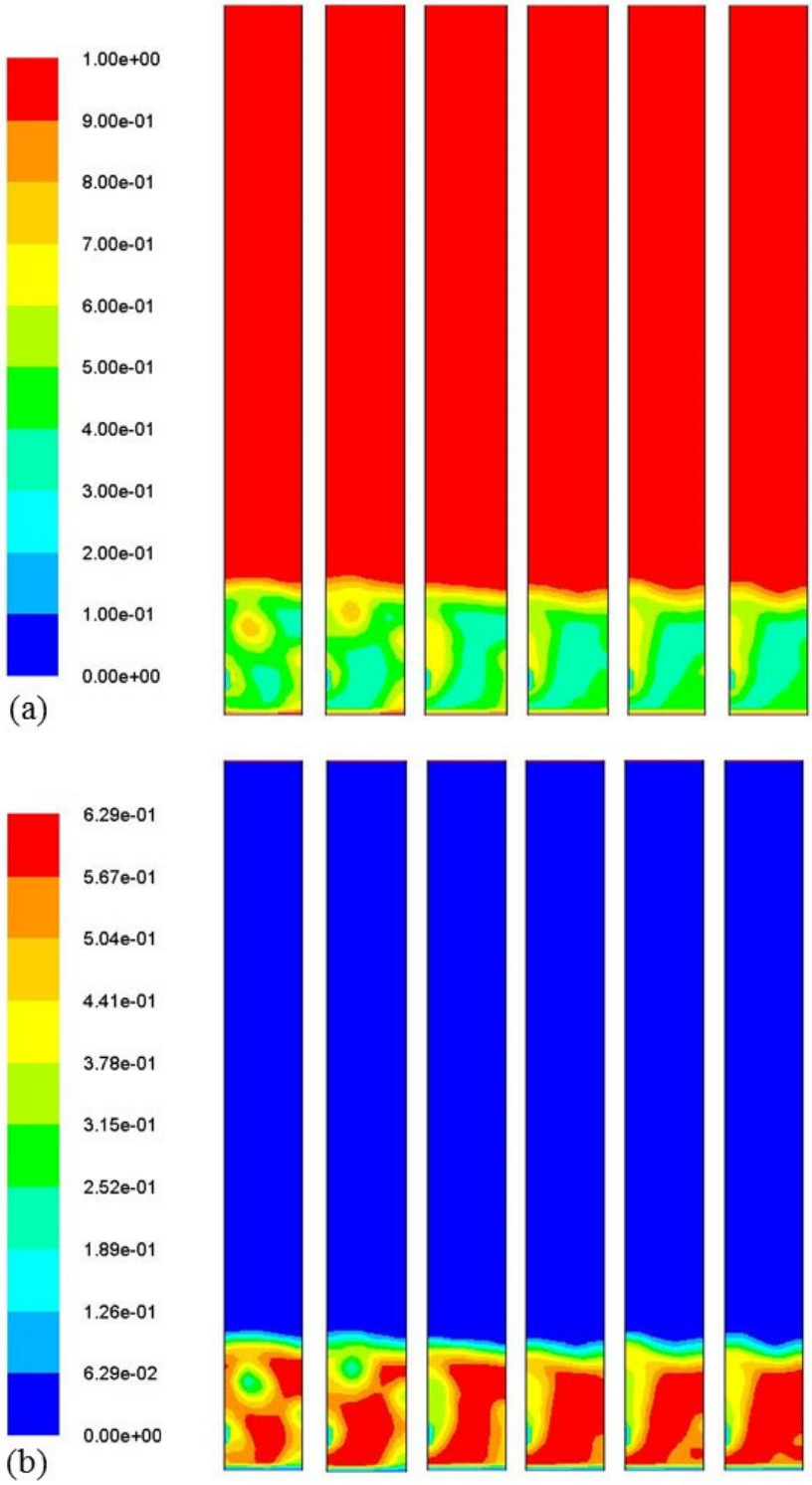

Figure 5.3. Instantaneous volume fraction of (a) gas phase (b) sand phase in a bubbling fluidized bed reactor with time interval of 0.1 sec between each profile.

Time-averaged volume fractions of the three phases in the fluidized bed reactor have also been plotted in Figure 5.4. This figure shows that there exist some segregation in the bed at this superficial gas velocity, which may affect the rate of heat and mass transfer and ultimately the rate of decomposition of cellulose. Hence, to let the pyrolysis happen at faster rates, it is recommended to use an optimized value of gas velocity.

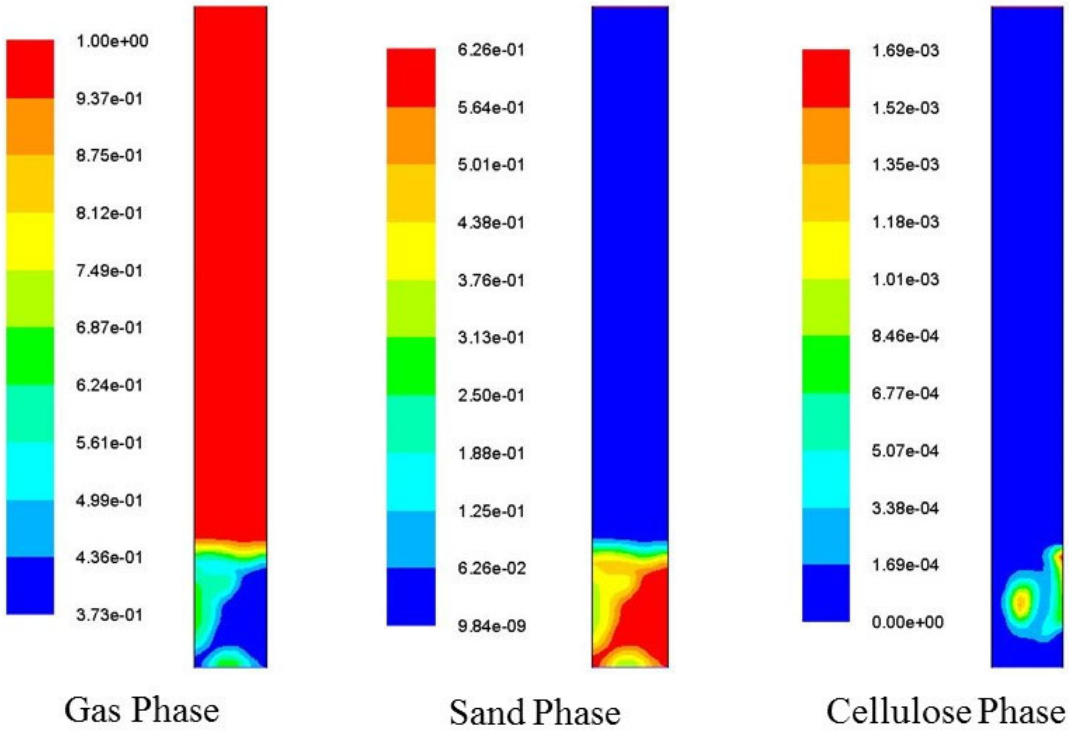

Figure 5.4. Time-averaged volume fraction profiles of three phases in the fluidized bed reactor.

Figure 5.5 shows instantaneous temperature profiles of gas phase (gas mixture of N_2, tar and gases), sand phase and the cellulose phase (mixture of cellulose, active cellulose and char).

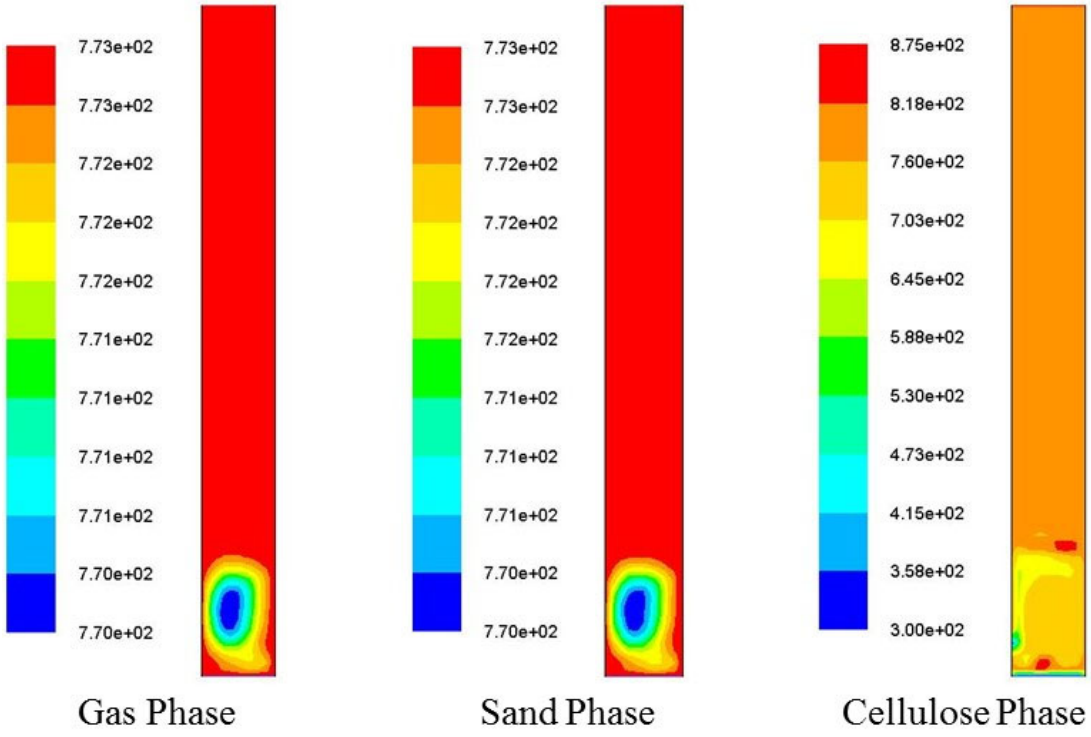

Figure 5.5. Instantaneous temperature profiles for gas, sand and cellulose phase in the fluidized bed reactor.

Since the operating temperature for reactor had been set to 773 K, there was a small variation in the temperatures of gas and sand phase. Sand was packed at the temperature of 773 K, and the gas phase also entered at the same temperature. The small change in temperature of both of these phases through the bed (772-773 K) could be due to production of volatiles n the fluidized bed as a result of cellulose decomposition. However, for cellulose there was a significant change in temperature through the fluidized because it was heated from its initial temperature of 300 to 300–773 K. However, the heating was rapid due to both conductive and convective heat transfers from the other two phases resulting in cellulose to stay at a temperature of 728 K through the most part of the reactor.

Time-averaged temperature profiles for the three phases gas phase, cellulose phase and the sand phase as a function of the reactor height are plotted in Figure 5.6. It is clear that the gas phase temperature was uniformly distributed in the recator near its intial value of 773 K. The temperature of sand also showed little variation through the bed. For the cellulose phase, the temperature profile did show a different behaviour. The temperature of cellulose decreased at the inlet of the feed where fresh cellulose entered

in the reactor at a temperature of 300 K. However, thereafter the temperature of cellulose increased rapidly due to the heat transfer between cellulose and heated gas.

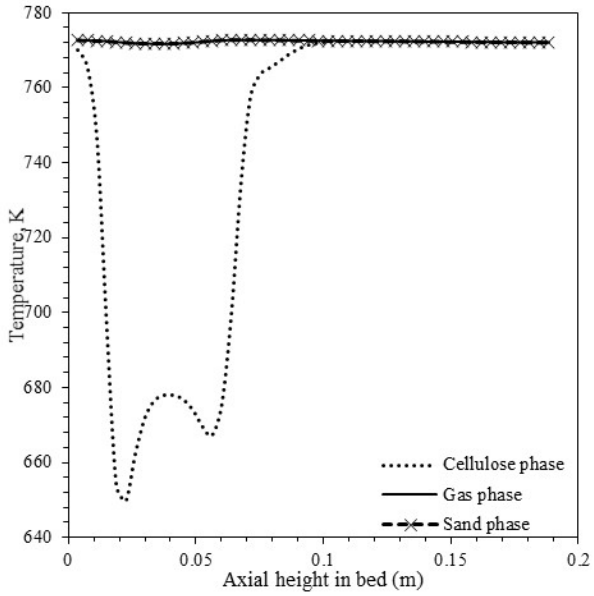

Figure 5.6. Time-averaged temperature profiles of three phases in fluidized bed reactor.

The time-averaged vertical velocity vectors for all three phases are shown in Figure 5.7, which shows that for gas phase the maximum value of gas velocity was more than its initial value due to production of volatiles (tar and gases). The gas-mixture flows in the upward direction in the centre of the column while solids particles recirculate in the downward direction along the reactor walls. The cellulose particles are mixed with the sand and gas phase near the feed inlet and then start to decompose. Solid particles flow down with the minimum averaged velocity. Sand particles keep circulating in the upward direction with the maximum velocity and flow down with the minimum velocity. The recirculation of particles promotes the mixing among the phases resulting in increased heat and mass transfer and rate of reaction.

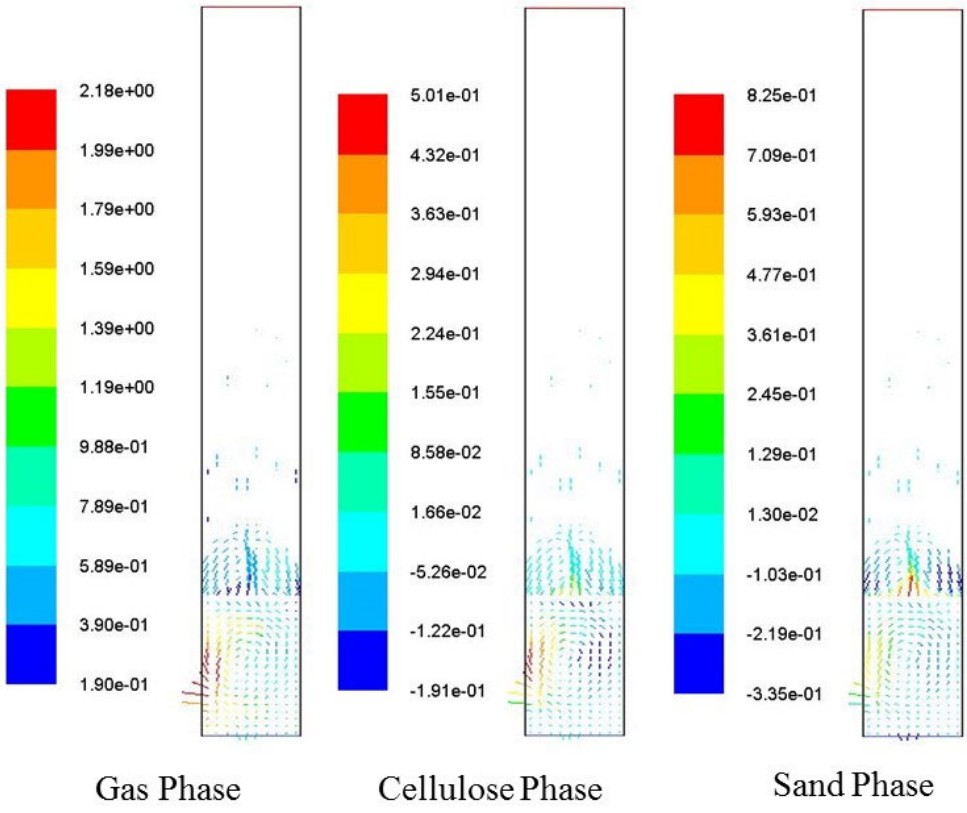

Figure 5.7. Time-averaged velocity vectors of the three phases (a) gas (b) cellulose (c) sand.

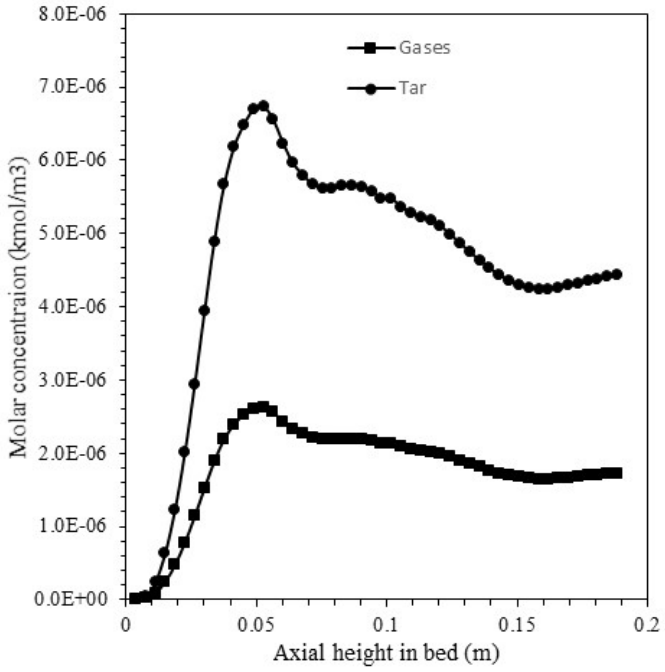

Figure 5.8. Molar concentration of tar and gases.

Plotted in Figure 5.8 are the molar concentrations of gas phase and tar as a function of reactor height. The concentration of both species was zero at the bottom of the reactor and before starting to increase near the feed inlet where cellulose entered in the reactor and started to pyrolyse. The rate of tar formation was higher than the gas formation reaction and hence the concentration of tar increased more rapidly in the bed region. As the tar particles moved along the bed height, it started to decompose to form gases, and its concentration decreased progressively. Since both tar and gases are elutriated out of the reactor along with the gas phase, their concentrations become constant after a certain height in the reactor.

Figure 5.9 compares the mass fraction of tar and gases leaving the reactor and fraction of char accumulating inside the reactor with and without DAEM kinetics. The results presented in the graph below validated the numerical values shown in Table 5.7. The fraction of tar was maximum near the feed inlet and then started to decrease as a result of tar cracking reaction. The yield of tar increased with DAEM, however trend for tar formation along the bed height was consistent in both cases. Fraction of gases decreased significantly because of the higher activation energy for this reaction and inclusion of standard deviation of .activation energy. Fraction of char increased in the bed region and then became nearly zero in the freeboard region. Charring was favoured because of high activation energy of reaction 3 as compared to reaction 2.

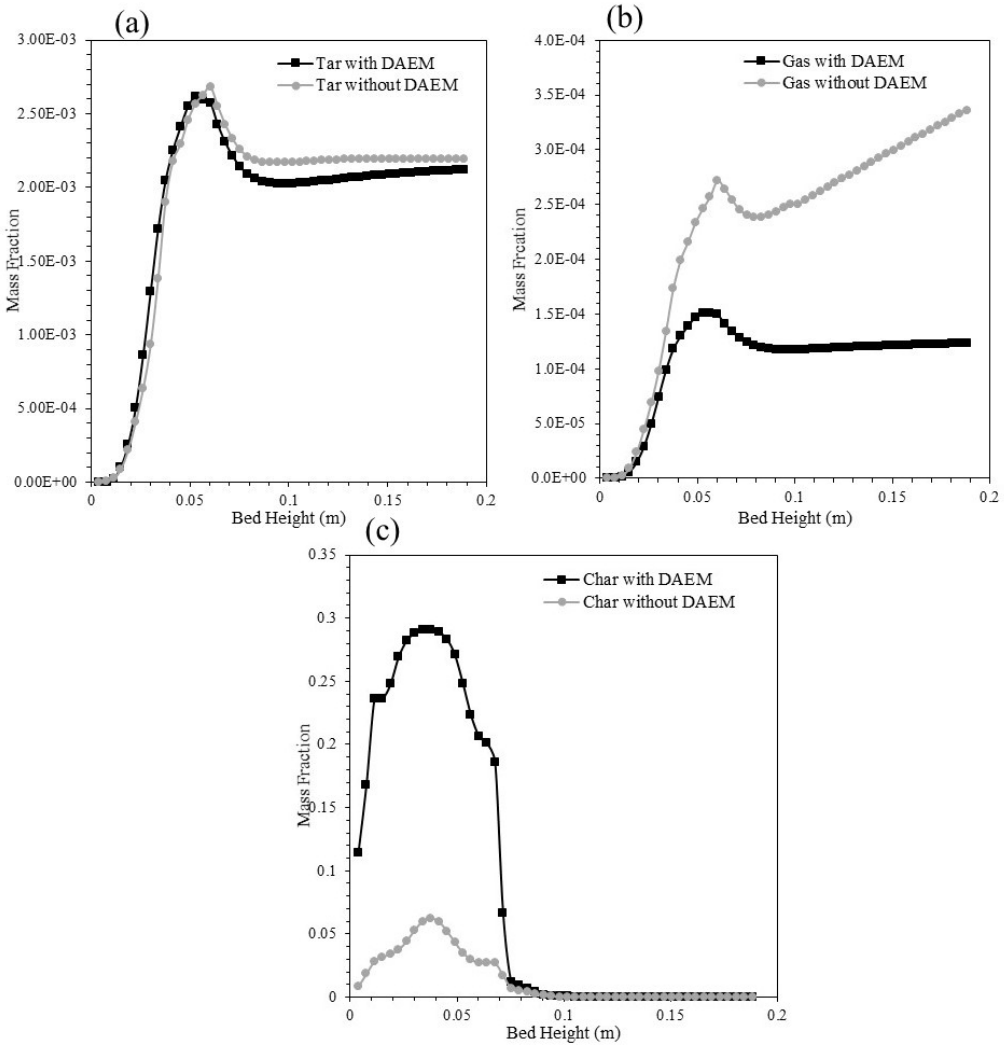

Figure 5.9. Mass fraction of pyrolysis product species (a) tar, (b) gas and (c) char.

5.5. Conclusions

A multi-phase CFD model has been developed for cellulose pyrolysis in a fluidized bed reactor. Firstly, the model was validated by making a comparison between pyrolysis product yields from experiments. The yield of bio-oil, char and gases was in good agreement with the experimental data. Once the model was validated, it was integrated with the distribution activation energy model. Kinetic parameters including the activation energy and standard deviation were collected from the data reported in Chapter 3. Using activation energy with the distribution function had a profound effect on the tar yield. The yield of char and gases were also affected significantly. The

predicted product yield with DAEM were in better agreement with experimental data in comparison to single activation energy model.

CHAPTER 6 CONCLUSIONS AND FUTURE RECOMMENDATIONS

6.1. Concluding Remarks

This chapter summarizes the key research findings of this study. First part of this work included prediction of kinetic parameters for cellulose using experimental data from TGA and modelling scheme such as DAEM. To know the effect of inorganic species on the product yield of cellulose pyrolysis, kinetics was also evaluated in the presence of NaCl. Secondly, a hydrodynamic model was developed to understand the mixing and segregation behaviour of cellulose particles in fluidized beds. Finally, these two have been integrated to develop a CFD model for analysing the cellulose pyrolysis in fluidized bed reactors with a range of distribution of activation energies. Below is a brief summary of the conclusion of this research:

6.1.1. Kinetic Modelling of Salt-loaded Cellulose Pyrolysis

First part of this work included prediction of kinetic parameters for cellulose using experimental data from TGA and modelling scheme such as DAEM. To know the effect of inorganic species on the product yield of cellulose pyrolysis, kinetics was also evaluated in the presence of NaCl. A set of modelling schemes were used to analyse the kinetics of pure cellulose and NaCl-loaded cellulose. Main conclusions drawn are:

- Increase in heating rate shifted the conversion and derivative of conversion towards higher temperatures for pure cellulose and NaCl-loaded cellulose with different concentrations of NaCl.
- Presence of inorganic salts specially the cations (Na^+) supressed the volatiles formation. Tar yield decreases significantly in the presence of small amount of salts.
- The presence of inorganic species in the pure cellulose increased the char yield. Similarly, gas yield also increased in the presence of inorganic species.
- For salt-loaded samples the production of char was affected by heating rate, it increased on increasing the heating rate.
- Loading of salt to the pure cellulose increased the char yield tremendously however, further increase in the concentration of salt did not increase the char yield.

6.1.2. Mixing and Segregation Behaviour of Cellulose in Fluidized Bed

Hydrodynamics of the cellulose in fluidized beds was modelled and analysed qualitatively and quantitatively:

- Particle segregation number (PSN) was used to quantify the mixing and segregation.
- Increase in the gas velocity promoted the mixing between cellulose and sand particles. PSN values decreased rapidly with an increase in the gas velocity from $1.0U_{mf}$ to $3.0U_{mf}$.
- Cellulose particles with larger diameters mix well with smaller and heavier particles of sand. PSN values showed less fluctuation and enhanced mixing. However, smaller particles of cellulose did not mix well with the larger particles of sand and showed fluctuations in PSN values.
- On increasing the fraction of lighter cellulose particles, the extent of segregation increased with an acceleration in the onset of segregation.
- While comparing the mixing and segregation patterns in 2-D and 3-D configurations, it was observed that the distribution of cellulose and sand phases in fluidized bed did not deviate with the configuration.

6.1.3. Distributed Activation Energy Modelling of Cellulose Pyrolysis in a Fluidized Bed Reactor

An integrated CFD model was also developed for cellulose pyrolysis by coupling the kinetics and hydrodynamics:

- CFD model developed for cellulose pyrolysis using Broido-Shafizadeh kinetic scheme with DAEM predicts the product yield in closer agreement with the experimental data rather than the model without DAEM.
- Specifying the cellulose pyrolysis kinetics using several values of distributed activation energies results in increase in tar yield.
- Gaussian distribution function also helps in determining the increase in the char yield and reduction in the gas yield.

6.2. Future Recommendations

Some recommendations for future work may include the following:

- Future work should consider the effect of inorganic species and their possible interactions with other components such as hemicellulose and lignin during kinetic modelling of biomass pyrolysis.
- CPD mechanism needs to be implemented in CFD model using Eulerian-Lagrangian framework to create greater understanding of particle-scale degradation inside the reactor.
- The kinetic parameters determined for NaCl-loaded cellulose needs to be coupled with CFD model to study the effect of inorganic species on the pyrolysis product yield at a reactor scale.
- Effect of operating parameters such as temperature, superficial gas velocity, feed flow rate and the design variables such as cellulose and sand particle diameter, particle density and volume fractions of the phase must be included in the multi-phase CFD model with DAEM.

APPENDIX A

Granular temperature model has been specified as phase property, neglecting the convective and diffusive terms, hence energy dissipation due to collisions and energy exchange will be given as:

$$\gamma_{\theta s} = \frac{12(1-e_{ss}^2)g_{0,ss}}{d_s\sqrt{\pi}}\rho_s\alpha_s^2\theta_s^{3/2}$$

$$\Phi_{ls} = -3K_{ls}\theta_s$$

$$\vec{R}_{ls} = K_{ls}(\vec{v}_l - \vec{v}_s)$$

K_{ls} = Momentum exchange co-efficient between the *lth*-fluid and *sth*-solid phase

Syamlal-O'brien symmetric model [222] has been used to specify the drag between solid particles. The model is of form:

$$K_{ls} = \frac{3(1+e_{ls})\left(\left(\pi/2\right) + C_{fr,ls}\left(\pi^2/8\right)\right)\alpha_s\rho_s\alpha_l\rho_l(d_l+d_s)^2 g_{0,ls}}{2\pi(\rho_l d_l^3 + \rho_s d_s^3)}|\vec{v}_l - \vec{v}_s|$$

Stress-strain tensor for solid phase

$$\bar{\bar{\tau}}_s = \alpha_s\mu_s[\nabla\vec{v}_s + \nabla\vec{v}_s^T] + \alpha_s\left(\lambda_s - \frac{2}{3}\mu_s\right)\nabla.\vec{v}_s\bar{\bar{I}}$$

Solid shear viscosity is obtained by adding the kinetic, collisional and frictional viscosities, such as:

$$\mu_s = \mu_{s,kin} + \mu_{s,col} + \mu_{s,fr}$$

Syamlal-O'brien model [224] has been used to define these viscosities which results in the expressions as:

$$\mu_{s,kin} = \frac{\alpha_s d_s\rho_s\sqrt{\theta_s\pi}}{6(3-e_{ss})}\left[1 + \frac{2}{5}(1+e_{ss})(3e_{ss}-1)\alpha_s g_{0,ss}\right]$$

$$\mu_{s,col} = \frac{4}{5}\alpha_s d_s\rho_s g_{0,ss}(1+e_{ss})\left(\frac{\theta_s}{\pi}\right)^2\alpha_s$$

Schaffer's relation [226] has been used to incorporate frictional stress for the solid phase near the packing limit:

$$\mu_{s,fr} = \frac{p_s \sin \emptyset}{2\sqrt{I_{2D}}}$$

To specify frictional pressure the model based on kinetic theory of granular flow has been used.

Additional to shear viscosity, there is solid bulk viscosity which includes the resistance of the granular particles to compression and expansion. The expression is given by Lun et al. [225]:

$$\lambda_s = \frac{4}{3}\alpha_s d_s \rho_s g_{0,ss}(1 + e_{ss})\left(\frac{\theta_s}{\pi}\right)^{1/2}$$

The pressure for the *sth* solid phase has been defined using the model given by Lun et al. [225] which is the sum of the kinetic term and the pressure because of collisions among particles.

$$p_s = \alpha_s \rho_s \theta_s + 2\rho_s(1 + e_{ss})\alpha_s^2 g_{0,ss}\theta_s$$

In the particles collision term there are two important parameters: e_{ss} is known as restitution coefficient and $g_{0,ss}$ is the radial distribution function.

For multiphase systems having N number of phases, the same equation has been modified as:

$$p_l = \alpha_l \rho_l \theta_l + \sum_{l=1}^{N} 2\frac{d_{ls}^3}{d_l^3}(1 + e_{ls})g_{0,ls}\alpha_l \alpha_s \rho_l \theta_l$$

The radial distribution is calculated according to Syamlal-O'brien [224]:

$$g_{0,kl} = \frac{1}{(1 - \alpha_s)} + \frac{3\left(\sum_{k=1}^{N} {\alpha_k}/{d_k}\right)}{(1 - \alpha_s)^2(d_s + d_l)} d_s d_l$$

BIBLIOGRAPHY

[1] World Energy Outlook, (2018). https://www.iea.org/renewables2018/ (accessed November 19, 2018).

[2] M. M, A. A, Lignin Degradation by Fungal Pretreatment: A Review, J. Plant Pathol. Microbiol. 08 (2017). doi:10.4172/2157-7471.1000398.

[3] F.X. Collard, J. Blin, A review on pyrolysis of biomass constituents: Mechanisms and composition of the products obtained from the conversion of cellulose, hemicelluloses and lignin, Renew. Sustain. Energy Rev. 38 (2014) 594–608. doi:10.1016/j.rser.2014.06.013.

[4] C. Di Blasi, Modeling chemical and physical processes of wood and biomass pyrolysis, Prog. Energy Combust. Sci. 34 (2008) 47–90. doi:10.1016/j.pecs.2006.12.001.

[5] S. V. Vassilev, D. Baxter, L.K. Andersen, C.G. Vassileva, An overview of the chemical composition of biomass, Fuel. 89 (2010) 913–933. doi:10.1016/j.fuel.2009.10.022.

[6] X. Guo, S. Wang, K. Wang, Q. Liu, Z. Luo, Influence of extractives on mechanism of biomass pyrolysis, J. Fuel Chem. Technol. 38 (2010) 42–46. doi:10.1016/S1872-5813(10)60019-9.

[7] K. Raveendran, A. Ganesh, K.C. Khilar, Influence of mineral matter on biomass pyrolysis characteristics, Fuel. 74 (1995) 1812–1822. doi:10.1016/0016-2361(95)80013-8.

[8] A. Trendewicz, R. Evans, A. Dutta, R. Sykes, D. Carpenter, R. Braun, Evaluating the effect of potassium on cellulose pyrolysis reaction kinetics, Biomass Bioener. 74 (2015) 15–25. doi:10.1016/j.biombioe.2015.01.001.

[9] J. Wang, M. Zhang, M. Chen, F. Min, S. Zhang, Z. Ren, Y. Yan, Catalytic effects of six inorganic compounds on pyrolysis of three kinds of biomass, Thermochim. Acta. 444 (2006) 110–114. doi:10.1016/j.tca.2006.02.007.

[10] C.A. Koufopanos, G. Maschio, A. Lucchesi, Kinetic Modelling of the Pyroysis of Biomass and Biomass Components, Can. J. Chem. Eng. 67 (1989) 75–84. doi:10.1002/cjce.5450670111.

[11] A.G.W. Bradbury, Y. Sakai, F. Shafizadeh, Kinetic Model for Pyrolysis of Cellulose., J Appl Polym Sci. 23 (1979) 3271–3280. doi:10.1002/app.1979.070231112.

[12] C.A. Koufopanos, N. Papayannakos, G. Maschio, A. Lucchesi, Modelling of the pyrolysis of biomass particles. studies on kinetics , Thermal and heat transfer effects ., Can. J. Chem. Eng. 69 (1991) 907–915.

[13] R.S. Miller, J. Bellan, A generalized biomass pyrolysis model based on superimposed cellulose, hemicellulose and lignin kinetics, Combust. Sci. Technol. 126 (1997) 97–137. doi:10.1080/00102209708935670.

[14] C. Di Blasi, Modelling the fast pyrolysis of cellulosic particles in fluid-bed reactors, Chem. Eng. Sci. 55 (2000) 5999–6013. doi:10.1016/S0009-2509(00)00406-1.

[15] A. V. Bridgwater, Review of fast pyrolysis of biomass and product upgrading, Biomass Bioener. 38 (2012) 68–94. doi:10.1016/j.biombioe.2011.01.048.

[16] D. Mohan, C.U. Pittman, P.H. Steele, Pyrolysis of wood/biomass for bio-oil: A critical review, Energy Fuels. 20 (2006) 848–889. doi:10.1021/ef0502397.

[17] L. Zhang, C. (Charles) Xu, P. Champagne, Overview of recent advances in thermo-chemical conversion of biomass, Energy Convers. Manag. 51 (2010) 969–982. doi:10.1016/j.enconman.2009.11.038.

[18] M.G. Rasul, M.I. Jahirul, W. Science, Recent developments in biomass pyrolysis for bio-fuel production : its potential for commercial applications pyrolysis process description pyrolysis classification, Recent Res. Environ. Geol. Sci. Recent. (2012) 256–265.

[19] M.I. Jahirul, M.G. Rasul, A.A. Chowdhury, N. Ashwath, Biofuels production through biomass pyrolysis- A technological review, Energies. 5 (2012) 4952–5001. doi:10.3390/en5124952.

[20] M.K. Bahng, C. Mukarakate, D.J. Robichaud, M.R. Nimlos, Current technologies for analysis of biomass thermochemical processing: A review, Anal. Chim. Acta. 651 (2009) 117–138. doi:10.1016/j.aca.2009.08.016.

[21] S. Yaman, Pyrolysis of biomass to produce fuels and chemical feedstocks, Energy Convers. Manag. 45 (2004) 651–671. doi:10.1016/S0196-

8904(03)00177-8.

[22] W.N.R.W. Isahak, M.W.M. Hisham, M.A. Yarmo, T.Y. Yun Hin, A review on bio-oil production from biomass by using pyrolysis method, Renew. Sustain. Energy Rev. 16 (2012) 5910–5923. doi:10.1016/j.rser.2012.05.039.

[23] A. Demirbas, Progress and recent trends in biofuels, Prog. Energy Combust. Sci. 33 (2007) 1–18. doi:10.1016/j.pecs.2006.06.001.

[24] H. Zhang, R. Xiao, D. Wang, G. He, S. Shao, J. Zhang, Z. Zhong, Biomass fast pyrolysis in a fluidized bed reactor under N_2, CO_2, CO, CH_4 and H_2 atmospheres., Bioresour. Technol. 102 (2011) 4258–64. doi:10.1016/j.biortech.2010.12.075.

[25] P.N. Sheth, B. V Babu, Kinetic Modeling of the Pyrolysis of Biomass, Environ. Eng. –. 4 (2006) 453–458.

[26] G. Várhegyi, M.J. Antal, E. Jakab, P. Szabó, Kinetic modeling of biomass pyrolysis, J. Anal. Appl. Pyrolysis. 42 (1997) 73–87. doi:10.1016/S0165-2370(96)00971-0.

[27] E. Ranzi, a Cuoci, T. Faravelli, a Frassoldati, G. Migliavacca, S. Pierucci, S. Sommariva, Chemical kinetics of biomass pyrolysis, Energy Fuels. 22 (2008) 4292–4300. doi:10.1021/ef800551t.

[28] R. Vinu, L.J. Broadbelt, Unraveling reaction pathways and specifying reaction kinetics for complex systems, Annu. Rev. Chem. Biomol. Eng. 3 (2012) 29–54. doi:10.1146/annurev-chembioeng-062011-081108.

[29] Corbetta, M, Pierucci, S, Ranzi, E, H. Bennadji, E.M. Fisher, Multistep kinetic model of biomass pyrolysis, Clean. Combust. (2013) 111–139. doi:10.1007/978-1-4471-5307-8.

[30] A. Sharma, V. Pareek, D. Zhang, Biomass pyrolysis - A review of modelling, process parameters and catalytic studies, Renew. Sustain. Energy Rev. 50 (2015) 1081–1096. doi:10.1016/j.rser.2015.04.193.

[31] A. Anca-Couce, Reaction mechanisms and multi-scale modelling of lignocellulosic biomass pyrolysis, Prog. Energy Combust. Sci. 53 (2016) 41–79. doi:10.1016/j.pecs.2015.10.002.

[32] S.R. A. Kersten, X. Wang, W. Prins, W.P.M. van Swaaij, Biomass pyrolysis in a fluidized bed reactor. Part 1: Literature review and model simulations, Ind. Eng. Chem. Res. 44 (2005) 8773–8785. doi:10.1021/ie0504856.

[33] X. Wang, S.R. A. Kersten, W. Prins, W.P.M. van Swaaij, Biomass pyrolysis in a fluidized bed reactor. Part 2: Experimental validation of model results, Ind. Eng. Chem. Res. 44 (2005) 8786–8795. doi:10.1021/ie050486y.

[34] K.L. Lam, A.O. Oyedun, C.W. Hui, Experimental and modelling studies of biomass pyrolysis, Chinese J. Chem. Eng. 20 (2012) 543–550. doi:10.1016/S1004-9541(11)60217-6.

[35] S. Papari, K. Hawboldt, A review on the pyrolysis of woody biomass to bio-oil: Focus on kinetic models, Renew. Sustain. Energy Rev. 52 (2015) 1580–1595. doi:10.1016/j.rser.2015.07.191.

[36] S. Sinha, A. Jhalani, M.R. Ravi, A. Ray, Modelling of pyrolysis in wood : A Review, SESI J. 10 (2000) 1–17. http://web.iitd.ac.in/~ravimr/Publications/IndianJournals/sesi-sanjiv.pdf.

[37] B. Moghtaderi, The state-of-the-art in pyrolysis modelling of lignocellulosic solid fuels, Fire Mater. (2006) 1–34. doi:10.1002/fam.891.

[38] B. V. Babu, Biomass Pyrolysis: a state-of-the-art review, Biofuels, Bioprod. Biorefining. (2008) 393–414. doi:10.1002/bbb.

[39] N. Prakash, T. Karunanithi, Kinetic Modeling in Biomass Pyrolysis - a review, J. Appl. Sci. Res. 4 (2008) 1627–1636.

[40] N. Prakash, T. Karunanithi, Advances in Biomass Pyrolysis Modeling and Simulation.pdf, Asian J. Sci. Res. 1 (2009) 1-27.

[41] S. Wang, G. Dai, H. Yang, Z. Luo, Lignocellulosic biomass pyrolysis mechanism A state of the art review, Prog. Energy Combust. Sci. 62 (2017) 33–86.

[42] R. Chan, Modelling and experimental verification physical and chemical processes during pyrolysis of a large biomass particle , Fuel 64 (1985) 1505–1513.

[43] G. Varhegyi, M.J. Antal, Kinetics of the thermal decomposition of cellulose ,

hemicellulose , and sugar cane bagasse, Energy Fuels (1989) 329–335.

[44] K. Hashimoto, I. Hasegawa, J. Hayashi, K. Mae, Correlations of kinetic parameters in biomass pyrolysis with solid residue yield and lignin content, Fuel. 90 (2011) 104–112. doi:10.1016/j.fuel.2010.08.023.

[45] R. Radmanesh, Y. Courbariaux, J. Chaouki, C. Guy, A unified lumped approach in kinetic modeling of biomass pyrolysis, Fuel. 85 (2006) 1211–1220. doi:10.1016/j.fuel.2005.11.021.

[46] S.S. Alves, J.L. Figueiredo, A model for pyrolysis of wet wood, Chem. Eng. Sci. 44 (1989) 2861–2869. doi:10.1016/0009-2509(89)85096-1.

[47] P. Ghodke, R.N. Mandapati, Investigation of particle level kinetic modeling for babul wood pyrolysis, Fuel. 236 (2019) 1008–1017. doi:10.1016/j.fuel.2018.09.084.

[48] J.E. White, W.J. Catallo, B.L. Legendre, Biomass pyrolysis kinetics: A comparative critical review with relevant agricultural residue case studies, J. Anal. Appl. Pyrolysis. 91 (2011) 1–33. doi:10.1016/j.jaap.2011.01.004.

[49] M.J. Antal, G. Vrhegyi, E. Jakab, Cellulose Pyrolysis Kinetics : Revisited Cellulose Pyrolysis Kinetics : Revisited, Society. 37 (1998) 1267–1275. doi:10.1021/ie970144v.

[50] F. Thurner, Mann, Kinetic investigation of wood pyrolysis, Ind. Eng. Chem. Process Des. Dev. 20 (1981) 482–488. doi:10.1021/i200014a015.

[51] D.S. Scott, J. Piskorz, D. Radlein, Liquid products from the continuous flash pyrolysis of biomass, Ind. Eng. Chem. Process Des. Dev. 24 (1985) 581–588. doi:10.1021/i200030a011.

[52] G. Varhegyi, E. Jakab, M.J. Antal, 95/01741 Is the Broido-Shafizadeh model for cellulose pyrolysis true?, Fuel Energy Abstr. 36 (1995) 119. doi:10.1016/0140-6701(95)93406-5.

[53] A. Cuoci, T. Faravelli, A. Frassoldati, S. Granata, G. Migliavacca, E. Ranzi, S. Sommariva, A General Mathematical Model of Biomass Devolatilization Note 1. Lumped kinetic models of cellulose, hemicellulose and lignin., 30th Meet. Ital. Sect. Combust. Inst. (2007) 1–6. http://www.combustioninstitute.it/proc/proc2007/data/papers/06 - Combustion

of Waste and Solid Fuels/06-02-Frassoldati-007-paper.pdf.

[54] A. Anca-Couce, R. Mehrabian, R. Scharler, I. Obernberger, Kinetic scheme of biomass pyrolysis considering secondary charring reactions, Energy Convers. Manag. 87 (2014) 687–696. doi:10.1016/j.enconman.2014.07.061.

[55] M. Hu, Z. Chen, S. Wang, D. Guo, C. Ma, Y. Zhou, J. Chen, M. Laghari, S. Fazal, B. Xiao, B. Zhang, S. Ma, Thermogravimetric kinetics of lignocellulosic biomass slow pyrolysis using distributed activation energy model, Fraser-Suzuki deconvolution, and iso-conversional method, Energy Convers. Manag. 118 (2016) 1–11. doi:10.1016/j.enconman.2016.03.058.

[56] R. Capart, L. Khezami, A.K. Burnham, Assessment of various kinetic models for the pyrolysis of a microgranular cellulose, Thermochim. Acta. 417 (2004) 79–89. doi:10.1016/j.tca.2004.01.029.

[57] A.K. Burnham, R.L. Braun, Global kinetic analysis of complex materials, Energy Fuels. 13 (1999) 1–22. doi:10.1021/ef9800765.

[58] A.K. Burnham, R.L. Braun, T.T. Coburn, E.I. Sandvik, D.J. Curry, B.J. Schmidt, R.A. Noble, An appropriate kinetic model for well-preserved algal kerogens, Energy Fuels. 10 (1996) 49–59. doi:10.1021/ef950142s.

[59] J.G. Reynolds, A.K. Burnham, P.H. Wallman, Reactivity of paper residues produced by a hydrothermal pretreatment process for municipal solid wastes, Energy Fuels. 11 (1997) 98–106. doi:10.1021/ef9600873.

[60] D. Dollimore, B. Holt, Thermal degradation of cellulose in nitrogen, J. Polym. Sci. 11 (1973) 1703–1711.

[61] A. Ortega, L.P. Maqueda, J.M. Criado, The problem of discerning Avrami-Erofeev kinetic models from the new controlled rate thermal analysis with constant acceleration of the transformation, Thermochim. Acta. 254 (1995) 147–152. doi:10.1016/0040-6031(94)02068-Y.

[62] J.G. Reynolds, A.K. Burnham, Pyrolysis decomposition kinetics of cellulose-based materials by constant heating rate micropyrolysis, Energy Fuels. 11 (1997) 88–97. doi:10.1021/ef960086a.

[63] M.J. Antal, Cellulose pyrolysis kinetics : The current state of knowledge, Ind. Eng. Chem. Res. 34 (1995) 703–717. doi:10.1021/ie00042a001.

[64] J. Bland, G. Silva, A detailed chemical kinetic model for pyrolysis of the lignin model compound chroman, AIMS Environ. Sci. 1 (2013) 12–25. doi:10.3934/environsci.2013.1.12.

[65] P.R. Patwardhan, R.C. Brown, B.H. Shanks, Product distribution from the fast pyrolysis of hemicellulose, ChemSusChem. 4 (2011) 636–643. doi:10.1002/cssc.201000425.

[66] D. Shen, R. Xiao, S. Gu, H. Zhang, The Overview of Thermal Decomposition of Cellulose in Lignocellulosic Biomass, Cellul. - Biomass Convers. (2013) 193–226. doi:10.5772/51883.

[67] C. Şerbănescu, Kinetic analysis of cellulose pyrolysis: a short review, Chem. Pap. 68 (2014) 847–860. doi:10.2478/s11696-013-0529-z.

[68] S. Wang, Q. Liu, Y. Liao, Z. Luo, K. Cen, A study on the mechanism research on cellulose pyrolysis under catalysis of metallic salts, Korean J. Chem. Eng. 24 (2007) 336–340. doi:10.1007/s11814-007-5060-x.

[69] S. C. Xiong, Q. , Aramideh, and Kong, Assessment of devolatilization schemes in predicting product yields of biomass fast pyrolysis, Environ. Sci. Technol. 33 (2014) 482–489. doi:10.1002/ep.

[70] K. Wan, Z. Wang, Y. He, J. Xia, Z. Zhou, J. Zhou, K. Cen, Experimental and modeling study of pyrolysis of coal, biomass and blended coal-biomass particles, Fuel. 139 (2015) 356–364. doi:10.1016/j.fuel.2014.08.069.

[71] P.R. Solomon, T.H. Fletcher, R.J. Pugmire, Progress in coal pyrolysis, Fuel. 72 (1993) 587–597. doi:10.1016/0016-2361(93)90570-R.

[72] P.G. Borah, R. C., Ghosh, P. and Rao, A review on Devolatilization of Coal in Fluidized Bed, Int. J. Energy Res. 35 (2011) 929–963.

[73] P.R. Solomon, D.G. Hamblen, Z.Z. Yu, M.A. Serio, Network models of coal thermal decomposition, Fuel. 69 (1990) 754–763. doi:10.1016/0016-2361(90)90042-O.

[74] E. M. Hambly, The chemical structure changes of coal, char, and tar during devolatilization., M. S. Thesis Brigham University, Provo, UT, 1998.

[75] S. Niksa, Predicting detailed products of secondary pyrolysis of diverse forms

of biomass, Proceedings of the Combustion Institute. 28 (2000) 2727-2733.

[76] M.A. Serio, A comprehensive model of biomass pyrolysis, Final report by Advanced Fuel Research Inc. (1997) 1-47.

[77] C. Sheng, J.L.T. Azevedo, Modeling biomass devolatilization using the chemical percolation devolatilization model for the main components, Proc. Combust. Inst. 29 (2002) 407–414. doi:10.1016/S1540-7489(02)80054-2.

[78] P.R. Solomon, Advanced Fuel-Devolatilization Model FG-DVC, (1980) 1–8.

[79] P.R. Solomon, D.G. Hamblen, M.A. Serio, Z.Z. Yu, S. Charpenay, A characterization method and model for predicting coal conversion behaviour, Fuel. 72 (1993) 469–488. doi:10.1016/0016-2361(93)90106-C.

[80] P.R. Solomon, H.H. King, Tar evolution from coal and model polymers: Theory and Experiments, Fuel. 63 (1983) 1302–1311. doi:10.1016/0016-2361(86)90078-5.

[81] M.A. Serio, D.G. Hamblen, J.R. Markham, P.R. Solomon, Kinetics of volatile product evolution in coal pyrolysis : Experiment and theory, Energy Fuels. 1 (1987) 138–152. doi:10.1021/ef00002a002.

[82] Solomon, P. R., D.G. Hamblen, Carangelo, R. M., and Serio, M.A., G. V Deshpande, A general model of coal devolatilization, Energy Fuels. 2 (1988) 405-422.

[83] P.R. Solomon, D.G. Hamblen, R.M. Carangelo, M. A Serio, G. V Deshpande, General model of coal devolatilizationt, Energy Fuels. 2 (1988) 405–422. doi:10.1021/ef00010a006.

[84] P.R. Solomon, M.A. Serio, R.M. Carangelo, R. Bassilakis, Coal analysis by TG-FTIR, Proceedings, 1989 International Conference on Coal Science, 1, 334-343.

[85] S. Niksa, FLASHCHAIN theory for rapid coal devolatilization kinetics. 1. Formulation, Energy Fuels. 5 (1991) 647–665.

[86] S. Niksa, FLASHCHAin theory for rapid coal devolatilization kinetics. 2. impact of Opertaing Conditions, Energy Fuels. 5 (1991) 665–673.

[87] S. Niksa, FLASHCHAIN theory for rapid coal devolatilization kinetics. 3. Modeling the behavior of various coals, Energy Fuels. 5 (1991) 673–683.

[88] S. Niksa, FLASHCHAIN Theory for Rapid Coal Devolatilization Kinetics. 4. Predicting ultimate yields from ultimate analyses alone, Energy & Fuels. 8 (1994) 659–670. doi:10.1021/ef00045a022.

[89] S. Niksa, Predicting the rapid devolatilization of diverse forms of biomass with bio-flashchain, Proc. Combust. Inst. 28 (2000) 2727–2733. doi:10.1016/S0082-0784(00)80693-1.

[90] S. Niksa, A.R. Kerstein, The distributed-energy chain model for rapid coal devolatilization kinetics. Part I: Formulation, Combust. Flame. 66 (1986) 95–109. doi:10.1016/0010-2180(86)90082-9.

[91] S. Niksa, The distributed-energy chain model for rapid coal devolatilization kinetics. Part II: Transient Weight Loss Correlations, Combust. Flame. 66 (1986) 111–119. doi:10.1016/0010-2180(86)90082-9.

[92] S. Niksa, Rapid Coal Devolatilization as an equilibrium flash distillation, ACS Div. Fuel Chem. Prepr. 32 (1987) 79–82. doi:DOI 10.1002/aic.690340509.

[93] T. H. Fletcher, A. R. Kerstein, R. J. Pugmire, M. Solumn and D. M. Grant, A chemical percolation model for devolatilization: Summary, Sandia Technical Report Sand, 1-66, 1992. doi:10.1017/CBO9781107415324.004.

[94] D.M. Grant, R.J. Pugmire, T.H. Fletcher, A.R. Kerstein, A chemical model of coal devolatilization using percolation lattice statistics, 322–332. https://web.anl.gov/PCS/acsfuel/.../Files/33_2_TORONTO_06-88_0322.pdf.

[95] T.H. Fletcher, A.R. Kerstein, R.J. Pugmire, D.M. Grant, Chemical percolation model for devolatilization. 2. Temperature and heating rate effects on product yields, Energy Fuels. 4 (1990) 54–60. doi:10.1021/ef00019a010.

[96] T.H. Fletcher, A.R. Kerstein, R.J. Pugmire, M.S. Solum, D.M. Grant, Chemical percolation model for devolatilization . 3. Direct Use of ^{13}C NMR data to predict effects of coal type, Energy Fuels. 6 (1992) 414–431. doi:10.1021/ef00034a011.

[97] R.S. Jupudi, V. Zamansky, T.H. Fletcher, Prediction of light gas composition in coal devolatilization, Energy Fuels. 23 (2009) 3063–3067. doi:10.1021/ef9001346.

[98] T.J. Wooters, L.L. Baxter, T.H. Fletcher, CPD model calculations of black

liquor and biomass pyrolysis., Abstr. Pap. 229th ACS Natl. Meet. San Diego, CA, United States, March 13-17, 2005. (2005) Fuel-047.

[99] T.H. Fletcher, H.R. Pond, J. Webster, J. Wooters, L.L. Baxter, Prediction of tar and light gas during pyrolysis of black liquor and biomass, Energy Fuels. 26 (2012) 3381-3387. doi:10.1021/ef300574n.

[100] A.D. Lewis, T.H. Fletcher, Prediction of sawdust pyrolysis yields from a flat-flame burner using the CPD model, Energy Fuels. 27 (2013) 942–953. doi:10.1021/ef3018783.

[101] A.D. Lewis, E.G. Fletcher, T.H. Fletcher, Pyrolysis and CO2 Gasification rates of biomass at high heating rate conditions, 8th U. S. Natl. Combust. Meet. 2020 (2013) 1-17.

[102] D.M. Alonso, S.G. Wettstein, J.A. Dumesic, Bimetallic catalysts for upgrading of biomass to fuels and chemicals, Chem. Soc. Rev. 41 (2012) 8075–8098. doi:10.1039/c2cs35188a.

[103] M.A. Serio, S. Charpenay, R. Bassilakis, P.R. Solomon, Measurement and modeling of lignin pyrolysis, 7 (1994) 107–124.

[104] Y. Chen, S. Charpenay, A. Jensen, M. A. Wójtowicz, M. A. Serio, Modeling of biomass pyrolysis kinetics, Symp. Combust. 27 (1998) 1327–1334. doi:10.1016/S0082-0784(98)80537-7.

[105] Y. Chen, S. Charpenay, A. Jensen, M.A. Serio, M.A. Wójtowicz, Modeling biomass pyrolysis kinetics and mechanisms, Fuel Energy Abstr. (1997) 96–102. http://www.ingentaconnect.com/content/els/01406701/1997/00000038/00000004/art84809.

[106] P.R.. Smith K. L, Smoot L.D, Fletcher Th.H, The structure and reaction processes of coal, Springer Science & Buisness Media, 31 Aug.1994. ISBN 0-306-44602-2.

[107] T.H. Fletcher, D. Barfuss, R.J. Pugmire, Modeling Light Gas and Tar Yields from Pyrolysis of Green River Oil Shale Demineralized Kerogen Using the Chemical Percolation Devolatilization Model, Energy Fuels. 29 (2015) 4921–4926. doi:10.1021/acs.energyfuels.5b01146.

[108] T.H. Fletcher, H.R. Pond, J. Webster, J. Wooters, L.L. Baxter, Prediction of tar

and light gas during pyrolysis of black liquor and biomass, Energy Fuels. 26 (2012) 3381–3387. doi:10.1021/ef300574n.

[109] W. De Jong, A. Pirone, M.A. Wojtowicz, Pyrolysis of Miscanthus Giganteus and wood pellets: TG-FTIR analysis and reaction kinetics, Fuel. 82 (2003) 1139–1147. doi:10.1016/S0016-2361(02)00419-2.

[110] M. Rabacal, M. Costa, M. Vascellari, C. Hasse, Kinetic modelling of sawdust and beech wood pyrolysis in drop tube reactors using advanced predictive models, Chem. Eng. Trans. 37 (2014) 79–84. doi:10.3303/CET1437014.

[111] G. Vizzini, a Bardi, E. Biagini, Prediction of rapid biomass devolatilization yields with an upgraded version of the Bio-CPD model,Italian Section of the Combustion Institute. 31st Meet. (2008) 1–6. http://143.225.115.225/proc/proc2008/data/papers/III/III-4.pdf.

[112] Biagini E, Falcitelli M, Tognotti L, A structural model for biomass devolatilization, Proceedings of 18th EUBCE, 2010. doi:10.5071/18thEUBCE2010-OB5.4.

[113] E. Biagini, M. Falcitelli, L. Tognotti, Devolatilisation and pyrolysis of biomasses : development and validation of structural models, 29th Meet. Combust. 2 (2006) 1–6.

[114] R. Alén, S. Rytkönen, P. McKeough, Thermogravimetric behavior of black liquors and their organic constituents, J. Anal. Appl. Pyrolysis. 31 (1995) 1–13. doi:10.1016/0165-2370(94)00811-E.

[115] M.S. Solum, C.L. Mayne, A.M. Orendt, R.J. Pugmire, J. Adams, T.H. Fletcher, Characterization of macromolecular structure elements from a Green River Oil shale, I. Extracts, Energy Fuels. 28 (2014) 453–465.

[116] T.H. Fletcher, R. Gillis, J. Adams, T. Hall, C.L. Mayne, M.S. Solum, R.J. Pugmire, Characterization of macromolecular structure elements from a Green River Oil shale, II. Characterization of pyrolysis products by 13C NMR, GC/MS, and FTIR, Energy Fuels. 28 (2014) 2959–2970. doi:10.1021/ef500095j.

[117] A.K. Burnham, X. Zhou, L.J. Broadbelt, Critical review of the global chemical kinetics of cellulose thermal decomposition, Energy Fuels. 29 (2015) 2906–

2918. doi:10.1021/acs.energyfuels.5b00350.

[118] H.B. Mayes, L.J. Broadbelt, Unraveling the reactions that unravel cellulose, J. Phys. Chem. A. 116 (2012) 7098–7106. doi:10.1021/jp300405x.

[119] S.H. Mushrif, V. Vasudevan, C.B. Krishnamurthy, B. Venkatesh, Multiscale molecular modeling can be an effective tool to aid the development of biomass conversion technology: A perspective, Chem. Eng. Sci. 121 (2015) 217–235. doi:10.1016/j.ces.2014.08.019.

[120] M. Zhang, Z. Geng, Y. Yu, Density functional theory (DFT) study on the dehydration of cellulose, Energy Fuels. 25 (2011) 2664–2670. doi:10.1021/ef101619e.

[121] M. Zhang, Z. Geng, Y. Yu, Density Functional Theory (DFT) study on the pyrolysis of cellulose: The pyran ring breaking mechanism, Comput. Theor. Chem. 1067 (2015) 13–23. doi:10.1016/j.comptc.2015.05.001.

[122] V. Agarwal, P.J. Dauenhauer, G.W. Huber, S.M. Auerbach, Ab initio dynamics of cellulose pyrolysis: Nascent decomposition pathways at 327 and 600 °C, J. Am. Chem. Soc. 134 (2012) 14958–14972. doi:10.1021/ja305135u.

[123] M.S. Mettler, S.H. Mushrif, A.D. Paulsen, A.D. Javadekar, D.G. Vlachos, P.J. Dauenhauer, Revealing pyrolysis chemistry for biofuels production: Conversion of cellulose to furans and small oxygenates, Energy Environ. Sci. 5 (2012) 5414. doi:10.1039/c1ee02743c.

[124] J. Huang, C. Liu, H. Tong, W. Li, D. Wu, Theoretical studies on pyrolysis mechanism of xylopyranose, Comput. Theor. Chem. 1001 (2012) 44–50. doi:10.1016/j.comptc.2012.10.015.

[125] V. Seshadri, P.R. Westmoreland, Concerted reactions and mechanism of glucose pyrolysis and implications for cellulose kinetics, J. Phys. Chem. A. 116 (2012) 11997–12013. doi:10.1021/jp3085099.

[126] X. Huang, D. Cheng, F. Chen, X. Zhan, A Density Functional Theory Study on Pyrolysis Mechanism of Lignin in Hydrogen Plasma, Ind. Eng. Chem. Res. 52 (2013) 14107–14115. doi:10.1021/ie401974j.

[127] X. Zhou, M.W. Nolte, H.B. Mayes, B.H. Shanks, L.J. Broadbelt, Experimental and mechanistic modeling of fast pyrolysis of neat glucose-based

carbohydrates. 2. Validation and evaluation of the mechanistic model, Ind. Eng. Chem. Res. 53 (2014) 13290–13301. doi:10.1021/ie502259w.

[128] Q. Lu, Y. Zhang, C.Q. Dong, Y.P. Yang, H.Z. Yu, The mechanism for the formation of levoglucosenone during pyrolysis of β-D-glucopyranose and cellobiose: A density functional theory study, J. Anal. Appl. Pyrolysis. 110 (2014) 34–43. doi:10.1016/j.jaap.2014.08.002.

[129] Q. Lu, B. Hu, Z. xi Zhang, Y. ting Wu, M. shu Cui, D. jia Liu, C. qing Dong, Y. ping Yang, Mechanism of cellulose fast pyrolysis: The role of characteristic chain ends and dehydrated units, Combust. Flame. 198 (2018) 267–277. doi:10.1016/j.combustflame.2018.09.025.

[130] R. Vinu, L.J. Broadbelt, A mechanistic model of fast pyrolysis of glucose-based carbohydrates to predict bio-oil composition, Energy Environ. Sci. (2012) 9808–9826. doi:10.1039/c2ee22784c.

[131] P.R. Patwardhan, J.A. Satrio, R.C. Brown, B.H. Shanks, Product distribution from fast pyrolysis of glucose-based carbohydrates, J. Anal. Appl. Pyrolysis. 86 (2009) 323–330. doi:10.1016/j.jaap.2009.08.007.

[132] H.B. Mayes, M.W. Nolte, G.T. Beckham, B.H. Shanks, L.J. Broadbelt, The Alpha-Bet(a) of Salty Glucose Pyrolysis: Computational Investigations Reveal Carbohydrate Pyrolysis Catalytic Action by Sodium Ions, ACS Catal. 5 (2015) 192–202. doi:10.1021/cs501125n.

[133] X. Zhou, M.W. Nolte, H.B. Mayes, B.H. Shanks, L.J. Broadbelt, Experimental and mechanistic modeling of fast pyrolysis of neat glucose-based carbohydrates. 1. Experiments and development of a detailed mechanistic model, Ind. Eng. Chem. Res. 53 (2014) 13274–13289. doi:10.1021/ie502260q.

[134] M.S. Mettler, A.D. Paulsen, D.G. Vlachos, P.J. Dauenhauer, The chain length effect in pyrolysis: bridging the gap between glucose and cellulose, Green Chem. 14 (2012) 1284. doi:10.1039/c2gc35184f.

[135] M.S. Mettler, A.D. Paulsen, D.G. Vlachos, P.J. Dauenhauer, Pyrolytic conversion of cellulose to fuels: levoglucosan deoxygenation via elimination and cyclization within molten biomass, Energy Environ. Sci. 5 (2012) 7864. doi:10.1039/c2ee21305b.

[136] T. McGrath, J. Hoffman, J. Wooten, M. Hajaligol, The effect of inorganics on the formation of PAH during low temperature pyrolysis of cellulose, Cellulose. 47 (2002). http://web.anl.gov/PCS/acsfuel/preprint archive/Files/47_1_Orlando_03-02_0062.pdf.

[137] P.R. Patwardhan, J.A. Satrio, R.C. Brown, B.H. Shanks, Influence of inorganic salts on the primary pyrolysis products of cellulose, Bioresour. Technol. 101 (2010) 4646–4655. doi:10.1016/j.biortech.2010.01.112.

[138] R. Font, A. Marcilla, E. Verdii, J. Devesa, Kinetics of the Pyrolysis of Almond Shells and Almond Shells Impregnated with CoC12 in a Fluidized Bed Reactor and in a Pyroprobe 100, Ind. Eng. Chem. Res. (1990) 1846–1855. doi:10.1021/ie00105a016.

[139] A. Jensen, K. Dam-Johansen, M. a. Wójtowicz, M. a. Serio, TG-FTIR Study of the Influence of Potassium Chloride on Wheat Straw Pyrolysis, Energy Fuels. 12 (1998) 929–938. doi:10.1021/ef980008i.

[140] C.Y. Yang, X.S. Lu, W.G. Lin, X.M. Yang, J.Z. Yao, TG-FTIR Study on Corn Straw Pyrolysis-influence of Minerals, Chem. Res. Chinese Univ. 22 (2006) 524–532. doi:10.1016/S1005-9040(06)60155-4.

[141] K. Wang, J. Zhang, B.H. Shanks, R.C. Brown, The deleterious effect of inorganic salts on hydrocarbon yields from catalytic pyrolysis of lignocellulosic biomass and its mitigation, Appl. Energy. 148 (2015) 115–120. doi:10.1016/j.apenergy.2015.03.034.

[142] X. Liu, Y. Dong, H. Yin, G. Zhang, Catalytic effect of $MgCl_2$ on cotton stalk pyrolysis for chemical production at low temperature, Can. J. Chem. Eng. 93 (2015) 1343–1348. doi:10.1002/cjce.22223.

[143] D.J. Nowakowski, J.M. Jones, Catalysis by potassium in the pyrolysis processes of biomass and basic biomass components, WREC (2005) 590–595.

[144] D.J. Nowakowski, J.M. Jones, Uncatalysed and potassium-catalysed pyrolysis of the cell-wall constituents of biomass and their model compounds, J. Anal. Appl. Pyrolysis. 83 (2008) 12–25. doi:10.1016/j.jaap.2008.05.007.

[145] D. Lv, M. Xu, X. Liu, Z. Zhan, Z. Li, H. Yao, Effect of cellulose, lignin, alkali and alkaline earth metallic species on biomass pyrolysis and gasification, Fuel

Process. Technol. 91 (2010) 903–909. doi:10.1016/j.fuproc.2009.09.014.

[146] F.-X. Collard, A. Bensakhria, M. Drobek, G. Volle, J. Blin, Influence of impregnated iron and nickel on the pyrolysis of cellulose, Biomass Bioener. 80 (2015) 52–62. doi:10.1016/j.biombioe.2015.04.032.

[147] P.T. Williams, P.A.Horne, The role of metal salts in the pyrolysis of biomass, Renew Energ. 4 (1994) 1-13.

[148] G. Yildiz, F. Ronsse, R. Venderbosch, R. van Duren, S.R.A. Kersten, W. Prins, Effect of biomass ash in catalytic fast pyrolysis of pine wood, Appl. Catal. B Environ. 168–169 (2015) 203–211. doi:10.1016/j.apcatb.2014.12.044.

[149] D. Mourant, Z. Wang, M. He, X.S. Wang, M. Garcia-Perez, K. Ling, C.Z. Li, Mallee wood fast pyrolysis: Effects of alkali and alkaline earth metallic species on the yield and composition of bio-oil, Fuel. 90 (2011) 2915–2922. doi:10.1016/j.fuel.2011.04.033.

[150] A. Trendewicz, R. Evans, A. Dutta, R. Sykes, D. Carpenter, R. Braun, Evaluating the effect of potassium on cellulose pyrolysis reaction kinetics, Biomass Bioener. 74 (2015) 15–25. doi:10.1016/j.biombioe.2015.01.001.

[151] E. Ranzi, M. Corbetta, F. Manenti, S. Pierucci, Kinetic modeling of the thermal degradation and combustion of biomass, Chem. Eng. Sci. 110 (2013) 1–11. doi:10.1016/j.ces.2013.08.014.

[152] Q. Eri, X. Zhao, P. Ranganathan, S. Gu, Numerical simulations on the effect of potassium on the biomass fast pyrolysis in fluidized bed reactor, Fuel. 197 (2017) 290–297. doi:10.1016/j.fuel.2017.01.109.

[153] S. Niksa, Predicting detailed product distributions for pyrolysis of diverse forms of biomass with bio-flashchain, Proc. Combust. Inst. 28 (2000) 2727-2733.

[154] H.B. Mayes, J. Tian, M.W. Nolte, B.H. Shanks, G.T. Beckham, S. Gnanakaran, L.J. Broadbelt, Sodium ion interactions with aqueous glucose: Insights from quantum mechanics, molecular dynamics, and experiment, J. Phys. Chem. B. 118 (2014) 1990–2000. doi:10.1021/jp409481f.

[155] X. Zhou, H.B. Mayes, L.J. Broadbelt, M.W. Nolte, B.H. Shanks, Fast pyrolysis of glucose-based carbohydrates with added NaCl Part 1: Experiments and development of a mehanistic model, AIChE J. 62 (2016) 766–777.

doi:10.1002/aic.

[156] X. Zhou, H.B. Mayes, L.J. Broadbelt, M.W. Nolte, B.H. Shanks, Fast pyrolysis of gluocse-based carbohydrates with added NaCl Part 2: validation and evaluation of the mechanistic model, AIChE J. 62 (2016) 778–791.

[157] T. Hosoya, H. Kawamoto, S. Saka, Cellulose-hemicellulose and cellulose-lignin interactions in wood pyrolysis at gasification temperature, J. Anal. Appl. Pyrolysis. 80 (2007) 118–125. doi:10.1016/j.jaap.2007.01.006.

[158] T. Hosoya, H. Kawamoto, S. Saka, Solid/liquid- and vapor-phase interactions between cellulose- and lignin-derived pyrolysis products, J. Anal. Appl. Pyrolysis. 85 (2009) 237–246. doi:10.1016/j.jaap.2008.11.028.

[159] N. Worasuwannarak, T. Sonobe, W. Tanthapanichakoon, Pyrolysis behaviors of rice straw, rice husk, and corncob by TG-MS technique, J. Anal. Appl. Pyrolysis. 78 (2007) 265–271. doi:10.1016/j.jaap.2006.08.002.

[160] C. Couhert, J.M. Commandre, S. Salvador, Is it possible to predict gas yields of any biomass after rapid pyrolysis at high temperature from its composition in cellulose, hemicellulose and lignin?, Fuel. 88 (2009) 408–417. doi:10.1016/j.fuel.2008.09.019.

[161] S. Wang, X. Guo, K. Wang, Z. Luo, Influence of the interaction of components on the pyrolysis behavior of biomass, J. Anal. Appl. Pyrolysis. 91 (2011) 183–189. doi:10.1016/j.jaap.2011.02.006.

[162] B. V Babu, A.S. Chaurasia, Modeling , simulation and estimation of optimum parameters in pyrolysis of biomass, Energy. Convers. Manag. 44 (2003) 2135–2158. doi:10.1016/S0196-8904(02)00237-6.

[163] B. V. Babu, A.S. Chaurasia, Pyrolysis of biomass: Improved models for simultaneous kinetics and transport of heat, mass and momentum, Energy Convers. Manag. 45 (2004) 1297–1327. doi:10.1016/j.enconman.2003.09.013.

[164] A. Bharadwaj, L.L. Baxter, A.L. Robinson, Effects of intraparticle heat and mass transfer on biomass devolatilization: Experimental results and model predictions, Energy Fuels. 18 (2004) 1021–1031. doi:10.1021/ef0340357.

[165] R. Difelice, G. Coppola, S. Rapagna, N. Jand, Modeling of biomass devolatilization in a fluidized bed reactor, Can. J. Chem. Eng. 77 (1999) 325–

332. doi:10.1002/cjce.5450770219.

[166] K. Papadikis, A. V. Bridgwater, S. Gu, CFD modelling of the fast pyrolysis of biomass in fluidised bed reactors, Part A: Eulerian computation of momentum transport in bubbling fluidised beds, Chem. Eng. Sci. 63 (2008) 4218–4227. doi:10.1016/j.ces.2008.05.045.

[167] P. Kaushal, J. Abedi, N. Mahinpey, A comprehensive mathematical model for biomass gasification in a bubbling fluidized bed reactor, Fuel. 89 (2010) 3650–3661. doi:10.1016/j.fuel.2010.07.036.

[168] Y. Wang, L. Yan, CFD studies on biomass thermochemical conversion, Int. J. Mol. Sci. 9 (2008) 1108–1130. doi:10.3390/ijms9061108.

[169] Q. Xue, T.J. Heindel, R.O. Fox, A CFD model for biomass fast pyrolysis in fluidized-bed reactors, Chem. Eng. Sci. 66 (2011) 2440–2452. doi:10.1016/j.ces.2011.03.010.

[170] Q. Xue, D. Dalluge, T.J. Heindel, R.O. Fox, R.C. Brown, Experimental validation and CFD modeling study of biomass fast pyrolysis in fluidized-bed reactors, Fuel. 97 (2012) 757–769. doi:10.1016/j.fuel.2012.02.065.

[171] A. Sharma, S. Wang, V. Pareek, H. Yang, D. Zhang, Multi-fluid reactive modeling of fluidized bed pyrolysis process, Chem. Eng. Sci. 123 (2015) 311–321. doi:10.1016/j.ces.2014.11.019.

[172] K. Papadikis, S. Gu, A. V. Bridgwater, CFD modelling of the fast pyrolysis of biomass in fluidised bed reactors: Modelling the impact of biomass shrinkage, Chem. Eng. J. 149 (2009) 417–427. doi:10.1016/j.cej.2009.01.036.

[173] K. Papadikis, S. Gu, A. V. Bridgwater, H. Gerhauser, Application of CFD to model fast pyrolysis of biomass, Fuel Process. Technol. 90 (2009) 504–512. doi:10.1016/j.fuproc.2009.01.010.

[174] J.M. Jones, M. Pourkashanian, A. Williams, D. Hainsworth, A comprehensive biomass combustion model, Renew. Energy. 19 (2000) 229–234. doi:http://dx.doi.org/10.1016/S0960-1481(99)00036-1.

[175] A.A. Rostami, M.R. Hajaligol, S.E. Wrenn, A biomass pyrolysis sub-model for CFD applications, Fuel. 83 (2004) 1519–1525. doi:10.1016/j.fuel.2003.09.024.

[176] A.B. da Silva, Review of devolatilisation models and their application to pulverised fuel combustion simulation, (n.d.).

[177] A.W. Nunn, T.R., Howard, J.B, Longwell, J.P. and Peters, Product compositions and kinetics in the rapid pyrolysis of sweet gum hardwood, Ind. Eng. Chem. Process Des. Dev. (1985) 836–844.

[178] B.M. Wagenaar, W. Prins, W.P.M. van Swaaij, Flash pyrolysis kinetics of pine wood, Fuel Process. Technol. 36 (1993) 291–298. doi:10.1016/0378-3820(93)90039-7.

[179] H. Lu, Experimental and modeling investigations of biomass particle combustion, Dep. Chem. Eng. PhD Thesis (2006).

[180] T.R. Nunn, J.B. Howard, J.P. Longwell, W.A. Peters, Product Compositions and kinetics in the rapid pyrolysis of sweet gum hardwood, Ind. Eng. Chem. Process Des. Dev. 24 (1985) 836–844.

[181] E. Biagini, M. Cioni, L. Tognotti, Development and characterization of a lab-scale entrained flow reactor for testing biomass fuels, Fuel. 84 (2005) 1524–1534. doi:10.1016/j.fuel.2005.02.001.

[182] E. Ranzi, P.E.A. Debiagi, A. Frassoldati, Mathematical modeling of fast biomass pyrolysis and bio-oil formation. Note I: Kinetic mechanism of biomass pyrolysis, ACS Sustain. Chem. Eng. 5 (2017) 2867–2881. doi:10.1021/acssuschemeng.6b03096.

[183] A.D. Paulsen, M.S. Mettler, P.J. Dauenhauer, The role of sample dimension and temperature in cellulose pyrolysis, Energy Fuels. 27 (2013) 2126–2134. doi:10.1021/ef302117j.

[184] C. Krumm, J. Pfaendtner, P.J. Dauenhauer, Millisecond pulsed films unify the mechanisms of cellulose fragmentation, Chem. Mater. 28 (2016) 3108–3114. doi:10.1021/acs.chemmater.6b00580.

[185] S. Mishra, P.S. Kharkar, A.M. Pethe, Biomass and waste materials as potential sources of nanocrystalline cellulose: comparative review of preparation methods, Carbohydr. Polym. 207 (2018) 418–427. doi:10.1016/j.carbpol.2018.12.004.

[186] T. Lin, E. Goos, U. Riedel, A sectional approach for biomass: Modelling the

pyrolysis of cellulose, Fuel Process. Technol. 115 (2013) 246–253. doi:10.1016/j.fuproc.2013.03.048.

[187] S. Ummartyotin, H. Manuspiya, A critical review on cellulose: From fundamental to an approach on sensor technology, Renew. Sustain. Energy Rev. 41 (2015) 402–412. doi:10.1016/j.rser.2014.08.050.

[188] Suhas, V.K. Gupta, P.J.M. Carrott, R. Singh, M. Chaudhary, S. Kushwaha, Cellulose: A review as natural, modified and activated carbon adsorbent, Bioresour. Technol. 216 (2016) 1066–1076. doi:10.1080/09614524.2018.1398716.

[189] J. Cai, W. Wu, R. Liu, An overview of distributed activation energy model and its application in the pyrolysis of lignocellulosic biomass, Renew. Sustain. Energy Rev. 36 (2014) 236–246. doi:10.1016/j.rser.2014.04.052.

[190] PITT, G. J., The kinetic of the evolution of volatile products from coal, Fuel. 41 (1962) 267–274. http://ci.nii.ac.jp/naid/10003393767/en/ (accessed March 6, 2019).

[191] D.B. Anthony, J.B. Howard, Coal devolatilization and hydrogastification, AIChE J. 22 (1976) 625–656. doi:10.1002/aic.690220403.

[192] A.K. Burnham, L.N. Dinh, A comparison of isoconversional and model-fitting approaches to kinetic parameter estimation and application predictions, J. Therm. Anal. Calorim. 89 (2007) 479–490. doi:10.1007/s10973-006-8486-1.

[193] H.L. Friedman, Kinetics of thermal degradation of char-forming plastics from thermogravimetry. Application to a phenolic plastic, J. Polym. Sci. Part C Polym. Symp. 6 (2010) 183–195. doi:10.1002/polc.5070060121.

[194] A.D. Lewis, Notes from Aaron Lewis for using CPD to predict biomass pyrolysis, (2010) 1-6. https://www.et.byu.edu/~tom/cpd/Bio-CPD-notes.htm.

[195] S. Perry, A global free-radical mechanism for nitrogen release during devolatilization based on coal chemical structure, Chem. Eng. Dep. (1999).

[196] A.D. Lewis, T.H. Fletcher, Predicting Sawdust pyrolysis yields using the cpd code with a tar cracking model, development. (2010) 1–6. http://acerc.byu.edu/Emily/Annual%20Conference/2010%20Presentations/Lewis,%20Aaron.pdf.

[197] G. Varhegyi, M.J. Antal, T. Szekely, F. Till, E. Jakab, G. Varhegyi, Simultaneous thermogravimetric-mass spectrometric studies of the thermal decomposition of biopolymers. 1. Avicel cellulose in the presence and absence of catalysts, Energy Fuels. 2 (1988) 267–272. doi:10.1021/ef00009a007.

[198] D. Liu, Y. Yu, J.I. Hayashi, B. Moghtaderi, H. Wu, Contribution of dehydration and depolymerization reactions during the fast pyrolysis of various salt-loaded celluloses at low temperatures, Fuel. 136 (2014) 62–68. doi:10.1016/j.fuel.2014.07.025.

[199] Z.A. Mayer, A. Apfelbacher, A. Hornung, Effect of sample preparation on the thermal degradation of metal-added biomass, J. Anal. Appl. Pyrolysis. 94 (2012) 170–176. doi:10.1016/j.jaap.2011.12.008.

[200] D. Liu, Y. Yu, Y. Long, H. Wu, Effect of MgCl2 loading on the evolution of reaction intermediates during cellulose fast pyrolysis at 325 ??C, Proc. Combust. Inst. 35 (2015) 2381–2388. doi:10.1016/j.proci.2014.05.026.

[201] Y. Yu, D. Liu, H. Wu, Formation and characteristics of reaction intermediates from the fast pyrolysis of NaCl- and $MgCl_2$ -loaded celluloses, Energ Fuels. 28 (2014) 245–253. doi:10.1021/ef401483u.

[202] T.H. Fletcher, R.J. Pugmire, Chemical percolation model for coal devolatilization, (1992). http://www.et.byu.edu/~tom/cpd/cpdcodes.html.

[203] T. Sonobe, N. Worasuwannarak, Kinetic analyses of biomass pyrolysis using the distributed activation energy model, Fuel. 87 (2008) 414–421. doi:10.1016/j.fuel.2007.05.004.

[204] A. Dufour, B. Ouartassi, R. Bounaceur, A. Zoulalian, Modelling intra-particle phenomena of biomass pyrolysis, Chem. Eng. Res. Des. 89 (2011) 2136–2146. doi:10.1016/j.cherd.2011.01.005.

[205] I. Milosavljevic, E.M. Suuberg, Cellulose Thermal Decomposition Kinetics: Global Mass Loss Kinetics, Ind. Eng. Chem. Res. 34 (1995) 1081–1091. doi:10.1021/ie00043a009.

[206] M. Essig, T. Lowary, G.N. Richards, E. Schenck, Influences of “Neutral” salts on thermochemical conversion of cellulose and of sucrose, in: Res. Thermochem. Biomass Convers., 143–154.

doi:10.1017/CBO9781107415324.004.

[207] P. Patwardhan, Understanding the product distribution from biomass fast pyrolysis, PhD Thesis, Iowa Atate University, Iowa, 2010. http://lib.dr.iastate.edu/etd/11767.

[208] P.N. Rowe, A.W. Nienow, Particle mixing and segregation in gas fluidised beds. A review, Powder Technol. 15 (1976) 141–147. doi:10.1016/0032-5910(76)80042-3.

[209] M.J. V Goldschmidt, J.M. Link, S. Mellema, J.A.M. Kuipers, Digital image analysis measurements of bed expansion and segregation dynamics in dense gas-fluidised beds, Powder Technol. 138 (2003) 135–159. doi:10.1016/j.powtec.2003.09.003.

[210] Y. Zhang, B. Jin, W. Zhong, Fluidization , Mixing and segregation of a biomass-sand mixture in a fluidized bed, Int. J. Chem. React. Eng. 6 (2008).

[211] L. Huilin, H. Yurong, D. Gidaspow, Hydrodynamic modelling of binary mixture in a gas bubbling fluidized bed using the kinetic theory of granular flow, Chem. Eng. Sci. 58 (2003) 1197–1205. doi:10.1016/S0009-2509(02)00635-8.

[212] L. Huilin, H. Yurong, D. Gidaspow, Y. Lidan, Q. Yukun, Size segregation of binary mixture of solids in bubbling fluidized beds, 134 (2003) 86–97. doi:10.1016/S0032-5910(03)00126-8.

[213] L. Huilin, D. Gidaspow, Hydrodynamics of binary uidization in a riser : CFD simulation using two granular temperatures, Chem. Eng. Sci. 58 (2003) 3777–3792. doi:10.1016/S0009-2509(03)00238-0.

[214] H. Iddir, H. Arastoopour, C.M. Hrenya, Analysis of binary and ternary granular mixtures behavior using the kinetic theory approach,Powder. Technol. 151 (2005) 117–125. doi:10.1016/j.powtec.2004.11.033.

[215] S. Qiaoqun, L. Huilin, L. Wentie, H. Yurong, Y. Lidan, D. Gidaspow, Simulation and experiment of segregating/mixing of rice husk-sand mixture in a bubbling fluidized bed, Fuel. 84 (2005) 1739–1748. doi:10.1016/j.fuel.2004.09.026.

[216] N.K.G. Keller, W. Bai, R.O. Fox, T.J. Heindel, Quantifying mixing in 3D binary particulate systems, Chem. Eng. Sci. 93 (2013) 412–422.

doi:10.1016/j.ces.2013.01.069.

[217] A. Sharma, S. Wang, V. Pareek, H. Yang, D. Zhang, CFD modeling of mixing/segregation behavior of biomass and biochar particles in a bubbling fluidized bed, Chem. Eng. Sci. 106 (2014) 264–274. doi:10.1016/j.ces.2013.11.019.

[218] W. Bai, N.K.G. Keller, T.J. Heindel, R.O. Fox, Numerical study of mixing and segregation in a biomass fl uidized bed, Powder Technol. 237 (2013) 355–366. doi:10.1016/j.powtec.2012.12.018.

[219] D. Gera, M. Syamlal, T.J. O'Brien, Hydrodynamics of particle segregation in fluidized beds, Int. J. Multiph. Flow. 30 (2004) 419–428. doi:10.1016/j.ijmultiphaseflow.2004.01.003.

[220] A. Fluent, ANSYS Fluent 12.0 user's guide, Ansys Inc. 15317 (2009) 1–2498. doi:10.1016/0140-3664(87)90311-2.

[221] D. Gidaspow, R. Bezburuah, Ding Jianmin, Hydrodynamics of circulating fluidized beds: Kinetic theory approach, in: 7th Fluid. Conf., (1992) 1–8.

[222] M. Syamlal, The particle-particle drag term in a multiparticle model of fluidization, Tech. Report. (1987) 1-25. doi:MC/21353-2373, NTIS/DE87006500.

[223] T. Hao, B. Park, Defining temperatures of granular powders analogously with thermodynamics to understand the jamming phenomena, 1–34.

[224] M. Syamlal, W. Rogers, T.J. O`Brien, MFIX documentation theory guide, Tech. Note. 1004 (1993) 1-52. doi:METC-9411004, NTIS/DE9400087.

[225] C.K.K. Lun, S.B. Savage, D.J. Jeffrey, N. Chepurniy, Kinetic theories for granular flow: inelastic particles in Couette flow and slightly inelastic particles in a general flowfield, J. Fluid Mech. 140 (1984) 223–256. doi:10.1017/S0022112084000586.

[226] D.G. Schaeffer, Instability in the evolution-equations describing incompressible granular flow, J. Differ. Equ. 66 (1987) 19–50.

[227] J.L. Sinclair, R. Jackson, Gas-particle flow in a vertical pipe with particle-particle interactions, AIChE J. 35 (1989) 1473–1486.

doi:10.1002/aic.690350908.

[228] N.K.G. Keller, Mixing and segregation in 3D multi-component two-phase fluidized beds using X-ray computed tomography, PhD Thesis, Iowa State University, Iowa, (2012).

[229] D. Kunii, O. Levenspiel, Fluidization Engineering, Second ed., Butterworth—Heinemann, series in Chemical Engineering 1992.

[230] K. Papadikis, S. Gu, A. V. Bridgwater, CFD modelling of the fast pyrolysis of biomass in fluidised bed reactors. Part B. Heat, momentum and mass transport in bubbling fluidised beds, Chem. Eng. Sci. 64 (2009) 1036–1045. doi:10.1016/j.ces.2008.11.007.

[231] S. Jalalifar, M. Ghiji, R. Abbassi, V. Garaniya, Numerical modelling of a fast pyrolysis process in a bubbling fluidized bed reactor, Conference paper (2017).

[232] S. Jalalifar, R. Abbassi, V. Garaniya, K. Hawboldt, Parametric analysis of pyrolysis process on the product yields in a bubbling fluidized bed reactor, Fuel 234 (2018) 616–625.

[233] J. Cai, W. Wu, R. Liu, An overview of distributed activation energy model and its application in the pyrolysis of lignocellulosic biomass, Renew. Sustain. Energy Rev. 36 (2014) 236–246. doi:10.1016/j.rser.2014.04.052.

[234] K. Kirtania, S. Bhattacharya, Coupling of a distributed activation energy model with particle simulation for entrained flow pyrolysis of biomass, Fuel Process. Technol. 137 (2015) 131–138. doi:10.1016/j.fuproc.2015.04.014.

[235] A. Soria-Verdugo, E. Goos, N. García-Hernando, Effect of the number of TGA curves employed on the biomass pyrolysis kinetics results obtained using the Distributed Activation Energy Model, Fuel Process. Technol. 134 (2015) 360–371. doi:10.1016/j.fuproc.2015.02.018.

[236] K. Czajka, A. Kisiela, W. Moroń, W. Ferens, W. Rybak, Pyrolysis of solid fuels: Thermochemical behaviour, kinetics and compensation effect, Fuel Process. Technol. 142 (2016) 42–53. doi:10.1016/j.fuproc.2015.09.027.

[237] Q. Xiong, F. Xu, E. Ramirez, S. Pannala, C.S. Daw, Modeling the impact of bubbling bed hydrodynamics on tar yield and its fluctuations during biomass fast pyrolysis, Fuel. 164 (2016) 11–17. doi:10.1016/j.fuel.2015.09.074.

[238] Q. Xiong, E. Ramirez, G. Wiggins, C.S. Daw, Coupling DAEM and CFD for simulating biomass fast pyrolysis in fluidized beds, Technical Report. (http://www.energy.gov/downloads/doe-public-access-plan.

[239] F. Shafizadeh, A.G.W. Bradbury, Thermal degradation of cellulose in air and nitrogen at low temperatures, J. Appl. Polym. Sci. 23 (1979) 1431–1442. doi:10.1002/app.1979.070230513.

[240] F. Shafizadeh, Introduction to pyrolysis of biomass, J. Anal. Appl. Pyrolysis. 3 (1982) 283–305. doi:10.1016/0165-2370(82)80017-X.

[241] C. Di Blasi, Numerical simulation of cellulose pyrolysis, Biomass Bioener. 7 (1994) 87–98.

[242] L.J. Curtis, D.J. Miller, Transport model with radiative heat transfer for rapid cellulose pyrolysis, Ind. Eng. Chem. Res. 27 (1988) 1775–1783. doi:10.1021/ie00082a007.

[243] J. Cai, T. Li, R. Liu, A critical study of the Miura – Maki integral method for the estimation of the kinetic parameters of the distributed activation energy model, Bioresour. Technol. 102 (2011) 3894–3899. doi:10.1016/j.biortech.2010.11.110.

[244] D.J. Gunn, Transfer of heat or mass to particles in fixed and fluidized beds, Int. J. Heat Mass Transf. 21 (1978) 467–476.